AD-A131 645 UNDERKEEL CLEARANCE STUDY(U) HYDRO RESEARCH SCIENCE 1/2
SANTA CLARA CA A B RUDAVSKY ET AL. SEP 81 HRS-092-81
N00014-80-C-0395

UNCLASSIFIED F/G 13/10 NL

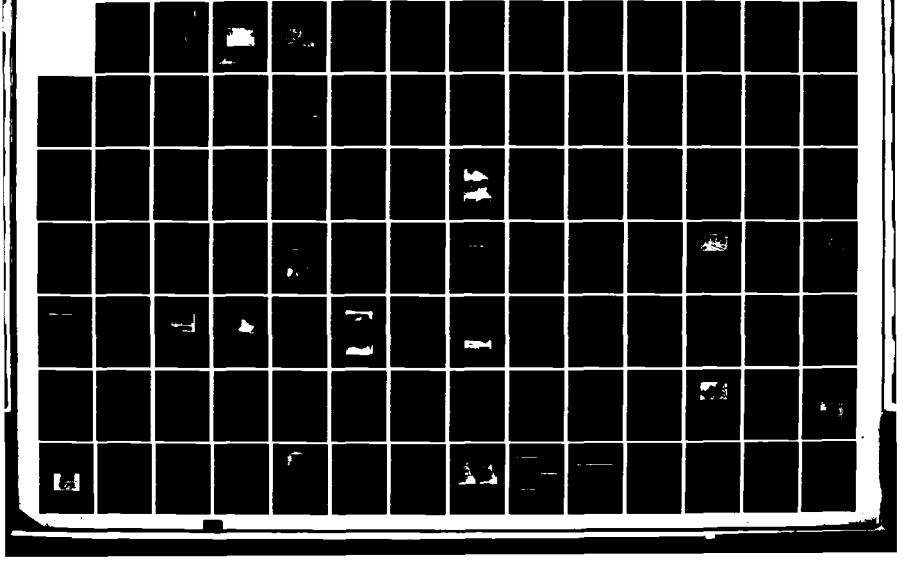

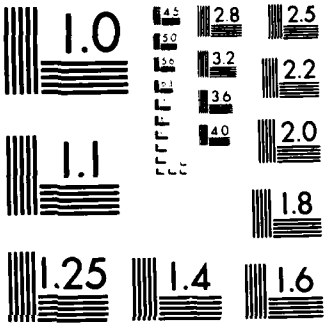

PHOTOGRAPH THIS SHEET

A131645

DTIC ACCESSION NUMBER

II

LEVEL

1

INVENTORY

Underkeel Clearance Study

DOCUMENT IDENTIFICATION Final, Mar 80 - Sept 81

Contract N0014-80-C-0395 Sept '81

DISTRIBUTION STATEMENT A
Approved for public release;
Distribution Unlimited

DISTRIBUTION STATEMENT

ACCESSION FOR	
NTIS GRA&I	☒
DTIC TAB	☐
UNANNOUNCED	☐
JUSTIFICATION	
BY Per Ltr. on file	
DISTRIBUTION / AVAILABILITY CODES	
DIST	AVAIL AND/OR SPECIAL
A	

DISTRIBUTION STAMP

DTIC
ELECTE
S AUG 23 1983 D
D

DATE ACCESSIONED

83 06 14 067

DATE RECEIVED IN DTIC

PHOTOGRAPH THIS SHEET AND RETURN TO DTIC-DDA-2

DTIC FORM OCT 79 70A

DOCUMENT PROCESSING SHEET

N00014-80-C-0395
Project Report HRS 092-81

UNDERKEEL CLEARANCE STUDY

prepared for

NAVAL FACILITIES ENGINEERING COMMAND

Alexandria, Virginia

by

Dr. A. B. Rudavsky
Wei-Yih Chow
James C. Wang
Jen-Men Lo

HRS Inc. HYDRO RESEARCH SCIENCE

3334 VICTOR COURT ■ SANTA CLARA, CALIFORNIA 95050 ■ 408 – 988-1027

N00014-80-C-0395
Project Report HRS 092-81

UNDERKEEL CLEARANCE STUDY

prepared for

NAVAL FACILITIES ENGINEERING COMMAND

Alexandria, Virginia

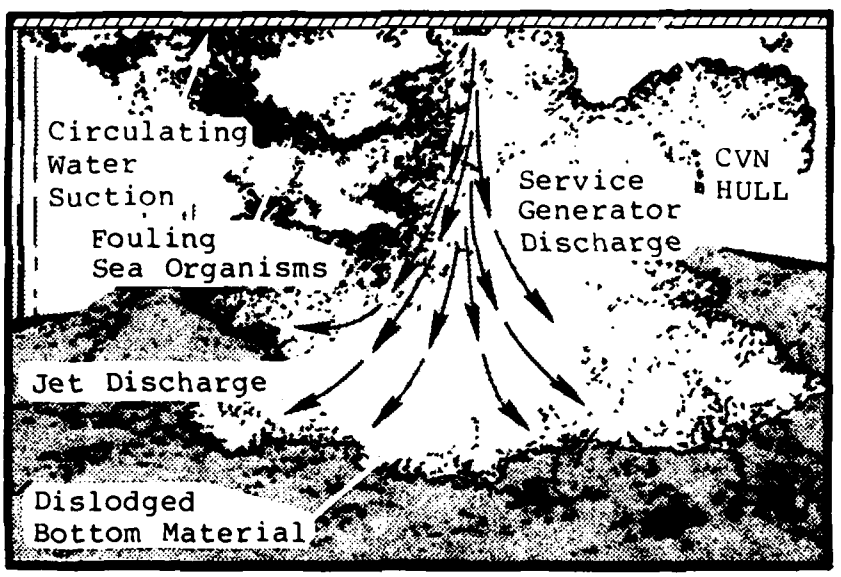

Cover photo illustrates one cause of CVN Fouling Problem.

by

Dr. A. B. Rudavsky
Wei-Yih Chow
James C. Wang
Jen-Men Lo

March 31, 1981

SECURITY CLASSIFICATION OF THIS PAGE (When Data Entered)

REPORT DOCUMENTATION PAGE

READ INSTRUCTIONS BEFORE COMPLETING FORM

1. REPORT NUMBER: N00014-80-C-0395

2. GOVT ACCESSION NO.:

3. RECIPIENT'S CATALOG NUMBER:

4. TITLE (and Subtitle): Underkeel Clearance Study prepared for Naval Facilities Engineering Command Alexandria, Virginia

5. TYPE OF REPORT & PERIOD COVERED: Final, March 1980 - September 1981

6. PERFORMING ORG. REPORT NUMBER: 1124

7. AUTHOR(s): Dr. A. B. Rudavsky, Jen-Men Lo, Wei-Yih Chow, James C. Wang

8. CONTRACT OR GRANT NUMBER(s): N00014-80-C-0395

9. PERFORMING ORGANIZATION NAME AND ADDRESS: Hydro Research Science (HRS, Inc.), 3334 Victor Court, Santa Clara, CA 95018

10. PROGRAM ELEMENT, PROJECT, TASK AREA & WORK UNIT NUMBERS: Element 64567N, Task 23702

11. CONTROLLING OFFICE NAME AND ADDRESS: PCO, ONR Dept Navy, 800 N. Quincy St, Arlington, VA 22217

12. REPORT DATE: published September 1981

13. NUMBER OF PAGES: 170

14. MONITORING AGENCY NAME & ADDRESS (if different from Controlling Office): Commander Atlantic Division, Naval Facilities Engineering Command, Attn: Mr. W.F. Gasser, Code 1025, Bldg W-5, Naval Station, Norfolk, VA 23511

15. SECURITY CLASS. (of this report): Unclassified

15a. DECLASSIFICATION/DOWNGRADING SCHEDULE:

16. DISTRIBUTION STATEMENT (of this Report)

DISTRIBUTION STATEMENT A
Approved for public release; Distribution Unlimited

17. DISTRIBUTION STATEMENT (of the abstract entered in Block 20, if different from Report)

18. SUPPLEMENTARY NOTES

19. KEY WORDS (Continue on reverse side if necessary and identify by block number)

Fouling
Marine Organisms
Sediments
Jets
Hydraulic Models
Numerical Models
Discharge Diffusers

20. ABSTRACT (Continue on reverse side if necessary and identify by block number)

Hydraulic model study was conducted to characterize the dynamic process of deep-draft vessel's sea-chest fouling, and to assess the flow patterns generated by suction and discharge of the sea chests in confined spaces. Onboard solutions were developed to minimize fouling of the sea chests by introducing diffuser structures at the discharge sea chests. A numerical model for assessing the flow patterns and suction foulings was also developed.

DD FORM 1 JAN 73 1473 EDITION OF 1 NOV 65 IS OBSOLETE

Unclassified

SECURITY CLASSIFICATION OF THIS PAGE (When Data Entered)

CONTENTS

CONTENTS (continued)

CONTENTS (continued)

CONTENTS (continued)

CONTENTS (continued)

LIST OF FIGURES

LIST OF FIGURES (continued)

LIST OF FIGURES (continued)

LIST OF TABLES

EXECUTIVE SUMMARY

THE PROBLEM — DECREASED OPERATIONAL READINESS OF CVN CLASS VESSELS

The operational readiness of aircraft carriers has for years been reduced by what would seem to be a minor problem -- the fouling of sea chests due to the ingestion of bottom sediment and marine organisms. Such fouling problems occur at both pier side and upon entering and leaving the berthing areas of certain Naval harbors.

Reference:
- Text Section 3.1

According to one Navy source, serious consequences can result from the inoperability of circulating water systems of CVN class vessels. Some typical problems have been reported [1] to include:

- Delays of flight operations for up to 12 hours following underway time, as catapults cannot be warmed at the pier.
- Underway evolutions cannot be conducted using the main engines, and tug assistance to anchorage is therefore often required.
- Frequent malfunctions of the turbine generator and distilling plant occur, in addition to excessive wear of the ship's machinery and pump components.

Such circulating water-system clogging has been found to occur at either the suction grating on the hull or on the tube sheet inside the condenser head. The exact causal factors were previously unknown, but were assumed to

- Text Sections 1.1, 3.1

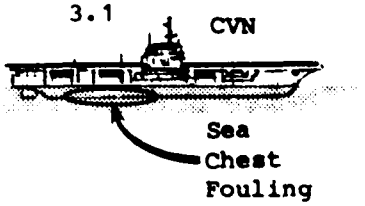

be: underkeel "migration" of marine organisms, sea chest suction, inadequate underkeel clearance, or a combination of these factors.

Before this study, little was known about the underkeel clearance required to alleviate such fouling problems. Prior to dredging to the proposed 50- plus 2-foot berthing depth for carriers, Norfolk Naval Base authorities wanted to be assured that the planned depth would alleviate the fouling problem.

- Text Sections 3.2.3, 3.2.4

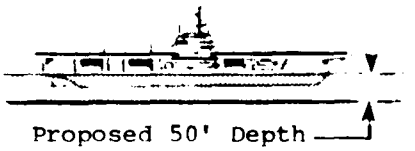

OBJECTIVES OF THE CURRENT STUDY

A Technology Development project was initiated by Naval Facilities Engineering Command (NAVFACENGCOM) to determine the underkeel clearance required to alleviate the fouling problem. The project was subsequently awarded to Hydro Research Science (HRS, Inc.) in the form of ONR Contract Number N00014-80-C-0395 dated 17 MAR 80.

The underlying objectives of the resulting HRS study were to: (a) investigate the underkeel requirements of aircraft carriers as related to the sea chest fouling problem, and (b) develop an on-board technology to control the fouling problems experienced by aircraft carriers in certain parts of Norfolk Harbor.

- Text Sections 1.2, 3.8
- Figure 3-4

PHYSICAL MODEL PREPARATION

Precision-constructed scale models of the selected CVN class service generator and main circulating cooling systems were then constructed. The models were placed in the HRS

- Text Section 4.1
- Appendix B
- Figures 4-1, 4-2, 4-3

Berthing Tank and fully instrumented for experimental purposes. The tank bottom was filled with sized walnut shell grains to simulate mud and algae to simulate marine organisms, and a dye probe was installed in the recirculating system to enable observation of the flow patterns.

IDENTIFICATION OF THE PRIMARY CAUSAL FACTOR

As a result of an intense hydraulic modeling investigation of the circulating cooling system fouling problems of Naval aircraft carriers during berthing and light off operations at port...the primary causal factor was identified as the sea-chest discharge jet.

The impingement of the jet on the berthing floor was found to cause dislodgement of bottom material. When the resuspended materials approached the suction sea chest, they were ingested and fouling occurred. Hydraulic model experimentation using an assumed average draft of 39 ft, with underkeel clearances of 5, 13, and 21 ft, corresponding to slip depths of 44, 52, and 60 ft, respectively, indicated that a strong "jet" persisted throughout the entire jet path.

An in-depth study was then conducted to characterize the velocity and pressure fields of the jets. It became obvious that onboard modifications would be potentially effective in controlling condenser fouling problems.

- Text Section 4.2
- Figure 4-4

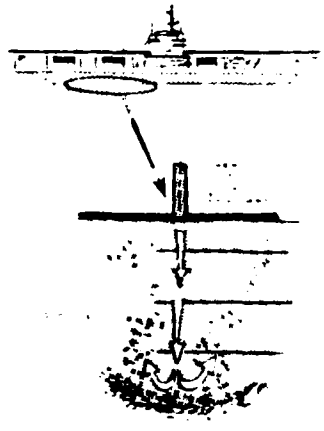

THE DIFFUSER AS THE ONBOARD SOLUTION

As the outcome of April/May 1980 meetings between HRS, NAVSEASYSCOM, NAVFACENGCOM

- Text Section 1.2.3

and LANTNAVFACENGCOM at the HRS Laboratory, it was agreed that HRS should pursue sea-chest "diffusers" as a viable onboard solution to the fouling problem.

The concept of diffuser design is to spread the flow through various physical arrangements such that the flow velocity is reduced and a uniform exit velocity obtained.

- Text Section 6.2

It was further agreed that the resulting diffuser designs were to be tested by HRS at potential underkeel clearances of 5 and 13 ft, corresponding to slip depths of 44 and 52 ft, utilizing physical-model test procedures.

- Text Section 1.2.2

THE ORIGINAL NAVSEASYSCOM DIFFUSER DESIGNS

NAVSEASYSCOM provided HRS with two preliminary sea-chest diffuser designs for evaluation. The diffuser impact chamber consisted of two semicircular cups concaved upward and located directly under the discharge line. The guide vanes located on the sides of the diffuser were designed to change the flow direction.

- Text Sections 6.3, 6.4

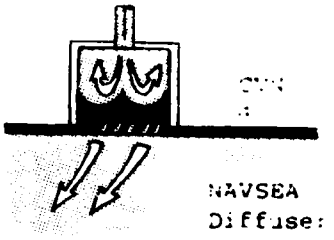

Rotational flow patterns were found in diffuser tests, the flow was branching into two streams due to the design of the two semicircular cups. It was evident that further modification of the diffuser was needed to achieve better flow distributions.

THE IMPROVED DIFFUSER DESIGNS

Onboard solutions were subsequently developed to obtain the optimized sea-chest dif-

- Text Section 6.0

fuser designs for the Service Generator (SG) cooling system. The optimized diffuser designs reduced the jet-produced disturbance of the berthing floor--also reducing the subsequent ingestion of suspended materials into the suction sea chest.

ASSESSMENT OF 5-FOOT KEEL CLEARANCE

- Text Sections 2.1, 6.7
- Appendix B

The existing 5-foot keel clearance or 44-foot slip depth was found to pose fouling problems because of the following reasons: (1) marine organisms usually "remain" within 6 ft from the sea floor, and (2) inadequate dispersions of the jet flow result from such "very confined" underkeel spaces.

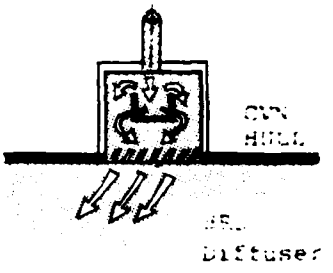

With the installation of the proposed diffuser, satisfactory reduction of flow velocity was accomplished. However, the 5-foot underkeel clearance will still impose potential sea-chest fouling problems.

It was therefore concluded that the existing 5-foot underkeel clearance is inadequate to prevent fouling of aircraft-carrier circulating cooling systems in the Norfolk Harbor environment.

THE SUPPORTING NUMERICAL-MODEL STUDY

- Text Section 5.0
- Appendix C, F

The objective of the numerical-model study was to develop a state-of-the-art numerical model relating the underkeel clearance of an aircraft carrier to the dynamics of sea-chest flow fields and related berthing floor behavior.

APPLICATIONS OF THE NUMERICAL MODEL

The numerical model was developed for the following purposes:

- Judging the stability of the bottom material by comparing the shear stress with the critical shear stress from Shields curve.
- Understanding the influence of underkeel clearance as it relates to the impingement of a jet.
- Estimating the volume of bottom material or marine organisms which could be ingested given a specified concentration and distribution of the organisms.
- Determining the jet center to suction center distance required to reduce the volume of ingested materials.

THE RESULTING CONCLUSIONS

The following conclusions resulted from this study:

- The jet discharge from the sea chest causes the marine life to be suspended and catapulted into the zone of influence of suction sea chest.
- The existing 5-foot underkeel clearance results in extreme jet strength, and extensive resuspension and insufflation of material.

- Text Section 2.1
- Figure 2-1

- Dredging the existing slips to 50 plus 2 ft to produce a 13-foot underkeel clearance would be beneficial, but would not cure the problem. A combination of onboard (diffuser installation) and offboard (dredging and facility modification) measures should provide the optimal means of reducing the problem.

- The discharge velocity of the main circulation pumps, although less than the service generators, is still sufficiently great to cause fouling when the pumps are operated at full capacity. It is technically feasible to diffuse the jet, but this study does not evaluate this option. If operationally acceptable, the fouling caused by the main circulation pumps could be reduced by throttling back when operating pier side. The main circulating cooling system was further investigated under reduced flow rates of 20,000 gpm and 8,750 gpm. Test results indicated that under low flow rate, the disturbance of sea floor was reduced.

- The diffuser designed for the service generator will reduce the strength of the discharge jet. Similar diffusers could be designed for other discharge openings. If desired by the Navy, the diffuser could be designed for

even smaller exit velocities. However, the louvered exit area would have to be expanded.

- Installation of the service generator diffuser must be considered as a partial solution. Deepening the berthing area by dredging, and possible additional facility modification measures to be investigated in a follow-on HRS study, are expected to solve the suction fouling problem.

RECOMMENDATIONS

Our recommendations for solving the suction fouling problems are:

- Deepening the berthing area to 50 plus 2-foot overdredge to achieve a 13-foot underkeel clearance.
- Installing the single-barrel and double-barrel diffusers designed for the service generator cooling system to suit the ship hull application. With the installation of the diffuser, the service generator discharge jet will be reduced in strength which will aid in alleviating sea-chest fouling.
- Utilizing other onboard and offboard remedial measures such as throttling back main circulation system pumps and modifying existing waterfront structures to minimize the dislodgement/transportation of organisms and sediment.

- Text Section 2.2

It is further recommended that a much larger scale sea-chest model be studied (model-to-prototype scale ratio of 1:4) to provide additional detailed information on flow patterns, back pressures, velocities, and localized phenomena not clearly revealed by the 1:10 hydraulic model study.

1.0 Introduction

1.0 INTRODUCTION

1.1 THE UNDERLYING PROBLEM

During "berthing" and "light off" operations in some ports, aircraft carriers sometimes experience heavy fouling of sea chests and condensers due to the ingestion of bottom sediment and marine organisms. [1] [2]*

Such clogging has been found to occur at either the suction opening grate on the hull bottom or on the tube sheet inside the condenser head. The causal factors were previously unknown, but were assumed to be: underkeel "migration" of marine organisms, sea-chest suction, inadequate underkeel clearance, or a combination of these factors.

1.2 THE CURRENT STUDY

Before this study, little was known about the underkeel clearance required to alleviate such fouling problems. Prior to dredging to the proposed 50- plus 2-foot berthing depth for carriers, Norfolk Naval Base wanted to be assured that the planned depth would alleviate the fouling problem.

A Technology Development project was therefore initiated by Naval Facilities Engineering Command (NAVFACENGCOM) to determine the underkeel clearance required to alleviate the problem. The project was subsequently awarded to Hydro Research Science (HRS, Inc.) in the form of ONR Contract Number N00014-80-C-0395 dated 17 MAR 80.

1.2.1 The Study Objectives. The underlying objectives of this study were to: (a) investigate the underkeel requirements of aircraft carriers as related to the sea-chest fouling problems, and (b) develop an onboard technology to control the fouling problems experienced by aircraft carriers in certain parts of Norfolk Harbor, primarily those berthed at Pier 12.

---

* Numbers in brackets [ ] refer to references in Annotated Bibliography, Appendix E.

1.2.2 Scope of the Study. As the outcome of meetings between HRS, NAVSEASYSCOM, NAVFACENGCOM, and LANTNAVFACENGCOM conducted in April and May 1980 at the HRS Laboratory, it was agreed that HRS was to pursue development of sea-chest "diffusers" as an onboard solution to the fouling problem. It was further agreed that the resulting diffuser designs were to be tested at underkeel clearances of 5, 13, and 21 ft using physical-model test procedures. The clearances conform to the average existing slip depth of 44 ft, a proposed dredging depth of 50 plus 2 ft, and a theoretical dredging depth of 60 ft, respectively.

> NOTE: HRS has received a subsequent contract to pursue the development of offboard fouling controls for the proposed Pier 11 and existing Pier 12 area at Naval Station, Norfolk, Virginia. The current report deals only with the onboard solutions developed in satisfaction of the cited contract.

1.2.3 Structure of the Study. To ensure satisfaction of the underlying objectives, the project was conducted as several discrete, but interrelated, phases. The primary phases included:

Phase 1 -- Analysis of the underlying problem and identification of potential onboard solution methodologies.

Phase 2 -- Physical-model experimentation to analyze the potential solutions... identifying the "most promising" for additional refinement.

Phase 3 -- Development of a working numerical model to assess underkeel flow fields and berthing floor behavior.

Phase 4 -- Comprehensive documentation of the project, including a Final Report and Bibliography, a User's Manual for the numerical model, and a narrated 16mm movie.

1.3 SOURCES OF INFORMATION

The following paragraphs identify the primary sources of information for this study. All of the cited sources were used extensively for the physical-model construction and test program, and were also drawn upon in developing this report.

1.3.1 NAVFACENGCOM, NAVSEASYSCOM, and LANTNAVFACENGCOM. General information on the structural aspects of Naval aircraft carriers was provided by NAVFACENGCOM. The following drawings were supplied:

- AOE Drawing No. 120-2286180 -- Sheets 1 and 2
- AOE Drawing No. 120-2287720 -- Sheets 2, 3, and 4
- CVN 69 Docking Drawing No. 845-4636304.

Additional information was obtained from: (a) communications between HRS and NAVFACENGCOM/NAVSEASYSCOM/LANTNAVFACENGCOM regarding the design of, and general information about, the sea chest, and (b) conferences held at HRS to discuss both the experimental program and the diffuser design.

1.3.2 Virginia Institute of Marine Science (VIMS). HRS entered into a contract with Virginia Institute of Marine Science (VIMS), performed by Dr. Robert Diaz, to study the hydrodynamic properties of the identified fouling marine organisms. The resulting data was utilized by the HRS project staff and is included as Appendix A of this report.

1.3.3 Literature Searches. Generalized data on hydrologic and sediment conditions near the study area were gathered via an extensive search of the available literature. [3] [4] [5] [6] [7]

1.4 STRUCTURE OF THIS REPORT

The remainder of this report documents the Technology Development project performed by HRS, Inc. For ease of readership, the report has been divided into two parts. Part I consists of a "less technical" summary of the project, and includes Sections 1 through 6. Part II contains more detailed technical information and data, and includes Appendix A through Appendix F. The contents of each section and appendix include:

--PART I--

Section 1 - INTRODUCTION

Section 2 - CONCLUSIONS AND RECOMMENDATIONS
A concise discussion of the study conclusions and the resulting recommendations.

Section 3 - THE PROBLEM
A summary of the fouling problem in terms of the available "pre-study" information and data.

Section 4 - THE ANALYSIS
A description of the analytical and physical model studies conducted by the HRS project staff.

Section 5 - THE NUMERICAL MODEL
Description of the state-of-the-art numerical model developed to relate "keel clearance" of Naval aircraft carriers to the dynamics of the flow field and related berthing floor behavior.

Section 6 - THE SOLUTIONS
Discussions of the HRS-developed solutions to the fouling problem, including conclusions and recommendations.

--PART II--

Appendix A - HYDRODYNAMIC PROPERTIES OF MARINE ORGANISMS
A summary of the data resulting from the marine organism investigations conducted by Dr. Robert Diaz of VIMS under contract to HRS, Inc.

Appendix B - PHYSICAL MODEL TESTS AND RESULTS
Descriptions of the physical model setup and test results.

Appendix C - DEVELOPMENT OF THE NUMERICAL MODEL
A detailed description of the working numerical model developed to permit assessment of the flow field beneath an aircraft carrier.

Appendix D - KEY WORDS AND DEFINITIONS
An alphabetical listing of the key technical and scientific terms used in this report, along with a concise definition of each term or abbreviation.

Appendix E - ANNOTATED BIBLIOGRAPHY
A state-of-the-art annotated bibliography of the primary references used to assess the fouling problem, and to determine the related state-of-the-art knowledge.

Appendix F - USER'S MANUAL
A simplified manual for Naval personnel using the numerical model described in Section 5.0 of this report.

Appendix G - CONVERSION FACTORS

Conversion Factors, Customary to SI Units of Measurements

2.0 Conclusions and Recommendations

2.0 CONCLUSIONS & RECOMMENDATIONS

2.1 CONCLUSIONS

As a result of an intense investigation of the circulating cooling system fouling problems of Naval aircraft carriers during berthing and light off operations at port...the primary causal factor was identified as the sea-chest discharge jet.

Hydraulic model experimentation with underkeel clearances of 5, 13, and 21 ft indicated that a strong "jet" persisted throughout the entire jet path. The impingement of the jet on the berthing floor was found to cause dislodgement of bottom material. When the resuspended materials approached the suction sea chests, fouling was found to be likely to occur.

An in-depth study of the flow field was then conducted to characterize the velocity and pressure field of the jets. Data were compared to the results from other investigators, and good correlations resulted.

> In order to control the condenser fouling, it became obvious that structural modifications to the ship would be required.

Onboard solutions were subsequently developed to minimize marine organism fouling of the circulating cooling system of aircraft carriers. Solutions were provided in the form of HRS-optimized sea-chest diffuser designs for the Service Generator (SG) cooling system. The optimized sea-chest designs acted to reduce the strength of the discharge jet, reducing jet-produced disturbance of the berthing floor, and subsequent ingestion of the suspended materials into the suction sea chest.

The existing 5-foot keel clearance, corresponding to an average existing slip depth of 44 ft, was found to pose fouling problems. It was found that: (1) marine organisms,

usually "remain" up to 6 ft from the sea floor,* and (2) inadequate dispersions of the jet flow result from such "very confined" underkeel spaces. It was therefore concluded that the existing 5-foot underkeel clearance is inadequate to prevent fouling of aircraft-carrier circulatory cooling systems in the current Norfolk port environment. A recommended 13-foot underkeel clearance, corresponding to a dredged depth of 50 plus 2 ft, together with the onboard discharge diffusers, will provide a more promising alternative.

In summary, the following conclusions resulted from this study:

- The jet discharge from the sea chest causes the marine life to be suspended and catapulted into the zone of influence of suction chest.
- The 5-foot underkeel clearance results in extreme jet strength and extensive resuspension and insufflation of material. (Figure 2-1 shows the suspension of the bottom material resulting from the strong discharge jet).
- The 13-foot underkeel clearance would be beneficial, but would not cure the problem. A combination of onboard and offboard measures should provide the optimal means of reducing the problem.
- The main circulation cooling system does not have to be operated at full capacity during light off operations and, therefore, was further investigated at reduced flow rates of 20,000 gpm and 8,750 gpm. Test results indicated that under low flow rate, the disturbance of the sea floor was reduced.

*Conversation with Dr. Robert Diaz, VIMS.

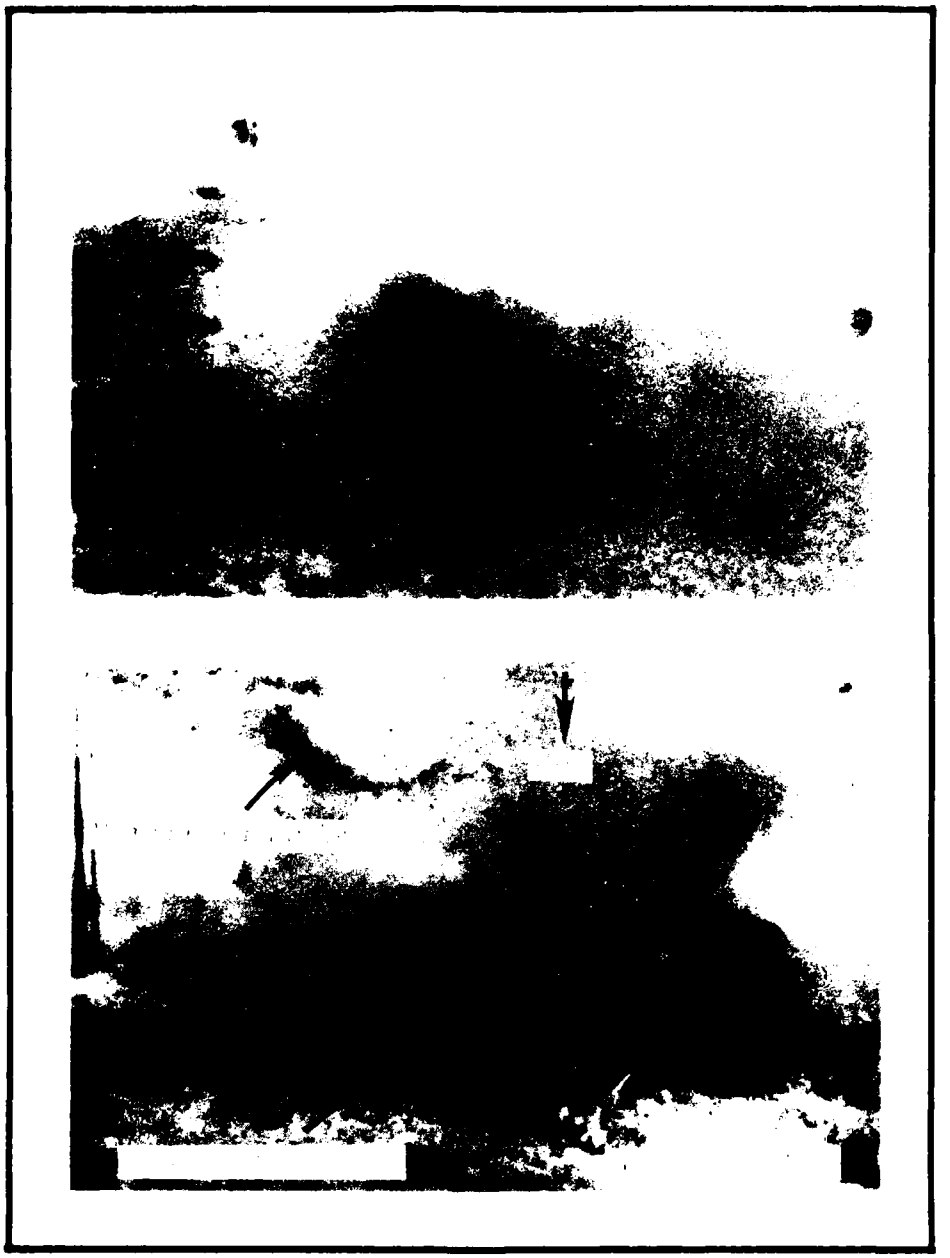

Figure 2-1

Suspension of Bottom Material
Resulting From Strong Jet Forces

- The diffuser designed for the service generator will reduce the strength of the discharge. Similar diffusers could be designed for other discharge openings. If desired by the Navy, the diffuser could be designed for even smaller exit velocities. However, the louvered exit area would have to be expanded.

- Installation of the service generator diffuser must be considered a partial solution. It is anticipated that the suction fouling problem can be solved by implementing the following:

  - Deepening the berthing area by dredging to 50 plus 2 ft

  - HRS follow-on study to investigate the possibility of additional measures.

2.2 THE RESULTING RECOMMENDATIONS

Our recommendations for solving the suction fouling problems are:

- Deepening the berthing area to achieve a 13-foot underkeel clearance.

- Installing the single-barrel and double-barrel diffusers designed for the service generator cooling system to suit the ship hull application. With the installation of the diffuser, the service generator discharge jet will be reduced in strength which will aid in alleviating sea-chest fouling.

- Utilizing other onboard remedial measures such as throttling back main circulation system pumps and modifying existing waterfront structures to minimize the dislodgement of organisms and sediments.

It is further recommended that a much larger scale sea-chest model be studied (model-to-prototype scale ratio of 1:4) to provide additional detailed information on flow patterns, back pressures, velocities, and localized phenomena which was not clearly revealed by the current 1:10 hydraulic-model study.

3.0 The Problem

3.0 THE PROBLEM

3.1 OVERVIEW

The operational readiness of aircraft carriers has for years been reduced by what would seem to be a minor problem -- the fouling of sea chests and condensers due to the ingestion of bottom sediment and marine organisms at pier side and when entering and leaving the berthing areas of certain Naval harbors.

According to one source, "the pattern is that marine organisms become lodged against the intake screens of the auxiliary and main condenser intakes...causing the cooling water temperatures to rise to such a point that the generating plants are rendered inoperative." [1]

Serious consequences occur as a result of such interruptions in the operability of CVN-class vessel seawater circulating water systems. Problems have been reported [1] to include:

- Inability to conduct inport testing of the steam plant or catapult.
- Delays of flight operations for up to 12 hours following underway time, as the catapults cannot be warmed at the pier.
- Pre-underway electrical and electronic testing is complicated because turbine generators are not available for ship's power...requiring operation with the limited power available from the ship's emergency diesel generators.
- Underway evolutions cannot be conducted at pier-side using the main engines, and tug assistance to temporary remote anchorage is therefore required.
- Frequent malfunctions of the turbine generator and distilling plant occur, in addition to excessive wear of the ship's machinery and pump components.

In most cases an aircraft carrier experiencing such sea-chest fouling problems has to proceed to anchorage and have the clogged screens cleaned by divers. In other cases the divers have had to clean the screens with the carrier in the berth. Such a cleaning operation is often very difficult in Norfolk Harbor, where the underkeel clearance is 5 ft or less for CVN-class vessels. Additionally, such cleaning operations take 6 or more hours to perform and are complicated by "the inability of divers to maintain a given position under the ship because of tidal flow, and loss of vision due to the "fluid" mud condition that exists up to a height of 6 ft from the slip bottom." [1]

> The remainder of this section of the report summarizes the particulars of the fouling problem in terms of the available "pre-study" information and data.

3.2 NORFOLK HARBOR

The following pages discuss the harbor itself, including: (a) the geographic location, (b) the overall configuration of the harbor, (c) current and proposed dredge depths, and (d) berthing facilities for CVN-class vessels.

3.2.1 Geographic Location. The Norfolk Harbor is located in the vicinity of the confluence of the James and Elizabeth Rivers, as illustrated in Figure 3-1, Norfolk Harbor Orientation. Naval vessels enter the Hampton Roads via the entrance reach from Chesapeake Bay, the Newport News Channel, or the Norfolk Harbor Reach.

3.2.2 Overall Configuration. The Norfolk Naval Station is located at Sewells Point. It includes all piers and slips on Sewells Point or approaches to the Point between Pier 12 and

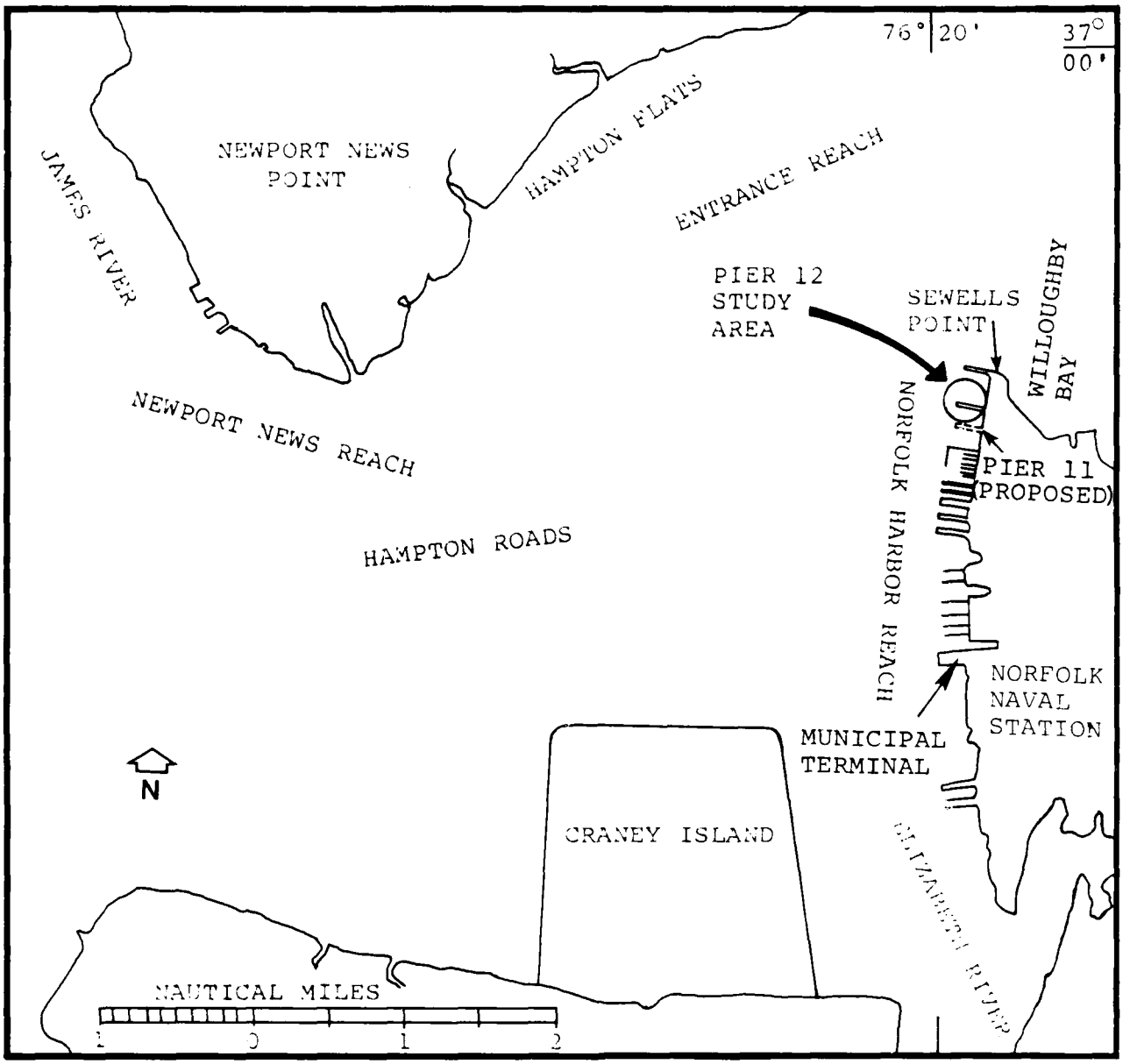

Figure 3-1

Norfolk Harbor Orientation

the Municipal Terminal to the west, and a small craft basin in Willoughby Bay. The study area for this project is within the Pier 12 berthing area.

3.2.3 Current and Proposed Dredge Depths. The Hampton Roads Entrance Reach, Norfolk Harbor Reach, and Newport News Channels are currently maintained at a depth of 45 ft below Mean Low Water (MLW). A plan to improve these channels by deepening the 45-foot channels to a depth of 55 ft below MLW, has been submitted by the Army Corps of Engineers. [8]

In the proposed Pier 11 and existing Pier 12 berthing areas, the Norfolk Naval Base is preparing a project for dredging the berthing depth of carrier berths to 50 ft.

3.2.4 CVN Berthing Facilities. The present berthing facilities for CV and CVN vessels (aircraft carriers) at Norfolk Harbor consists of slips at Pier 12...with occasional berthing at Pier 7. [4] Additional carrier berthing will be provided by Pier 11, proposed for construction adjacent to Pier 12 during 1982-1983.

3.3 HYDROLOGIC CONDITIONS

The hydrological conditions at the Chesapeake Bay/James River Estuary for the present study were divided into two categories: the average condition, and the extreme condition.

3.3.1 The Average Condition. The average hydrological conditions of the Chesapeake Bay/James River have been reported by previous investigators. [3] [9] The reported hydrological data include water depth, tidal current, wind, water temperature, and salinity for various locations throughout the James River Estuary. These existing data comprised the basic hydrologic information used in the physical model study.

3.3.2 The Extreme Condition. The extreme hydrologic conditions of the Chesapeake Bay/James River occur when a hurricane sweeps through the area. Existing reports describe various extreme conditions. [10] [11] [12] [13] Hurricane Connie, for example, precipitated from 5 to 6 inches of rainfall in 1955, causing up to 4.5-foot storm surges near Hampton Roads.

> Selected typical extreme conditions of the proposed Pier 11 and existing Pier 12 berthing sites are treated in detail in another related HRS study which concentrates on offboard solutions to the fouling problem.

3.4 HYDRAULIC CONDITIONS

The two key parameters of estuarine hydraulics are: (a) the velocity of tidal currents, and (b) the tidal circulation patterns.

3.4.1 Current Velocity. Preliminary information on Norfolk Harbor surface and bottom currents is scarce. However, one field study [14] reported a current velocity of more than 1 knot near the bottom off Sewells Point, and less than 0.5 knots in the access channel off Pier 12.

As for the Newport News Channel, the report stated that the currents do not always follow the channel, and the average velocity in mid-channel at strength of flood or ebb is about 1.5 knots. Information on the velocity near Pier 12 (the north side) indicated that the bottom and surface currents rarely exceed 0.2 knots.

Because of the nominal current within the berthing area, zero current velocity was assumed for the underkeel clearance study.

3.4.2 Circulation Patterns. The circulation in Hampton Roads is not identical for flood and ebb tides. According to Neilson and Boule, [15] the flood tide predominates over Hampton Flats. The flow up the James River turns sharply around Newport News Point. The flow toward the Elizabeth River divides into two streams -- some of the flow moves to the west just north of Craney Island, and the remainder moves into the Elizabeth River proper. Eddies are believed to form in the lee of both Sewells Point and Craney Island during flood tide.

Neilson and Boule [15] also reported that during ebb tide, the flow down the James River is directed toward the shoreline south of Sewells Point. The early flood in the Elizabeth River and late ebb in the James River occur at the same time. The flow towards Sewells Point, therefore, branches into two streams: The first stream entering the Elizabeth, and the second stream moving out of the river mouth.

3.5 BOTTOM SOIL CONDITIONS

Sediments dredged from within Pier 12 berths range from silt to coarse clay, and are probably the result of the flocculating* of suspended sediment and the bedload sediment movement from the rivers flowing into Hampton Roads. [4] The sediment characteristics in the study area and other harbors are reported elsewhere. [16] [17] [18] [19] [20] These sediments are further discussed in the following paragraphs.

3.5.1 Soil Classification. The predominant sediment type within Pier 12 consists of silts and clays (mud). Four sediment samples collected in Pier 12 had median particle sizes of 5.5, 6.2, 6.3, and 7.0 microns -- therefore comprising a medium- to fine-silt sediment.

---

* Flocculating -- The collection or uniting of suspended sediment to form a mass.

3.5.2 Sediment Composition. A survey of the sediment at both slips of Pier 12 [6] revealed four basic sediment compositions at the site:

- Black homogeneous mud, smooth when rubbed between the fingers, and of the consistency of pudding. From 30 to 35% solid by weight.
- Coarse medium-brown sand, containing shell fragments. Comprised 76% solid by weight.
- Black clay and sand mixture, containing shell fragments. Comprised 56% solid by weight.
- Gray mud, containing fine sand grains. Comprised 44% solid by weight.

3.6 THE "FOULING" MARINE ORGANISMS

The bottom-sediment cumulation at the Norfolk Naval Station poses a problem, for it is expensive to dredge. However, the clogging of aircraft-carrier circulating cooling systems by marine organisms poses an even greater problem.

The following paragraphs summarize the characteristics of the marine organisms. More complete information has been included in Appendix A of this report.

3.6.1 Species Involved in Fouling Problems. The specific sea-chest fouling organisms identified in the Norfolk Harbor include the hydroid Sertularia argentea and the bryozoan Alcyonidium verrilli. Photographs of actual samples of each from Norfolk Harbor appear as Figures 3-2 and 3-3. At Pier 12 the hydroid is believed to contribute from 90 to 95 percent of sea-chest fouling problems. The remaining 5 to 10 percent of the fouling problems involve the bryozoan. [2] [10] Both the hydroids and the bryozoans move in the lower portion of the water column and have densities ranging from 1.03 to 1.15.

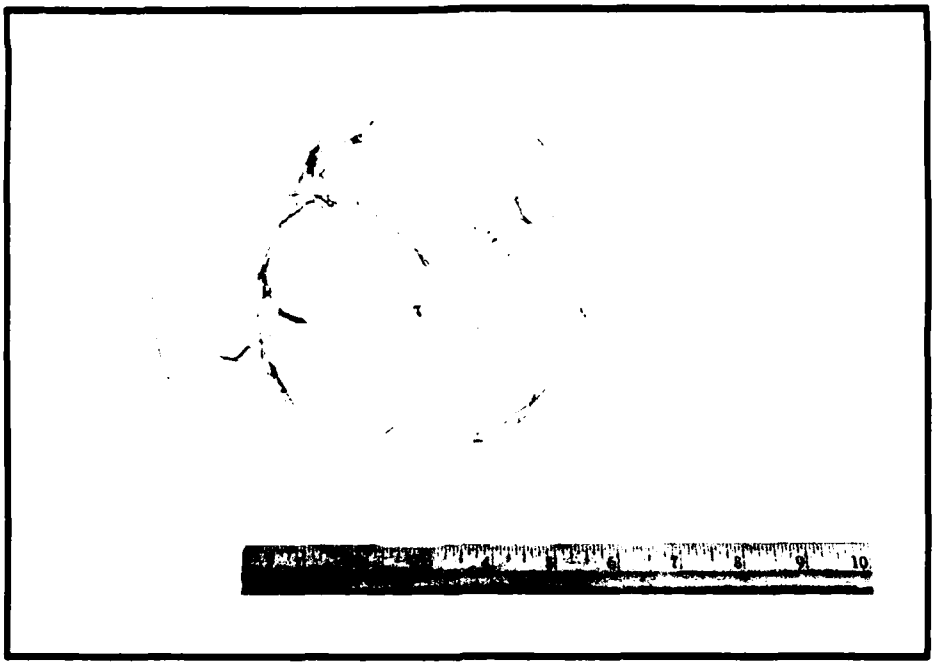

Figure 3-2
Photo of Hydroids from Norfolk Harbor

Figure 3-3
Photo of Bryozoans from Norfolk Harbor

3.6.2 Seasonal Growth Patterns. The hydroid is composed of colonies ranging from 10 to 12 inches high, with multiple branches. It is a "winter species" which achieves peak growth from November to February. Branches and side branches tend to break off during winter storms and are carried away by the current. Such branches continue to grow after separation from the parent colony. [2]

3.7 VESSEL-RELATED PARAMETERS

The remainder of this section of the report is concerned with the vessel-related parameters critical to understanding the reported CVN sea-chest fouling problems.

3.7.1 Vessel Circulating Water Systems. The current study concentrated on fouling problems associated with the two primary CVN-class seawater circulating water systems: (1) the Main Circulating Water system, and (2) the Service Generator (SG) system.

3.7.2 Sea-Chest Discharge Flow Rates. The pumping capacity of the circulating cooling systems of the subject aircraft carrier* ranges from 3,450 to 25,000 gallons per minute (gpm). Within the scope of the present study, the 25,000-gpm flow rate of the main circulating system and the 5,890 gpm of the service generator system, comprised the variables under investigation.

3.7.3 "Assumed" Operating Ranges. For the purposes of this study, the operating ranges of the circulating cooling systems were divided into three pumping rates. These "assumed" operating ranges consisted of 100, 80, and 35 percent of full-operating capacity.

---

* The Naval aircraft carrier used as the "model" for this study was the USS Dwight D. Eisenhower (CVN 69).

3.7.4 Light Off Operations. During "light off" operations, the service generators pump at full capacity. The main circulating system may, however, be operated at lower rates such as 10 or 20 percent of full capacity.

3.8 BERTHING-RELATED PARAMETERS

The following pages summarize the primary berthing-related parameters associated with the sea-chest fouling problems of CVN vessels in Norfolk Harbor.

3.8.1 General Orientation of a Berthed Vessel. To provide a basic point of reference, the orientation of a capital ship at berth is illustrated in Figure 3-4, Sectional Orientation of a Capital Ship at Berth.

3.8.2 Operating Load Drafts. The maximum operating load drafts of Naval aircraft carriers is reported to range from 37 to 40 ft. [4] The load draft, in turn, relates directly to the underkeel clearance for a given berthing location.

3.8.3 Underkeel Clearance. The circulating cooling system sea chests of Naval aircraft carriers are located on the underside of the vessel. In the case of an operating load, draft of from 37 to 40 ft in a berthing position or channel with a 45-foot depth (the current condition)...only 5 to 8 ft of underkeel clearance exists at low tide.

The suction and discharge openings of the sea chest must, in turn, operate within the current 5- to 8-foot underkeel clearance.

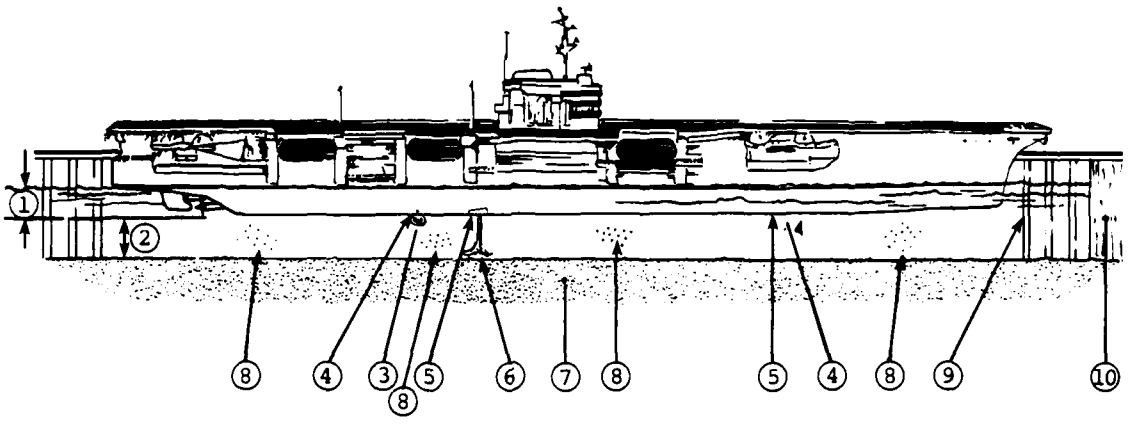

LEGEND

1 Draft
2 Underkeel Clearance
3 Typical Zone of Withdrawal
4 Suction Sea Chest
5 Discharge Sea Chest
6 Typical Discharge Action
7 Deformable Material Berthing Bottom
8 Marine Organisms
9, 10 Peripheral Confinement

Figure 3-4

Sectional Variation of a Capital Ship at Berth

This study investigated several underkeel clearances using an assumed average draft of 39 ft, including: (a) a 5-foot clearance corresponding to the existing average Pier 12 CVN berthing depth of 44 ft, (b) a 13-foot underkeel clearance corresponding to the proposed dredged depth of 50 plus 2-foot overdredge, and (c) a 21-foot underkeel clearance corresponding to a hypothetical lower depth limit of 60 ft for experimental purposes.

4.0 The Analysis

4.0 THE ANALYSIS

Extensive state-of-the-art physical modeling procedures were utilized to analyze the sea-chest fouling problem. This section of the report consists of a "less technical" summary of the modeling procedures utilized to analyze the problem and then identify and refine the most promising onboard solutions.

> More detailed information on this aspect of the study has been included in Appendix B of this report.

4.1 THE PHYSICAL MODEL

4.1.1 The Berthing Tank. A platform was constructed and installed in the permanent HRS Berthing Tank. To aid the reader, a photo of the Berthing Tank appears as Figure 4-1.

Precision-constructed scale models* of the selected CVN-class service generator (SG) and main circulating (MC) cooling system were then placed in the tank and fully instrumented for experimental purposes. The tank bottom was filled with sized walnut-shell grains to simulate mud and algae to simulate marine organisms, and a dye probe was installed in the recirculating system to enable observation of the flow patterns.

4.1.2 The Sea Chest Models. Two pairs of SG cooling system intake and discharge openings and one pair of the main circulating system openings were modeled. The underkeel clearance for preliminary tests was first set at 21 ft and later set at 5 and 13 ft. A schematic layout of the modeled sea chests is detailed in Figure 4-2. A photo of the sea chest model appears as Figure 4-3.

---

* Models were constructed per the dimensions of CVN 69, the "model" for this study.

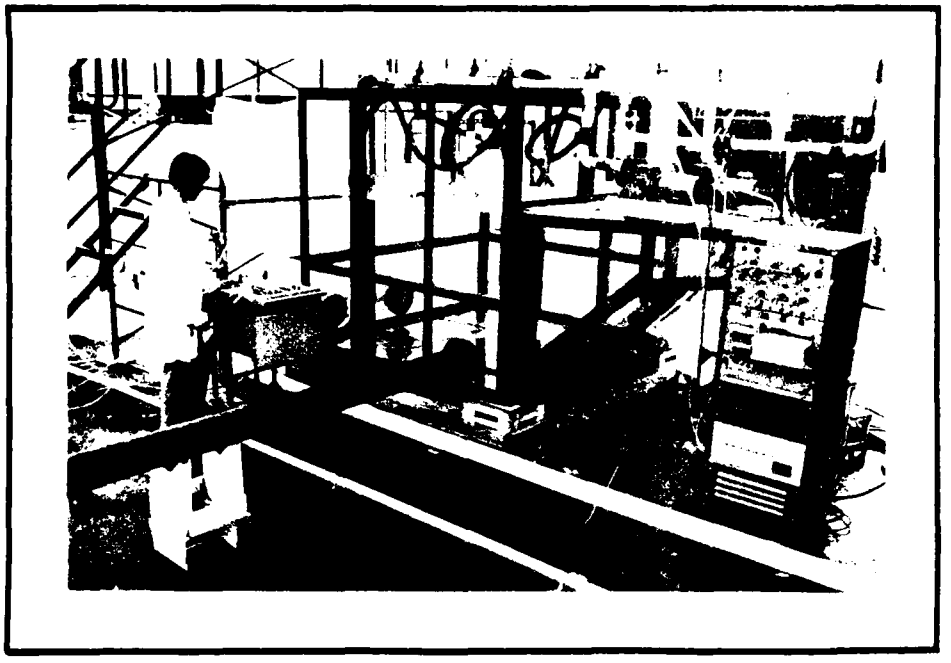

Figure 4-1
HRS Berthing Tank

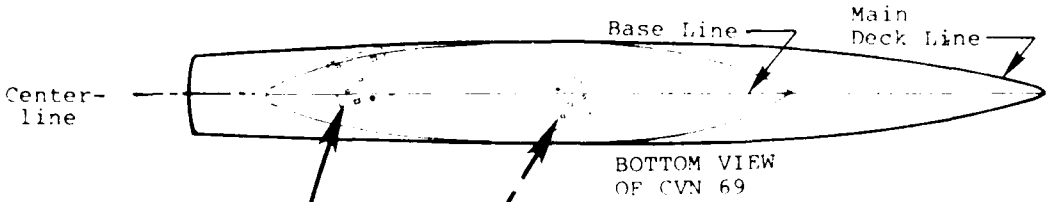

DIMENSIONS OF MODELED AFT OPENINGS
OF CVN 69 /ESSEL

Number	Service Description	Dimension (Inches)
41	#4 Main Circ. (MC) Suction	42+13/16 x 28+13/16
43	#4 SG/CG Sea-water Suction	38+5/8 x 31+7/8
45	#4 SG/CG Sea-water Discharge	16 DIA
46	#4 Main Circ. Discharge	69+13/16 x 46+13/16
53	#3 SG Seawater Suction	37+1/8 x 30+3/8
57	#3 SG Seawater Discharge	16 DIA

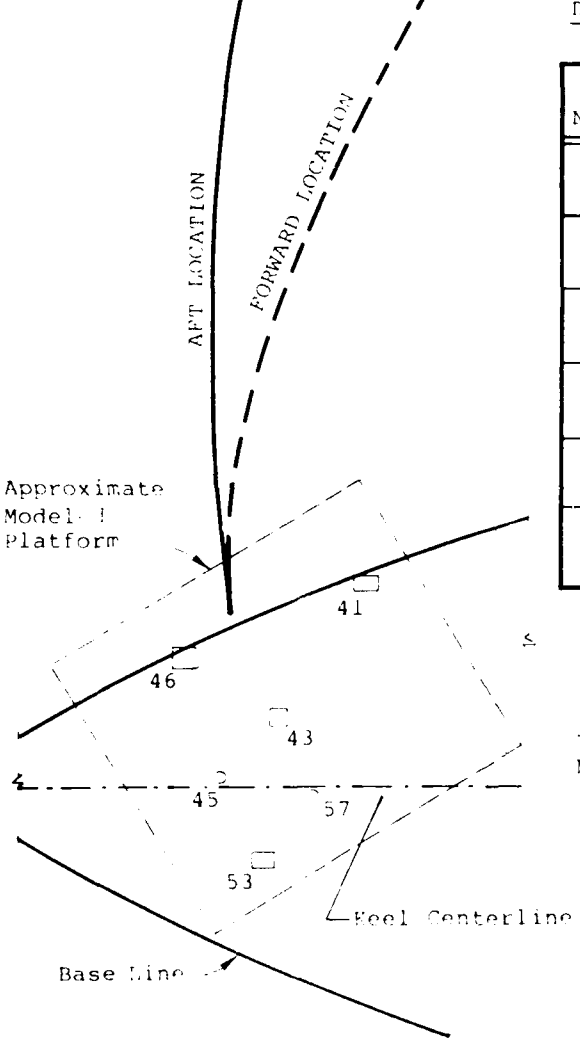

DETAIL VIEW OF MODELED PLATFORM

Note: Forward and aft opening locations are symmetrical

Figure 4-2

Layout of Modeled Sea Chests

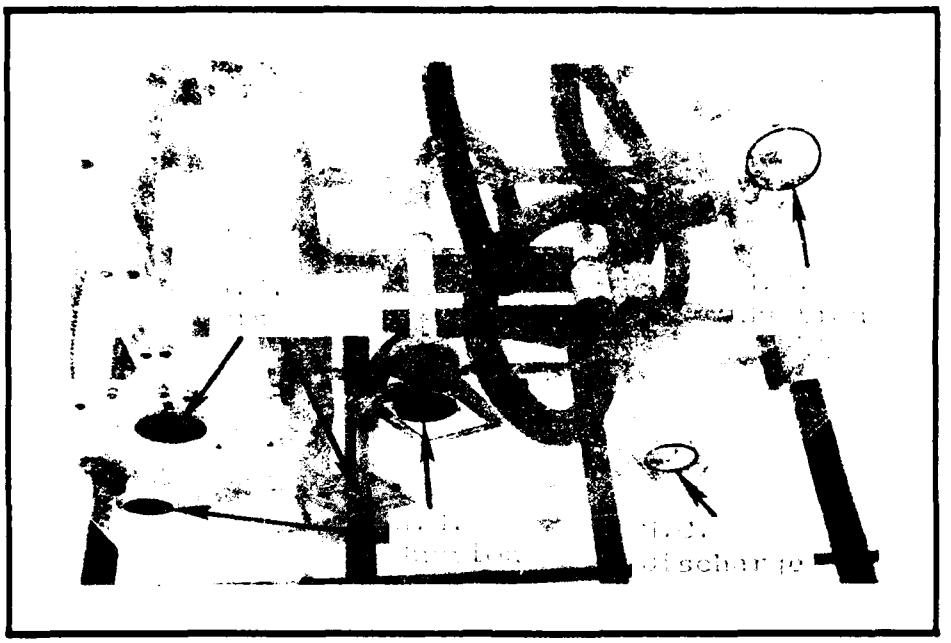

Figure 4-3
Sea Chest Model

4.2 THE PRELIMINARY ANALYSIS

Prior to conducting an extensive physical-model experimentation, a problem-oriented preliminary analysis was performed. The results are summarized on the following pages.

4.2.1 Suction Operations. Preliminary tests of the SG condenser unit suction were conducted with a flow rate of 5,890 gpm. Very little activity was observed near the suction sea chest. The influence zone was limited to the vicinity of the suction sea chests.

The velocity at the immediate area (within 1 foot) surrounding the suction opening was found to be 1.2 ft/sec. The decrease of velocity with distance was very noticable. Within a 4-foot radius, the velocity dropped to 0.2 ft/sec.

The tests indicated that suction action alone was not the major cause of the sea-chest organism fouling. A typical velocity distribution at the suction sea chest is shown in Figure 4-4.

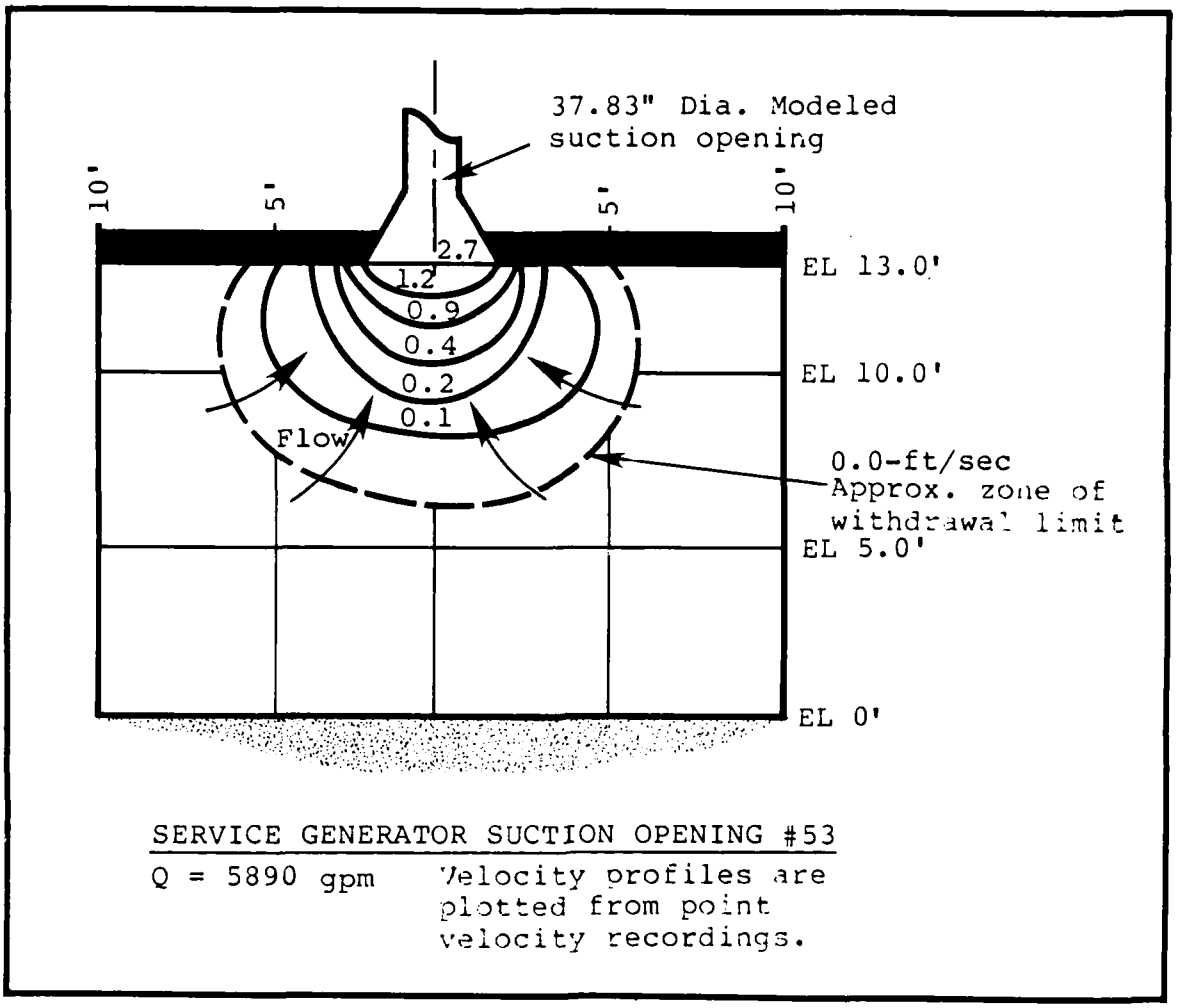

Figure 4-4
Typical Velocity Distribution at the Suction Sea Chest

Observations were also made at the main circulating system suction sea chest. Similar phenomena were observed, leading to the conclusion that the suction action, by itself, did not pose a serious sea-chest fouling problem.

4.2.2 Discharge Operations. Observations of the discharge sea-chest operations were made on a pair of service-generator condenser units (suction and discharge) with a flow rate of

5,890 gpm. Test results revealed that a very strong jet flow, shooting downward from the sea chest, penetrated deep into the surrounding water, impinged on the sea floor, and caused substantial disturbance to the bottom material.

This jet action resuspended the bottom particles, dispersing them into the surrounding environment. Part of the suspended material floated upward and was carried by the circulation current. As such floatages approached the suction influence zone, the suction action pulled the particles into the sea chest inlets. It was therefore concluded that:

The jet is the primary causal factor behind organism-fouling of sea chests.

In order to ensure clear understanding of these jet and scour processes, the following pages detail the HRS analyses of: (1) the jet impinging on a solid boundary, and (2) the jet impinging on a movable boundary.

4.3 ANALYSIS OF JET IMPINGING ON A SOLID BOUNDARY

Experiments were conducted on both the SG cooling system and the main circulating system. The following pages detail the experimental results.

4.3.1 The Service Generator (SG) Discharge. The SG discharge sea chest has circular cross sections. The SG jet velocity profile, therefore, tends to be axisymmetric about the centerline of the circular pipe, and results in a symmetric flow field under the sea chest.

A photograph of the circular jet patterns created by the SG system appears as Figure 4-5. The SG discharge velocity distribution measurements for a flow rate of 5,890 gpm indicated that the maximum exit velocity V_o at an elevation of 13 ft above the solid bottom was 10.5 ft/sec. The maximum

velocity at an elevation of 5 ft was determined to be 7 ft/sec. At 2 ft from the jet centerline near the solid boundary, the radial velocity was 4.5 ft/sec -- which can move 1/2-inch-size medium gravel on a noncohesive sand bed.

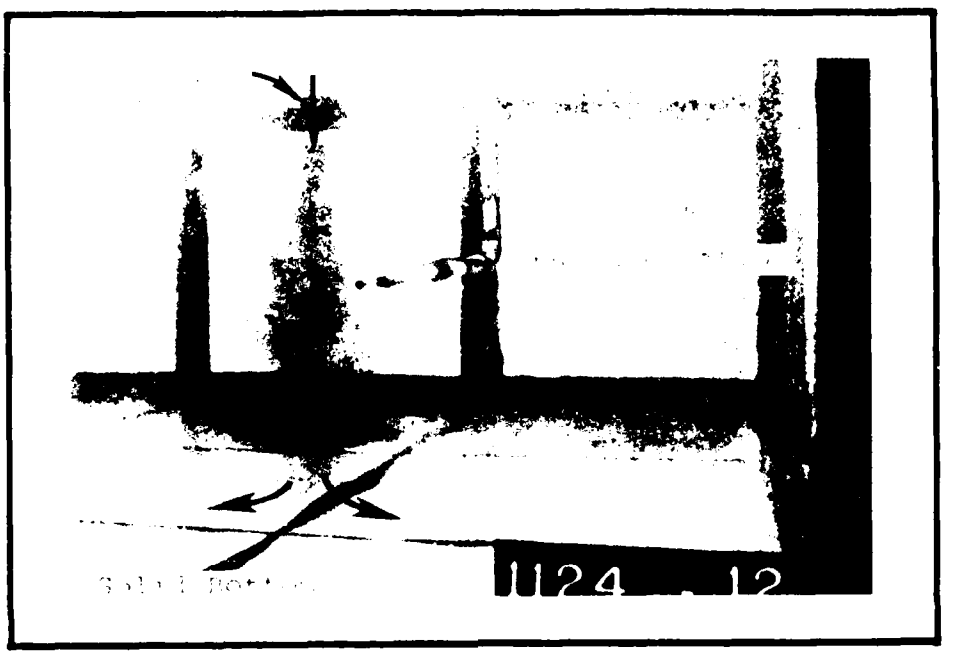

Figure 4-5
SG Circular-Jet Patterns

4.3.2 The Main Circulating System Discharge. The main circulating system discharge creates an elliptical jet pattern. For the main circulating system discharge sea chest at full capacity of 25,000 gpm, the maximum exit velocity V_o was 6.6 ft/sec at an elevation of 13 ft above the solid bottom. The maximum axial velocity was 4.7 ft/sec at an elevation of 5 ft above the solid bottom. At 7.5 aft of the vessel, the radial velocity near the solid bottom was approximately 2.5 ft/sec, which can move fine gravel of a size up to 0.2 inch on a noncohesive sand bed.

A photograph of the elliptical jet patterns produced by the main circulating system appears as Figure 4-6.

The main circulating system discharge sea chest was also tested with a reduced flow rate of 20,000 gpm (80%) and 8,750 gpm (35%). The maximum exit velocities were 4.70 ft/sec and 2.32 ft/sec, respectively, and the maximum bottom radial velocities were 2.15 ft/sec and 1.01 ft/sec.

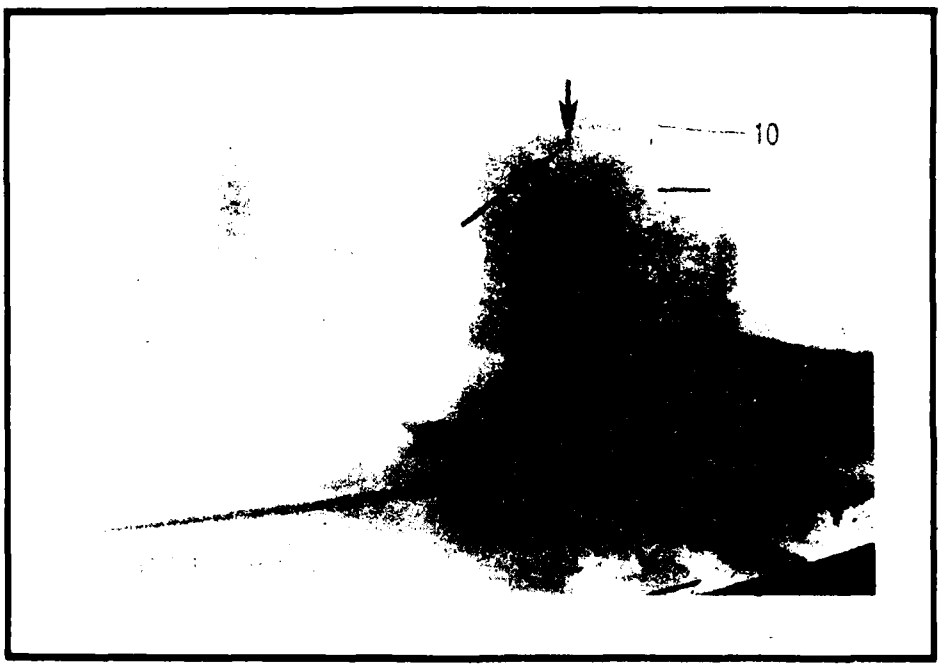

Figure 4-6
Main Circulating System Jet Patterns

Detailed velocity distributions for both SG and Main Circulating Systems are included in Appendix B of this report.

4.4 ANALYSIS OF JET IMPINGING ON A MOVABLE BOUNDARY

To date, there has not been a clear understanding of jet erosion mechanisms on movable boundaries. Few investigations of jet erosion have been conducted. [22] [23] [24] [25] None of the studies reported conclusive findings on jet erosion mechanisms, nor did they report velocity distributions. To

gain an understanding of the erosion mechanism and the flow field in the vicinity of the scoured area, a test program of jet impingement onto a movable boundary was conducted.

4.4.1 Movable Boundary Test Variables. This test program was conducted to observe the effects of circular jet impingement on the sea bottom. Materials used in the study included sand (to simulate sand) and walnut shell grains (to simulate mud). The underkeel clearance was set at 13 ft, with a flow rate of 5,890 gpm.

4.4.2 Jet Impinging on Sand Bottom. Tests of the jet impinging on sand showed that the jet eroded the bottom sand outward, resulting in a scour hole with the bottom about 15.5 ft below the discharge opening. The velocity at 11 ft below the discharge opening was found to have a magnitude of 52% of its original strength. At 15 ft below the discharge opening, the velocity still maintained 32% of its original strength. The radial velocity at 13 ft below had a magnitude of about 3 ft/sec, which is capable of moving 0.4-inch gravel.

A photograph of the effect of the jet impingement on a sand bottom appears as Figure 4-7, Typical Sand Bottom Scour Effects.

4.4.3 Jet Impinging on Mud Bottom. The jet impinging on mud is a dynamic process. Tests showed that the jet dug down into the bottom layer, resulting in a scour hole about 16 ft below the discharge opening. The mechanism of jet impinging on mud bottom is discussed in Appendix B, Paragraph B.5.2.4. The velocity measurement revealed that at 11 ft below the discharge opening, the jet still possessed 54% of its original strength. However, a measurement at 14 ft below showed the velocity to be only 20% of the original strength. Figure 4-8 shows the typical mud bottom scour effects.

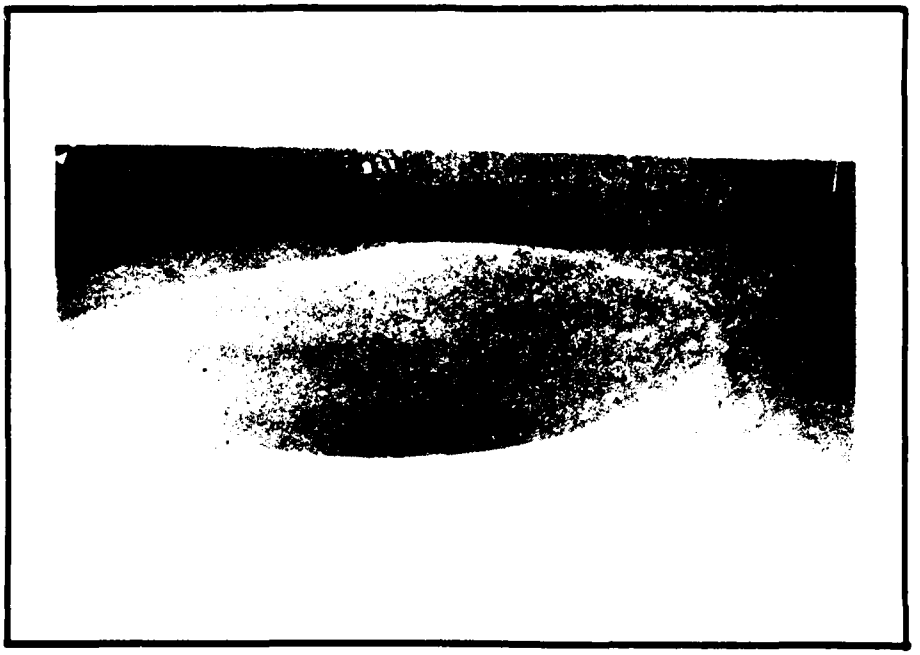

Figure 4-7
Typical Sand Bottom Scour Effects

Figure 4-8
Typical Mud Bottom Scour Effects

4.5 MOVABLE BOUNDARY WITH MARINE ORGANISMS

4.5.1 Hydrodynamic Properties of the Organisms. To ensure that the hydrodynamic properties of the marine organisms were properly treated in the physical-model study, HRS contracted with Virginia Institute of Marine Sciences (VIMS) to study selected properties of each of the species. Performed by Dr. Robert Diaz, the study produced the key results as summarized in the following paragraphs:

- The initiation of motion for live hydroids requires a velocity of about 0.05 to 0.11 feet per second (fps). For live bryozoans, a velocity of 0.34 to 0.41 fps will move the species. As to the mixture of live and dead colonies, the required velocities are 0.15 fps for hydroids, and 0.30 fps for bryozoans.
- The fall velocity of hydroids ranges from 0.02 to 0.12 fps for live colonies, and 0.09 to 0.39 fps for dead colonies. The fall velocities are from 0.21 to 0.29 fps for live bryozoans, and from 0.09 to 0.21 fps for dead bryozoans.

4.5.2 The Marine Organism Test Variables. Green algae were used to simulate the transport properties of the hydroids for visual perception and qualitative assessment. The algae were arranged in the test setup so that a portion was implanted into the bottom walnut-shell layer, and a portion was suspended in the water, simulating the sea-bottom environment. A collection device for the algae was placed at the middle section of the simulated suction pipeline. This collection device consisted of a circular conduit section, with several layers of screen baffle spaced inside the conduit as interception mesh.

A test of the service generator discharge jet was conducted using a 13-foot underkeel clearance. In the test the jet flow dug into the bottom layer, disturbing the buried algae. The algae were then lifted and carried by the flow. Those carried into the region of influence of the suction sea chest subsequently disappeared into the suction pipelines.

Test results revealed that: (a) at 5,890 gpm, 12.5% of the algae was insufflated, (b) at a pumping rate of 4,800 gpm, about 9% of the algae was ingested, and (c) at the much lower pumping rate of 2,100 gpm, only 2% of the algae was ingested. A photograph of the marine organism movable boundary test appears as Figure 4-9.

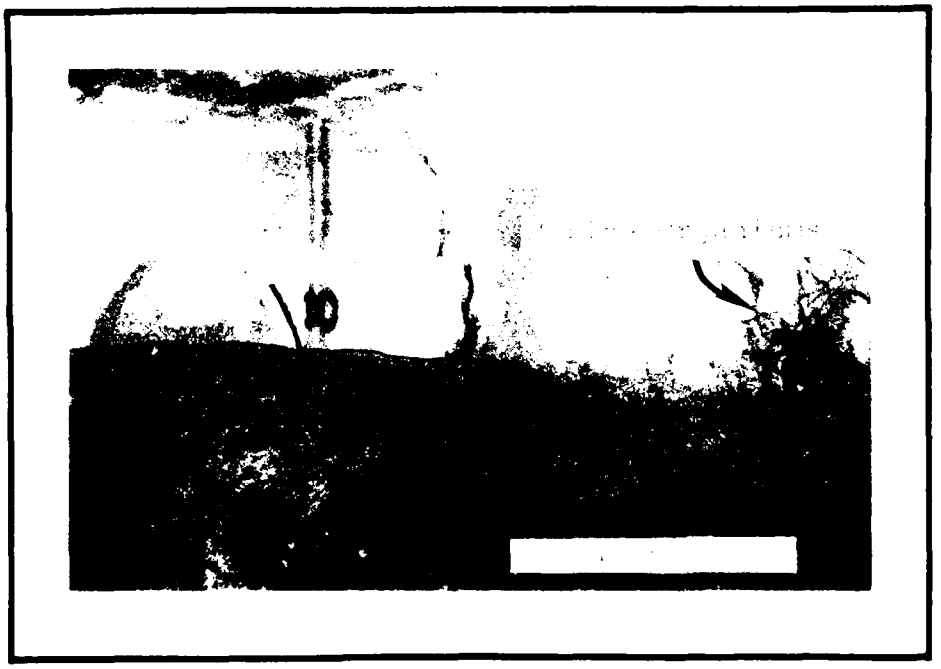

Figure 4-9

Resulting Scour Patterns from
One Pair of SG Cooling System Openings

A test was also conducted for the operation using two pairs of service generator openings (intake and discharge) and one pair of main circulating system openings with a 13-foot underkeel clearance. The results revealed an ingestion of about 11% of the algae into one of the service generator suction lines.

It was therefore concluded that even with the berthing area dredged to 50 ft, the fouling problem will still occur.

4.6 CONCLUSIONS FROM MOVABLE-BOUNDARY TESTS

The following conclusions were drawn from the results of the previously-cited movable-boundary tests:

- The discharge jet impinging on a movable boundary is a dynamic process which results in scouring of the bottom material.
- This scouring action only exists locally, and reaches an equilibrium condition such that the perpetuating eddie flow is contained within the scoured area.
- The disturbance of the bottom layer caused by the discharge jet scouring results in the sea-chest fouling problem.

5.0 The Numerical Model

5.0 THE NUMERICAL MODEL

The objective of this phase of the study was to develop a state-of-the-art numerical model relating the underkeel clearance of an aircraft carrier to the dynamics of sea-chest flow fields and the related berthing floor behavior.

5.1 OVERVIEW

The scope of this phase of the study encompassed:

- Conducting a general compilation and analysis of: (a) the physical model results, and (b) the mathematical formulations for the relevant fluid mechanics phenomena (suction and discharge flow patterns within various fields of confinement).
- Developing the algorithm for the numerical model and coding the computer program intended to satisfy the study objectives.
- Performing validation tests of the numerical model.
- Documenting the numerical model study and developing a User's Manual.

5.2 THE DATA COMPILATION

Physical-model data on both suction and discharge jet were compiled. The data on velocity, pressure, and shear stress were then tabulated and compared with other investigator's findings [26] [27] [28] [29]. Major attention was focused on the discharge jet data, as the jet was identified as the main driving force behind the fouling problem.

5.3 THE ALGORITHMS

The algorithms used to develop the working numerical model included both suction and discharge jet simulations. These algorithms are discussed in the following paragraphs.

5.3.1 Suction Simulations. A finite difference model was developed to predict the suction flow field. The fluid was assumed to be inviscid, incompressible, and irrotational. After defining the governing equations and boundary conditions, a finite difference form with the successive over-relaxation (S.O.R.) method was developed to calculate the velocities at any point confined under the keel.

> Detailed information related to the development of the formulation and its associated boundary conditions is included in Appendix C of this report.

5.3.2 Discharge Simulations. The flow field resulting from the jet discharge posed a very complicated problem. There are no existing, related general mathematical formulations. The present simulation of the jet discharge based upon HRS physical-model results is, however, in good agreement with the results of previous investigations. [26] [29]

Two very different bottom-boundary conditions were studied: (a) fixed (flat) boundary, and (b) movable boundary. The fixed-boundary numerical model of the discharge jet simulated the flow field velocities, the bottom pressure, and the bottom shear stress. The movable-boundary numerical model simulated the flow field velocities related to the underkeel clearances.

5.4 NUMERICAL VS PHYSICAL MODEL RESULTS

Figures 5-1 through 5-4 compare numerical-model versus physical-model results related to: jet discharge velocities, suction velocities, bottom pressure, and the bottom stress for fixed boundary.

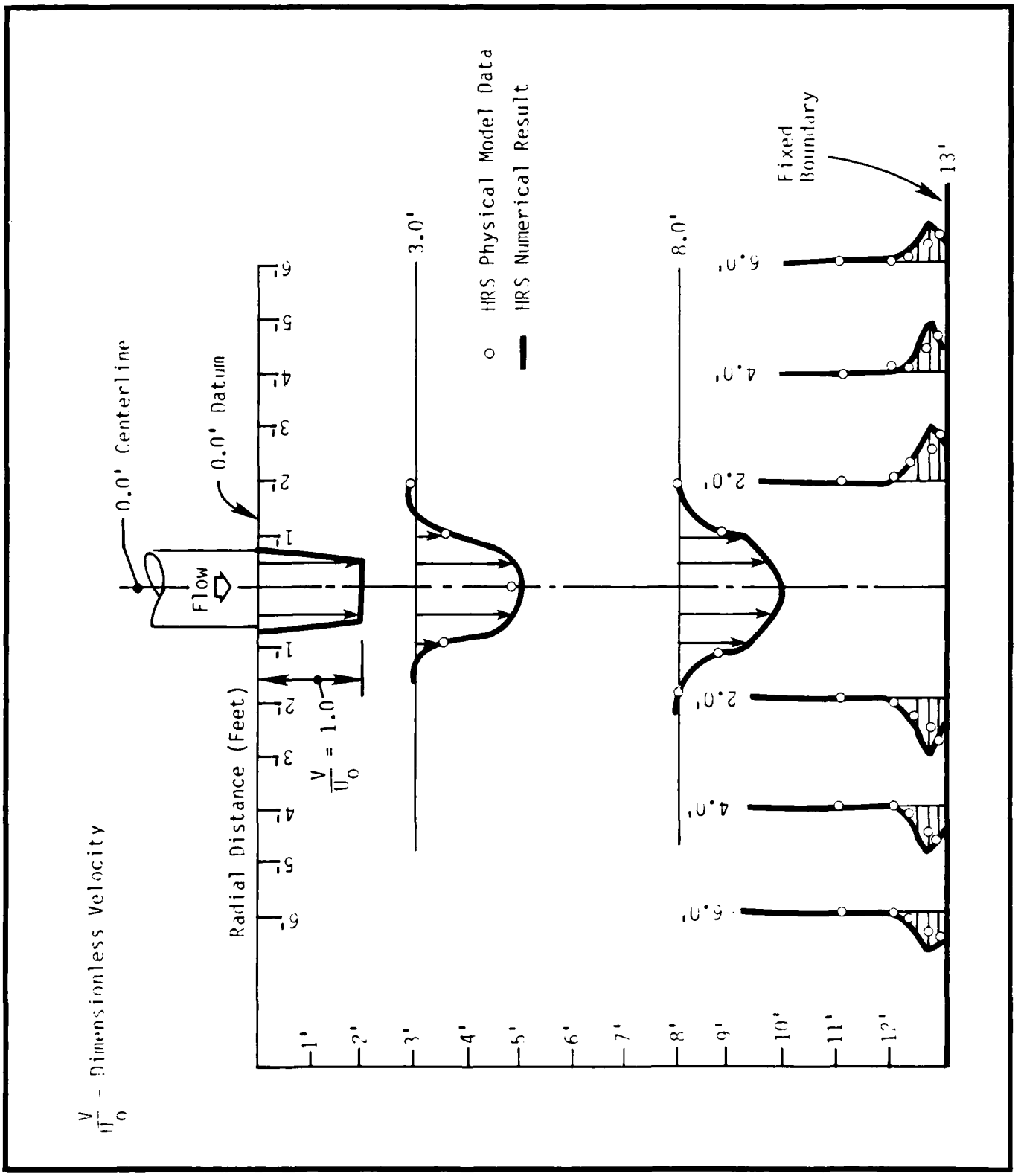

Figure 5-1

Flow Field for the Impingement of a Jet on Fixed Boundary

(Comparison of numerical results with physical model results)

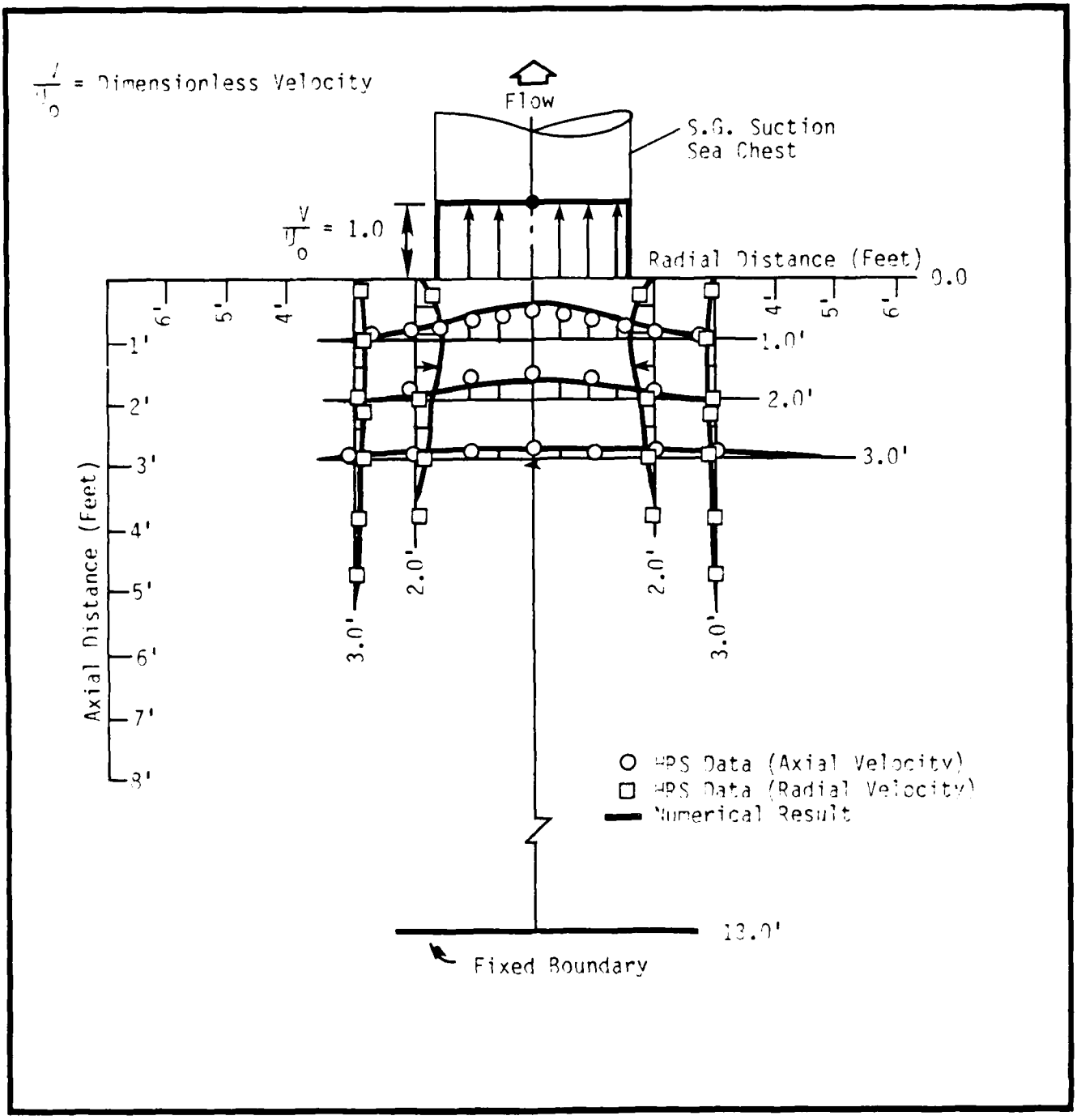

Figure 5-2

Suction Flow Field on Fixed Boundary

(Comparison of numerical results with physical model results)

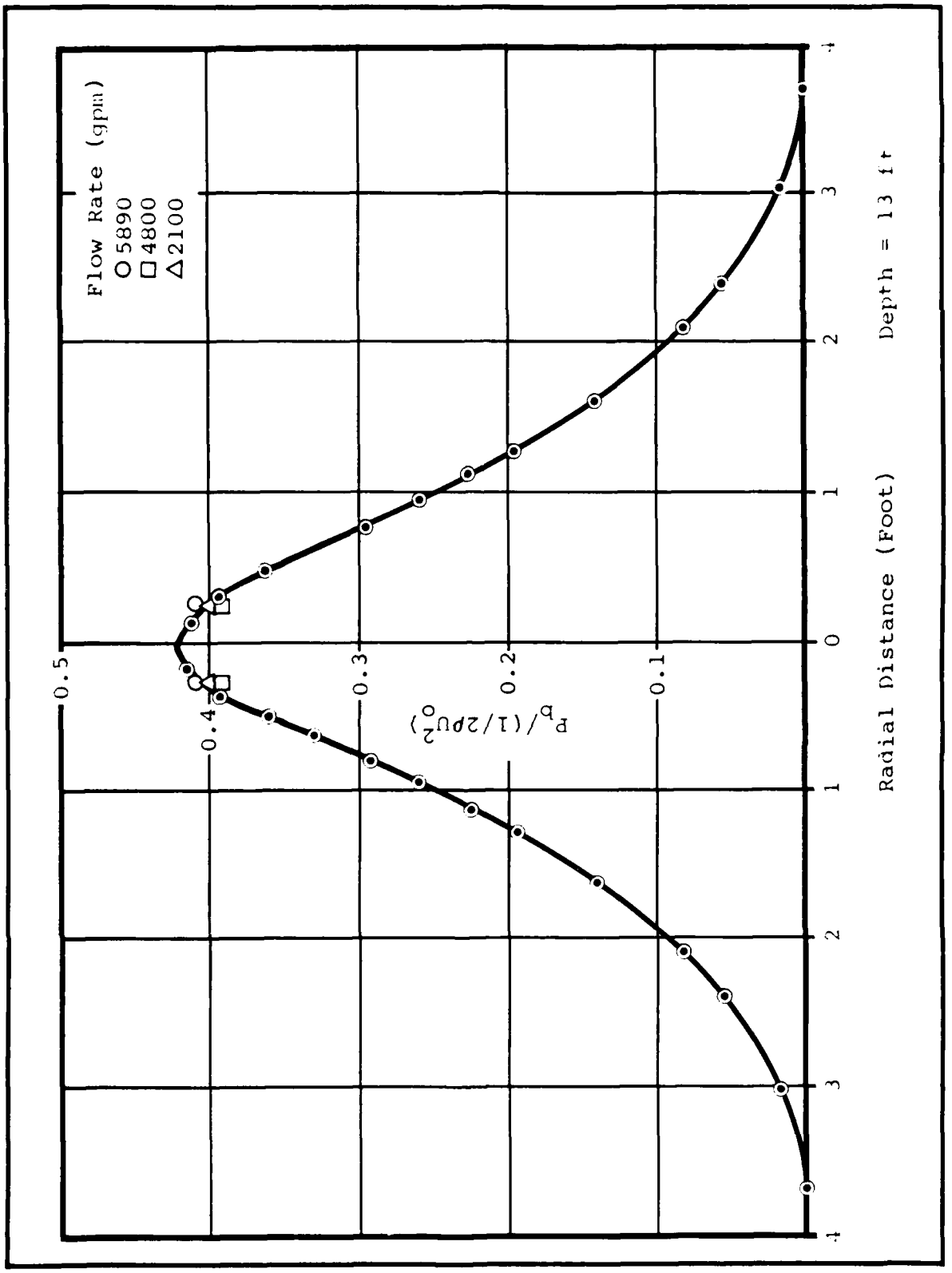

Figure 5-3

Bottom Pressure Distribution for the Impingement of a Jet on Fixed Boundary

(Comparison of numerical results with physical model results)

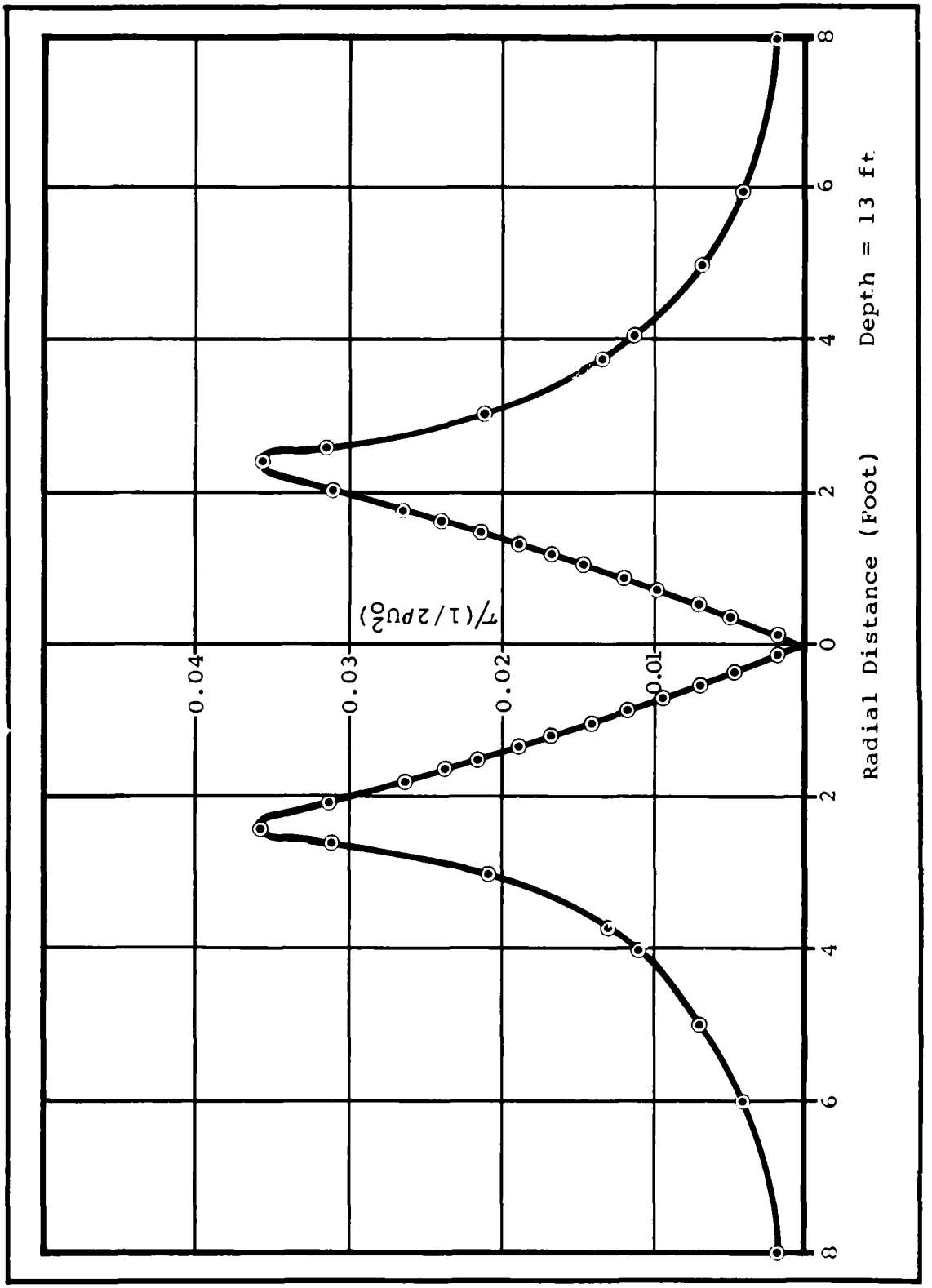

Figure 5-4

Bottom Shear Stress Distribution for the Impingement of a Jet on Fixed Boundary

Figures 5-5 and 5-6 summarize the numerical model for the jet discharge flow field on a movable bottom. Two different simulated bottom materials are represented: (a) mud, and (b) sand. The numerical model results yielded a significant agreement with the physical model results.

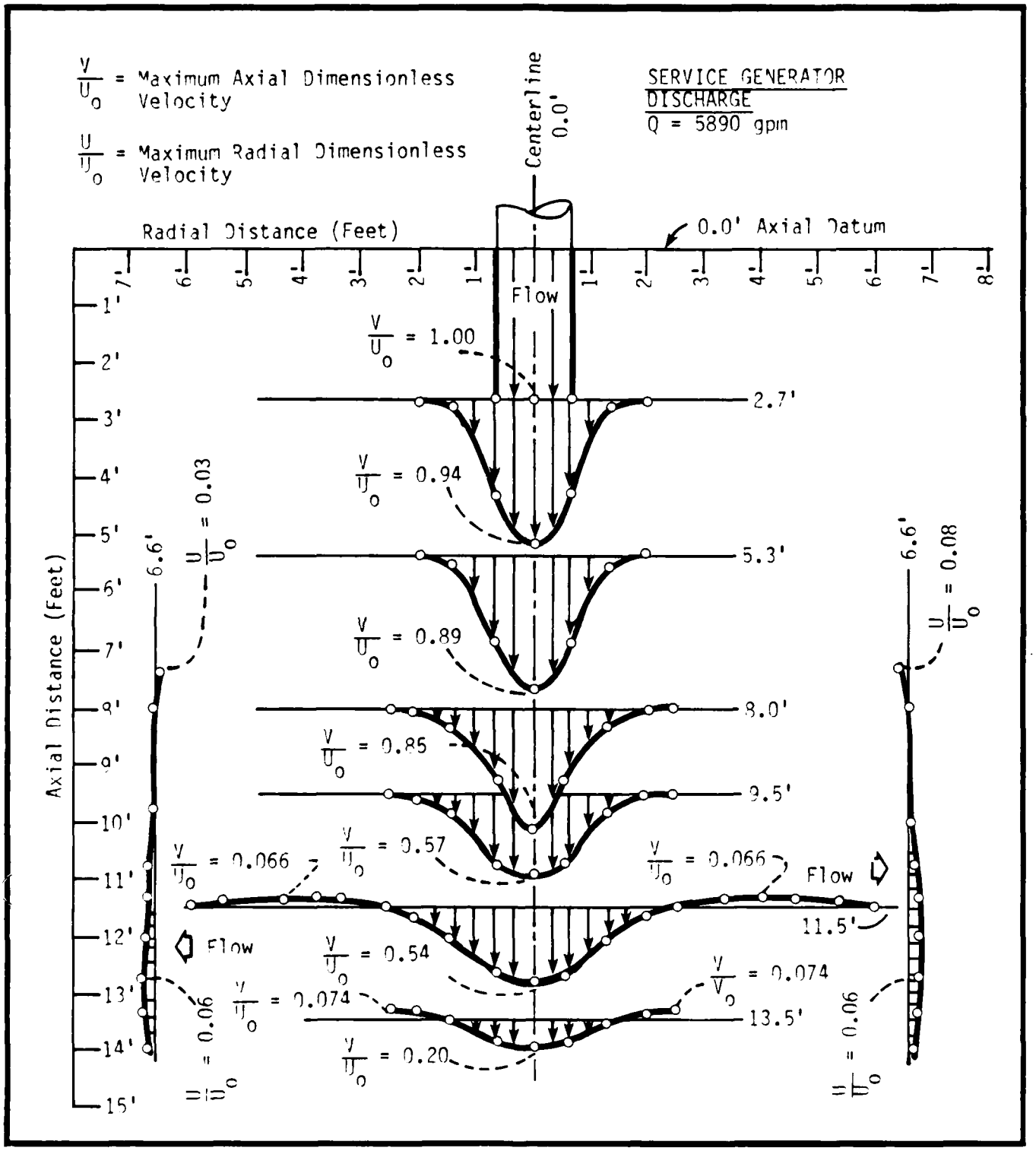

Figure 5-5

Flow Field on Movable Bottom (Mud)

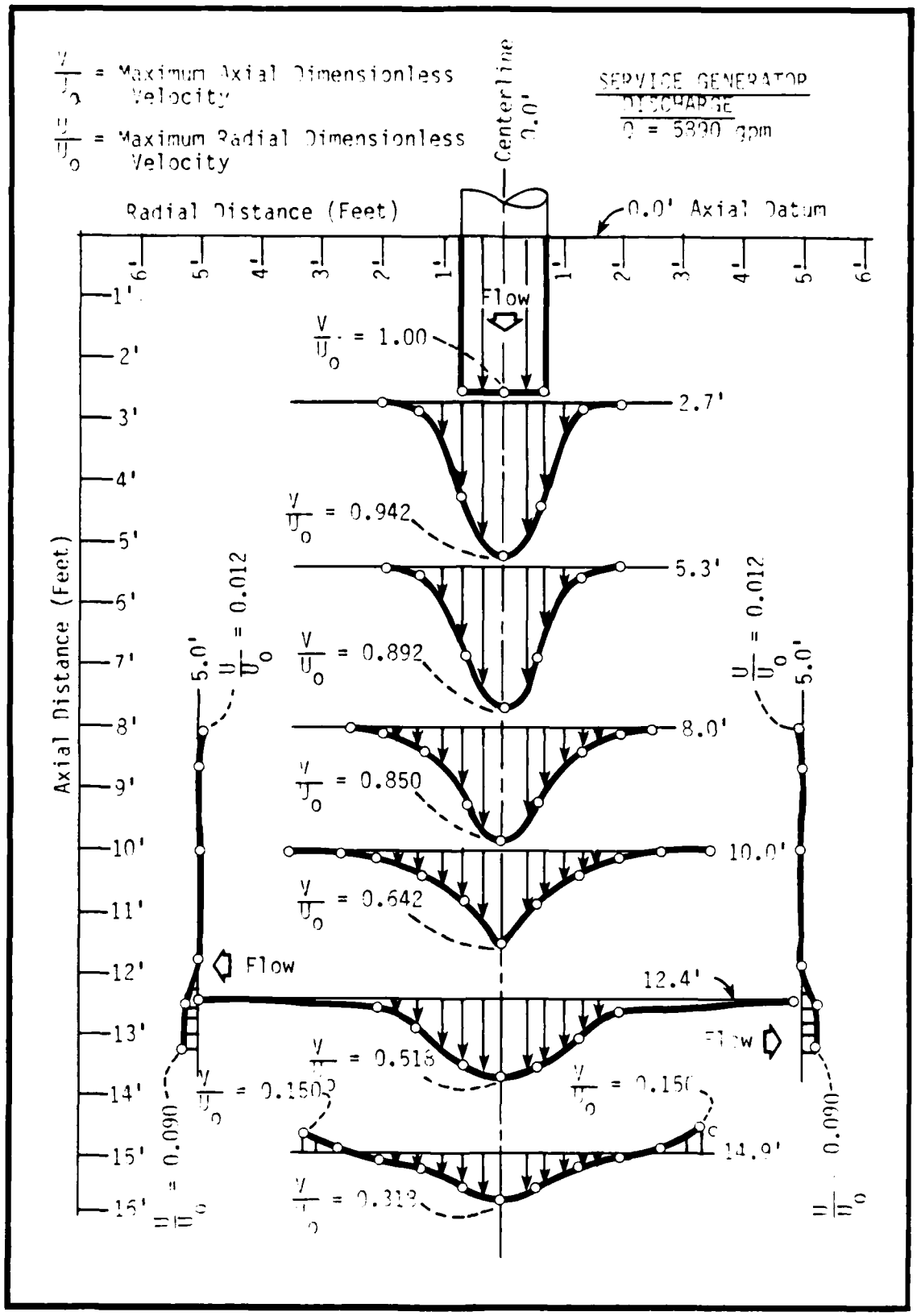

Figure 5-6

Flow Field of Jet on Movable Bottom (Sand)

5.5 APPLICATIONS AND LIMITATIONS OF THE MODEL

For a fixed (flat) boundary, the numerical model provides a means of predicting the jet impingement on: the flow velocities, bottom pressure, and shear stress for jet impingement and suction. The model was developed for the following purposes:

- Judging the stability of the bottom material by comparing the shear stress with the critical shear stress from Shields curve.
- Understanding the influence of underkeel clearance (water depth) as it relates to the impingement of a jet.
- Estimating the volume of bottom material or marine organisms which could be ingested given a specified concentration and distribution of the organisms.
- Determining the jet-center-to-suction-center distance required to reduce the volume of ingested materials.

For the impingement of a jet on a movable boundary the present model is not a general model because of the lack of formulation for mud environment and state-of-the-art difficulties faced in defining a mathematical approach to the problem.

6.0 The Solutions

6.0 THE SOLUTIONS

The analysis of the results of the fouling tests and scour studies indicated that with the original sea-chest configuration, fouling phenomena will occur with each of the three underkeel clearances of 5, 13, and 21 ft. Since sediment buildup can also be expected to create dredging problems, it was concluded that the design of additional control mechanisms would be required to minimize organism fouling and prevent sediment buildup problems. Various solutions can be applied to the aircraft carrier or to the estuary environment to control sediment and organism foulings.

6.1 PRACTICAL SOLUTIONS TO FOULING PROBLEMS

Practical solutions to the fouling problem fall into two categories: (a) onboard solutions and (b) offboard solutions. The onboard solutions include fouling control devices installed on the carrier itself.

Offboard solutions can further be subdivided into onsite solutions and peripheral solutions. Onsite solutions include those provided at the berthing area; peripheral solutions are those provided within the harbor for sediment control.

6.1.1 Onboard Solutions. Although various concepts could be applied to develop onboard solutions, this study concentrated on the use of diffusers.

The criteria provided to HRS for diffuser velocity reduction designs was a space of 4 x 3.5 x 4 ft for the single-barrel diffuser, and a space of 8 x 3.5 x 4 ft for the two-barrel diffuser. An exit velocity of 2.5 ft/sec was agreed by both NAVSEASYSCOM and NAVFACENGCOM to be acceptable, although HRS was prepared to further reduce the exit velocity.

6.1.2 Onsite Solutions. Various onsite solution techniques could be applied to the ship berthing area, including: (a) fencing pier slips with a barrier curtain, (b) providing jet arrays to sweep out bottom sediments, (c) using a crater-sink sediment bypassing system to pump sediment out, or (d) solidifying the sea floor to prevent deep digging of the sea bottom by jets. Only the "solidification of sea floor" option has been included in this study. The remaining onsite solutions will be investigated in a separate HRS research project of Piers 11 and 12.

6.1.3 Peripheral Solutions. Potential peripheral area sediment control techniques include: flushing, exclusion, trapping, and circulation. These techniques and methodologies will be further discussed in the above-cited Piers 11 and 12 study report.

6.2 DIFFUSER DESIGN CONCEPT

The concept of the diffuser design is to spread the flow through various physical arrangements such that the flow velocity will be reduced and a uniform exit velocity obtained. Such a dissipation of energy could be accomplished in three basic ways: (a) via direct impact, (b) via implantation of roughness elements, and (c) via geometric considerations. Each of these basic techniques is discussed in the following paragraphs.

6.2.1 Impact Considerations. Direct impact of the flow on a physical structure provides the most effective method of dissipating energy. Usually an impact chamber or an impact baffle plate is used for such a purpose. Caution must be used during design stages, however, to ensure that the structure can withstand the impact pressure.

6.2.2 Implantation of Roughness Elements. Utilizing roughness elements to slow down a flow is also a common method of dissipating energy. However, ease of construction is usually a critical consideration.

6.2.3 Change of Geometry. Changing the structural geometry of a structure to better guide the flow through, comprises another effective method of adjusting flow velocity distributions [30].

6.3 THE PRELIMINARY DIFFUSER DESIGN

The optimal design criteria for the diffuser design included:

- Compact diffuser space
- Capability of withstanding ship motions
- Optimal diffuser head loss
- Ease of design, construction, and installation.

Based on the cited design criteria, a series of diffuser designs was developed, tested, and evaluated. Figure 6-1 illustrates the conceptual design of the diffuser and its components. Twenty-four different configurations of the diffuser design were tested. Figure 6-2 is a photograph of the various diffuser designs tested by HRS. The experimental evaluation of the design indicated that the perforated impact plate and louver arrangement was an effective design.

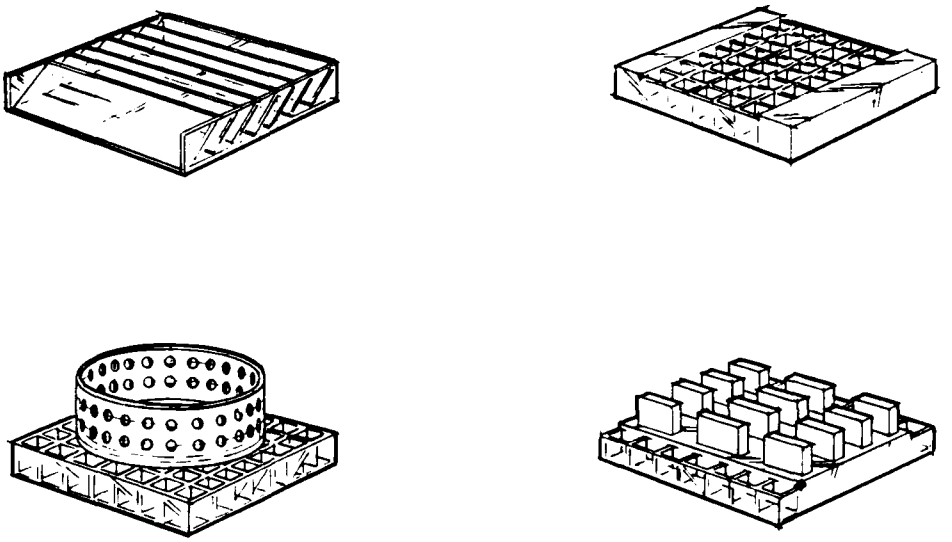

EXAMPLES OF VARIOUS CONCEPTS TESTED

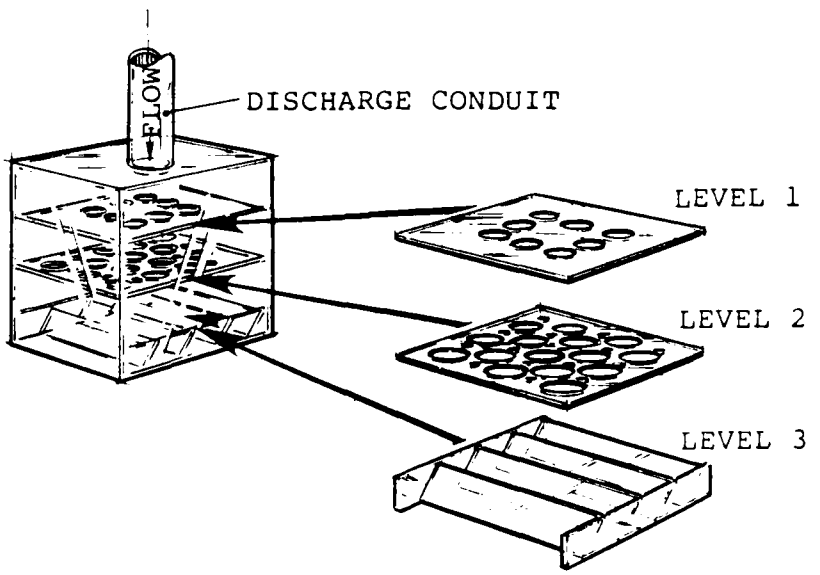

ARTIST'S CONCEPT OF DIFFUSER MODEL SHOWING THREE LEVELS OF INSERTS

Figure 6-1

Conceptual Design of the Diffuser and Components

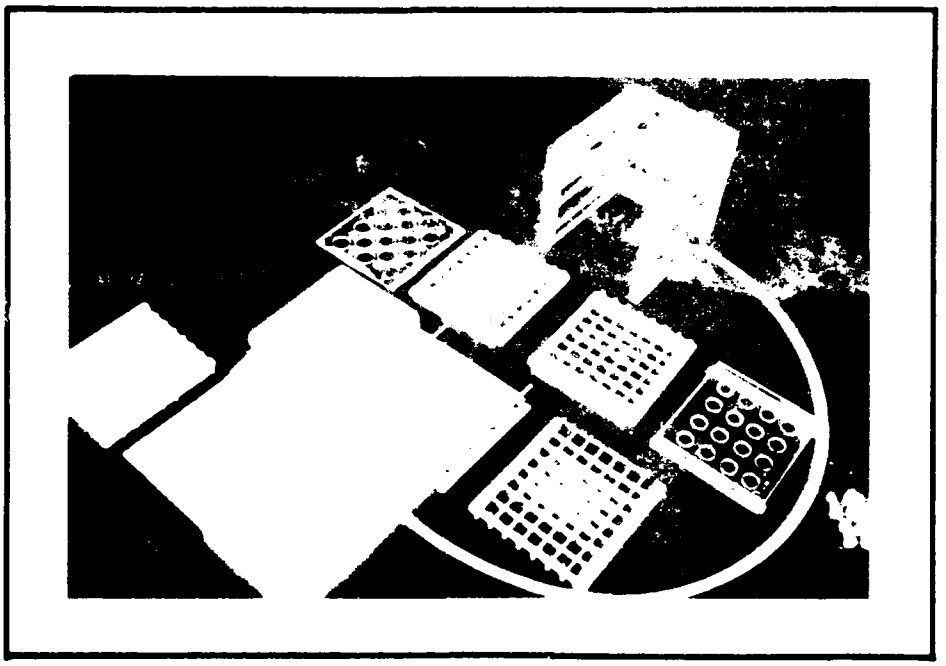

Figure 6-2
Diffuser Designs Tested by HRS

6.4 THE SINGLE-BARREL DIFFUSER

The single-barrel diffuser is used in the SG condenser unit. The dimension of the diffuser was limited to a box structure 4 ft long by 3-1/2 ft wide by 4 ft deep.

6.4.1 Preliminary NAVSEASYSCOM Designs. NAVSEASYSCOM provided HRS with two preliminary sea-chest diffuser designs for evaluation. As shown in Figure 6-3, the impact chamber consisted of two semicircular cups concaved upward and located directly under the discharge line. The guide vanes, located on the sides, were designed to change flow direction.

Tests of the diffuser yielded rotational flow patterns, with the discharge branching into two streams, due to the design of the two semicircular cups. It was evident that further modification of the impact chamber was required to achieve better flow distributions.

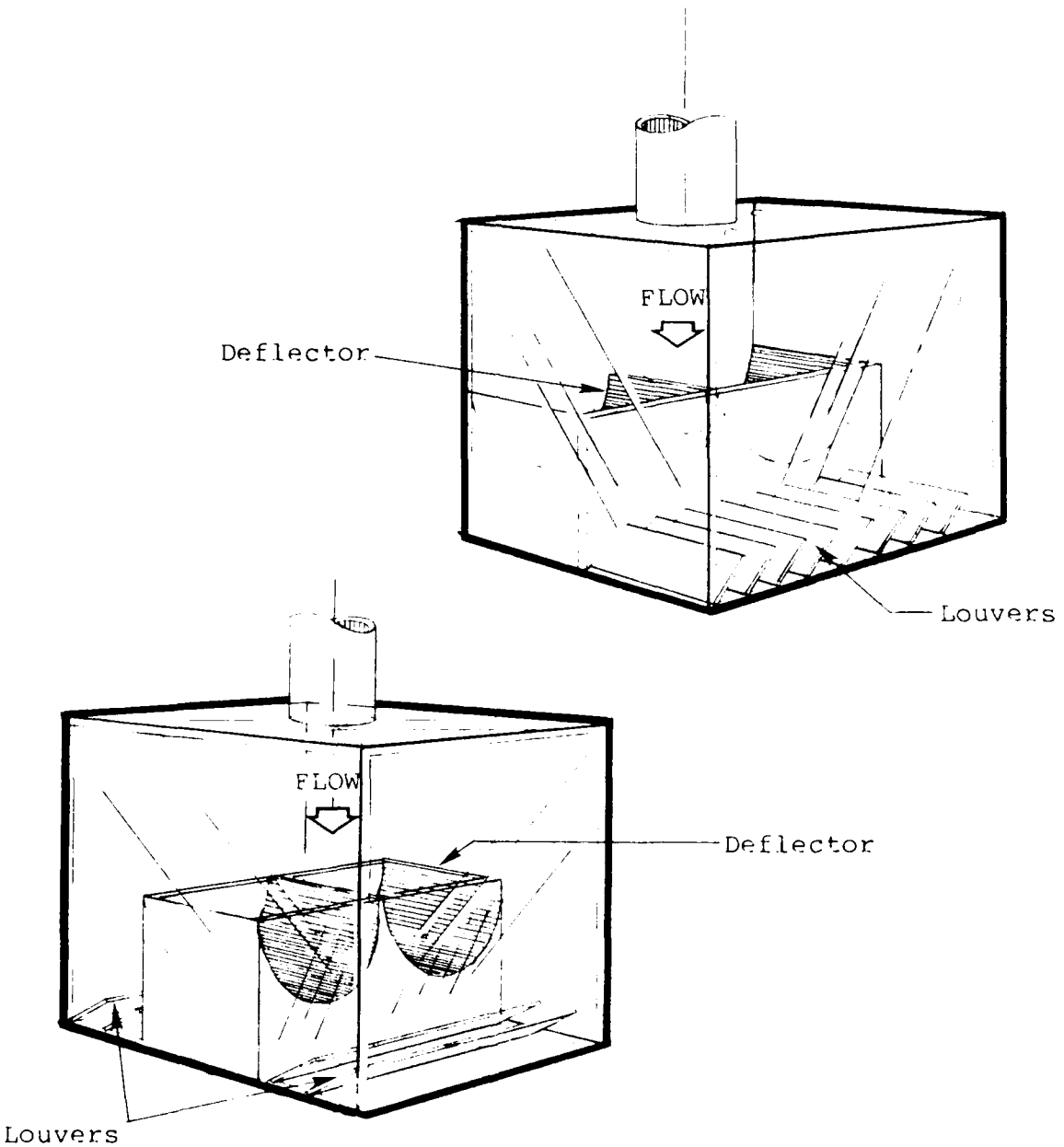

Figure 6-3

NAVSEASYSCOM Preliminary Diffuser Designs

6.4.2 Single-Barrel Diffuser Development. Various impact chamber arrangements were tested and compared with the original two NAVSEASYSCOM semicircular impact chamber diffusers. The configurations included an enclosed and a semi-enclosed rectangular chamber both with and without a roof structure, plus a circular impact chamber and impact plates. Figure 6-4 shows the different components tested.

The evaluation of these various arrangements revealed that the semi-enclosed rectangular chamber with rows of perforated 3-inch circular openings at the side walls, and with bottom slots, provided satisfactory velocity distributions at the louvered exit.

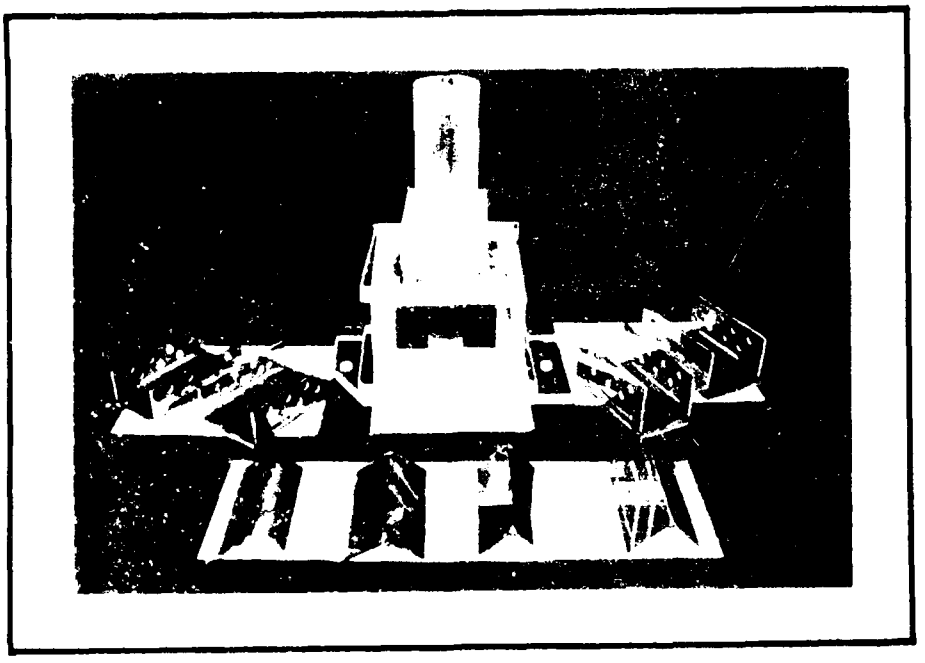

Figure 6-4
Diffuser Test Components

6.4.3 Final Single-Barrel Design. The final single-barrel diffuser design was obtained as the result of the optimization

tests. Figure 6-5 shows the final design of the single-barrel diffuser. This design was tested at pumping conditions of 5,890, 4,800 and 2,100 gpm with keel clearance of 13 ft. The results of these tests revealed a maximum velocity of 2.8 ft/sec at the exit. This velocity was reduced to 1.3 ft/sec near the sea floor in the direction away from the suction sea chest (see Figure 6-11). The back pressure to the discharge pipe was equal to 10 inches of water head for a pumping rate of 5,890 gpm. Figure 6-6 illustrates the dimensions of the final recommended single-barrel diffuser.

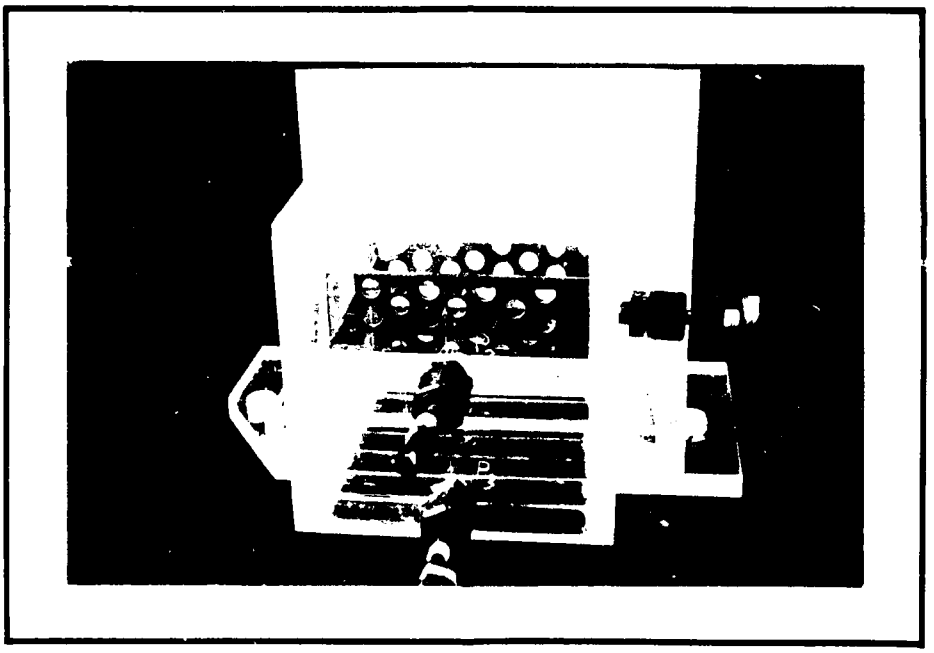

Figure 6-5
Final Design of the Single-Barrel Diffuser

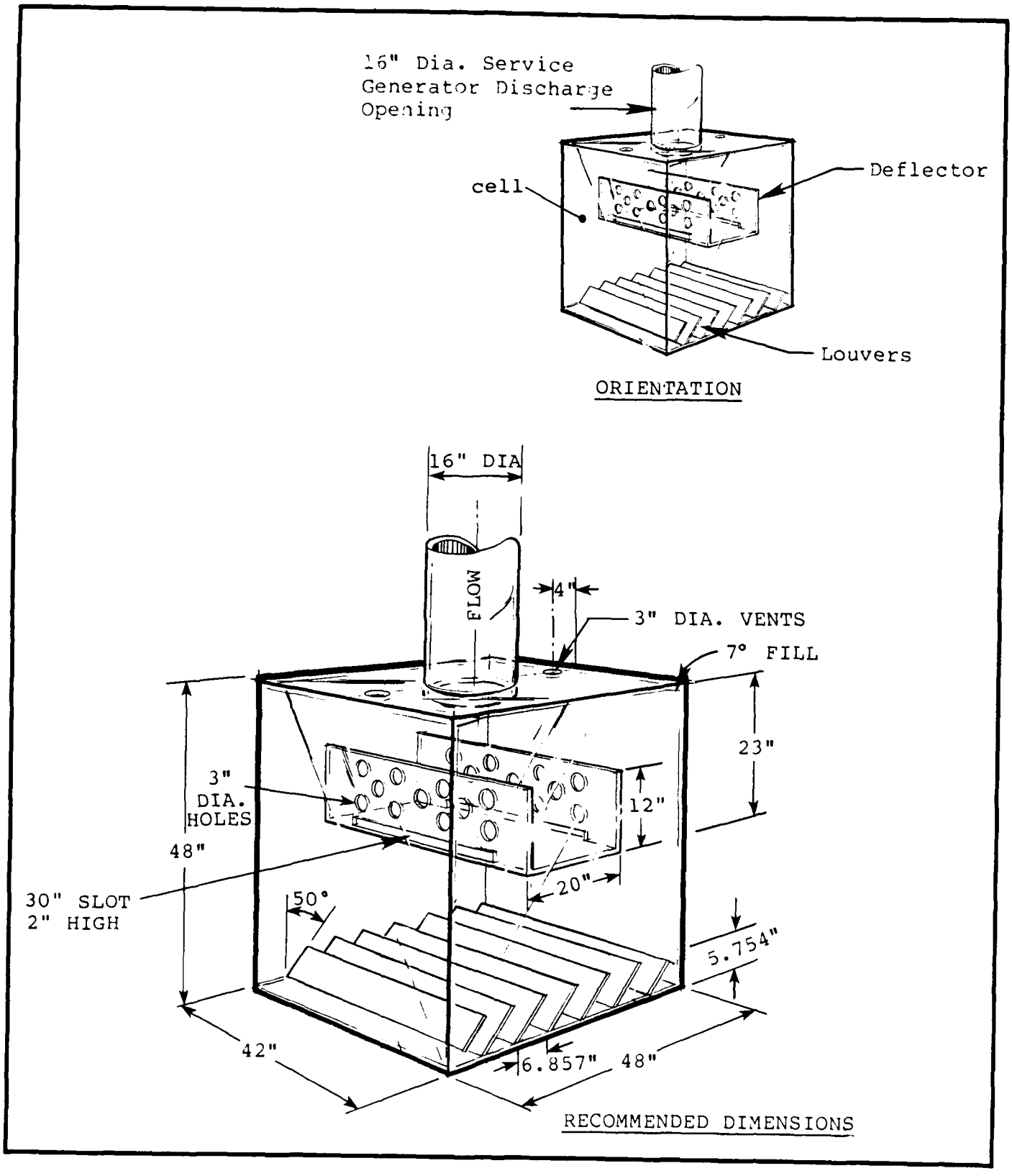

Figure 6-6

Final Recommended Single-Barrel Diffuser

6.5 THE DOUBLE-BARREL DIFFUSER

The preliminary design dimensions for the double-barrel discharge diffuser were 8 ft long by 3-1/2 ft wide by 4 ft deep. The inner barrel has an impact diverter with a roof design to divert the flow toward a 2-ft-diameter lightening hole on the separation wall between the inner and the outer barrels. In the other compartment, seven louvers located at the bottom guide the flow in the direction of the stern. Figure 6-7 illustrates the preliminary double-barrel diffuser design.

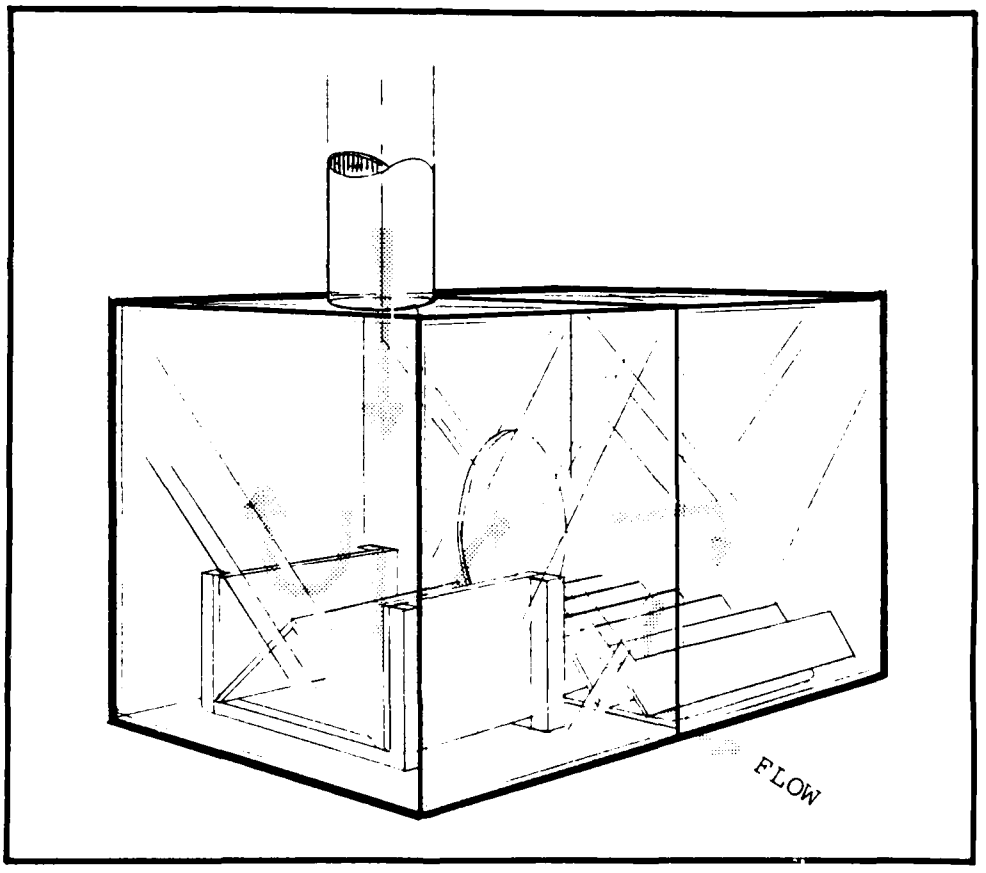

Figure 6-7
Preliminary Double-Barrel Diffuser Design

6.5.1 Double-Barrel Diffuser Development. The diffuser was subjected to base tests to determine the effectiveness of the velocity reduction. Observation of the flow patterns revealed uneven-flow velocity distributions at the louver exit. These distributions were found to result from the diversion of incoming flow at the inner barrel through the lightening hole. When the flow entered the outer compartment at high momentum, it impacted on the outside wall, then deflected back with concentrated jet flow patterns out of the louvers.

6.5.2 Final Double-Barrel Design. As with the single-barrel discharge diffuser, several impact arrangements were tested. These arrangements included rectangular and circular chambers with perforated walls at the inner compartment to dissipate energy, and a baffle beam design at the outer compartment to redistribute the flow.

Evaluations indicated that a design incorporating a semi-enclosed rectangular impact chamber at the inner compartment, and two parallel baffle beams with port-to-starboard orientation at the outer compartment, provided a good exit velocity distribution. This design is therefore recommended as an effective onboard solution. The final recommended design is presented in Figures 6-8, 6-9, and 6-10.

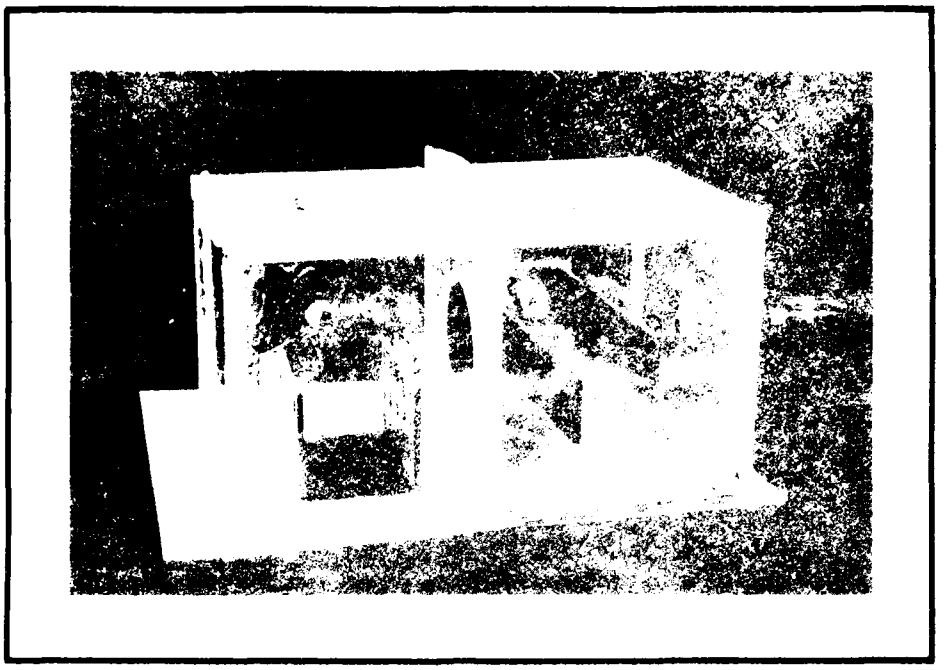

Figure 6-8
Final Design of the Double-Barrel Diffuser

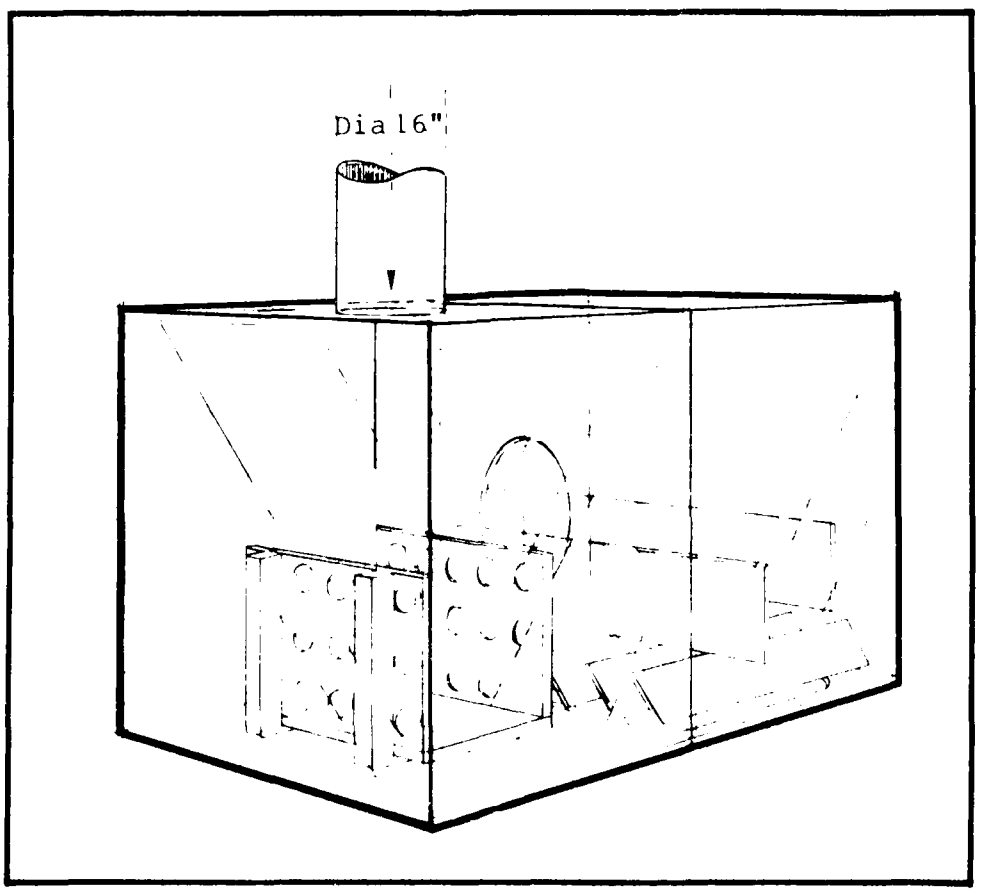

Figure 6-9
Final Recommended Double-Barrel Diffuser

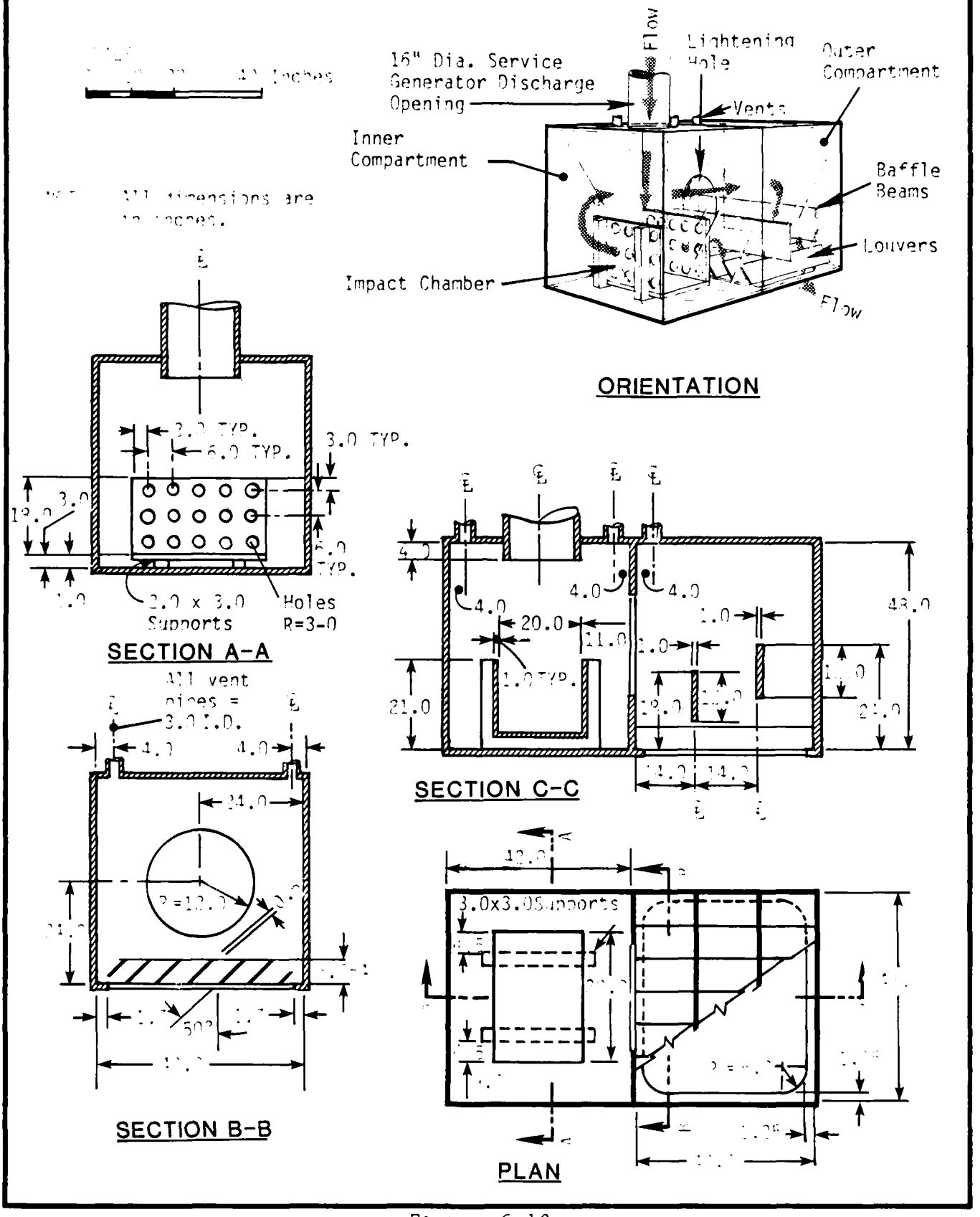

Figure 6-10

Final Recommended Double-Barrel Diffuser

6.6 VERIFICATION STUDIES

The final recommended diffuser designs were then subjected to various operational conditions to verify their operational characteristics.

6.6.1 Pier-Side Berthing Simulation. With the discharge diffusers in place, pumping rates of 5,890, 4,800 and 2,100 gpm were tested for the SG discharge sea chests. A dye probe was used to observe the exit flow patterns, and an electromagnetic velocity meter was used to measure the velocity distributions.

Excellent flow conditions were obtained. Figure 6-11 shows the flow patterns resulting from the two final diffusers. Figure 6-12 shows the flow patterns and velocity measurements obtained from these tests.

6.6.2 Ship-In-Motion Simulation. An alternative method of ship-in-motion simulation was adopted by moving the flow beneath the stationary platform to obtain the relative velocities. The flow patterns of a ship moving at speeds of 5 and 12 knots with a pumping rate of 5,890 gpm on the SG discharge were recorded, and are shown in Figure 6-13. The results indicated that with the diffuser as the onboard solution, problems will not be encountered during ship-moving operations.

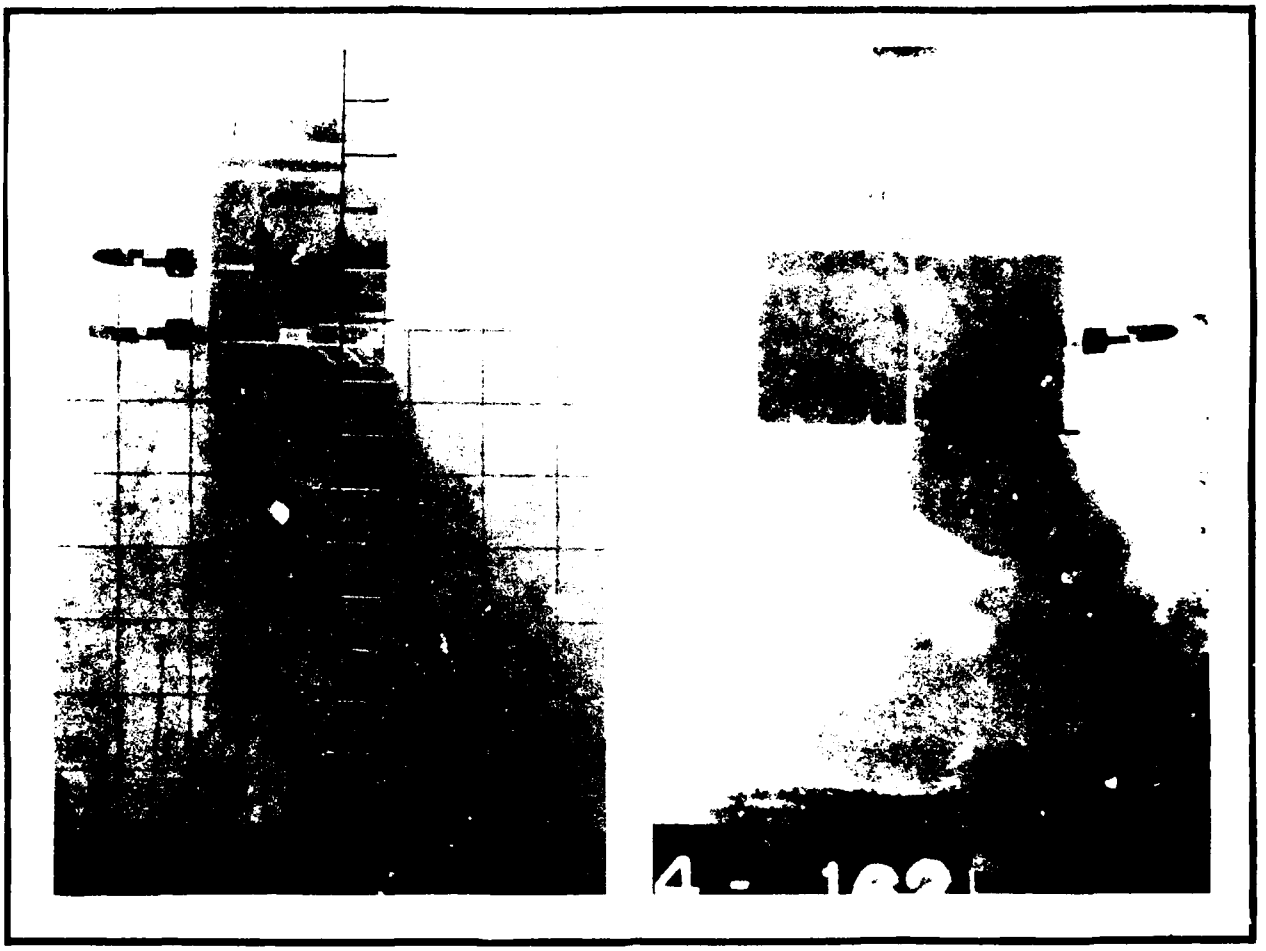

Figure 6-11

Flow Patterns Resulting from Two Final Diffusers

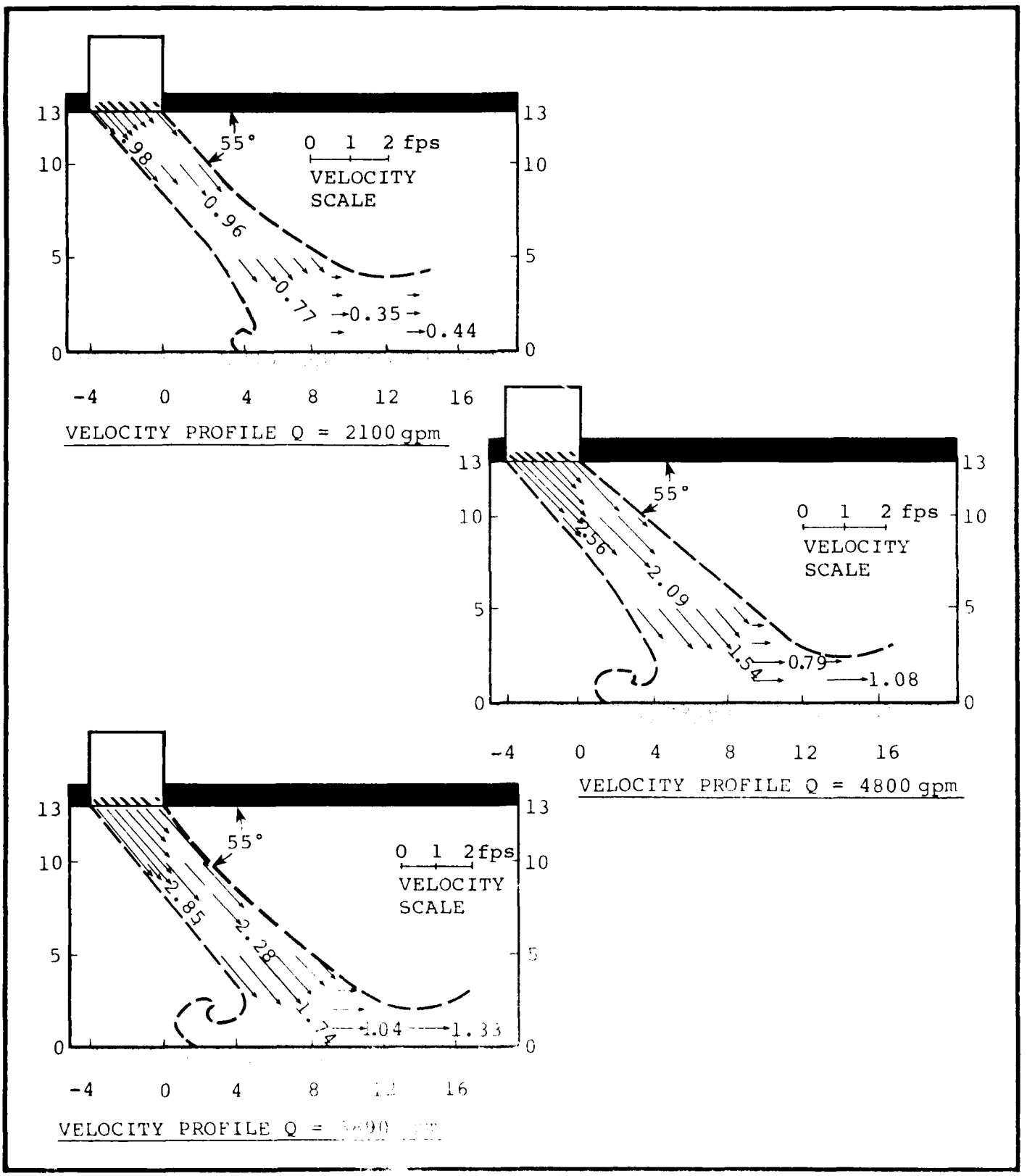

Figure 6-12

Pipe-Stub Diffuser Flow Patterns

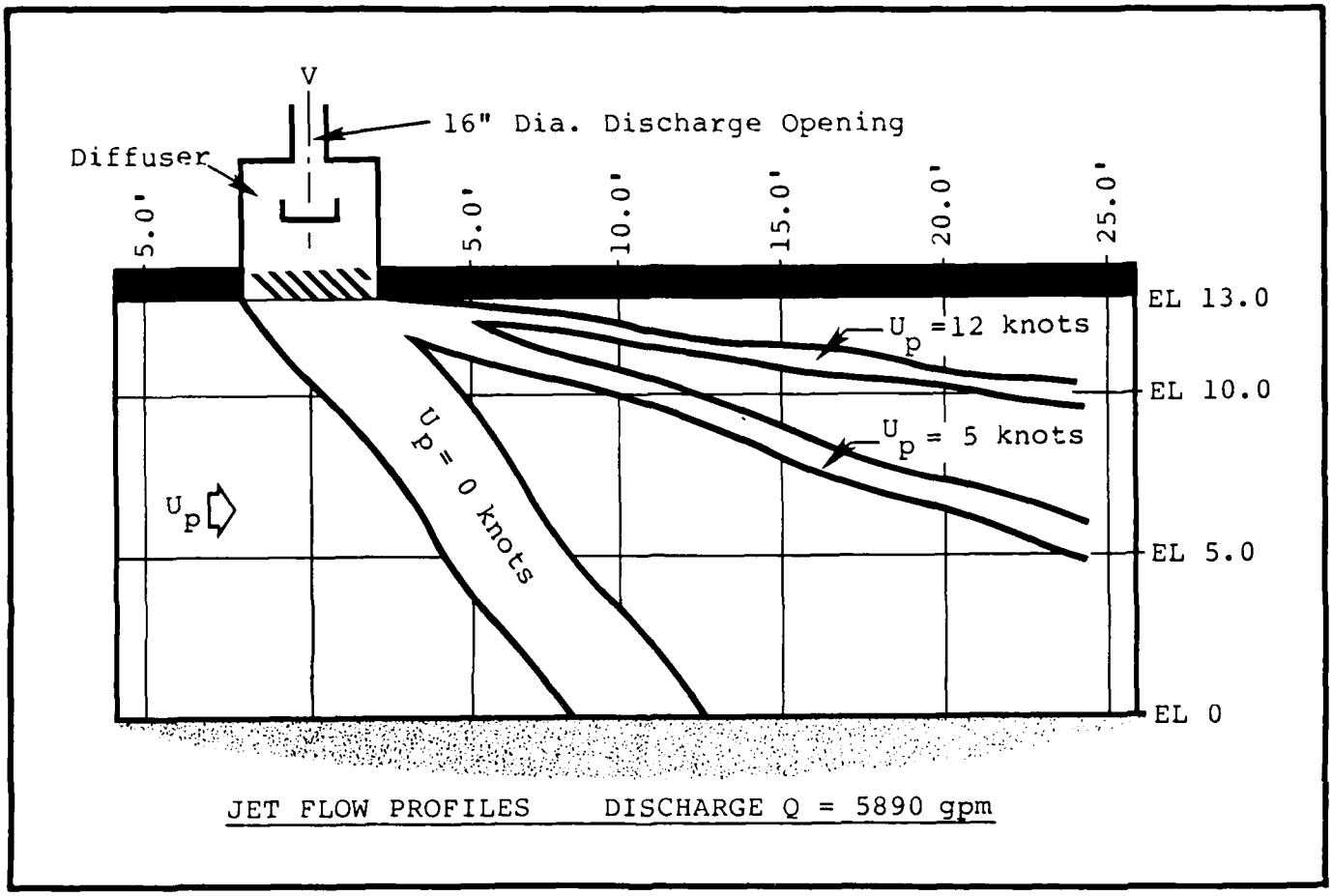

Figure 6-13
Flow Patterns from Moving-Ship Simulation

6.6.3 Sea Bottom Scouring and Fouling Tests. Both single- and double-barrel discharge diffusers were tested using a thick layer of mixed walnut-shell/green algae lying at the bottom of the berthing tank. Flow rates of 5,890, 4,800, and 2,100 gpm were examined using a 13-foot underkeel clearance. The primary purposes of this test were to qualitatively assess the scouring of the bottom material, and to investigate the insufflation of material into the suction sea chests.

Observation of the sea-bottom material scouring revealed that the bottom layer was only superficially disturbed, and a slight depression produced. Very small amounts of the floating material approached the suction sea chest as a result of this minor disturbance of the flow field.

6.7 CONCLUSIONS ON ONBOARD SOLUTIONS

The previously described test program concluded the study on the SG diffuser units. The problem of the main circulating cooling system had not yet been solved. However, according to the Navy personnel, the main circulating cooling system does not have to be operated at full capacity during berthing and light off operations. This provides a very promising fouling control measure by simply cutting down the pumping rate on the main circulating system sea chests.

It was concluded that with the diffuser as the onboard solution, and deepening of the berthing area to 50 ft, the fouling of the suction sea chest can be minimized.

6.8 CONCEPT OF SOLIDIFICATION OF SEA FLOOR

An alternative technique for controlling the fouling phenomena could utilize the previously discussed "jet on solid boundary" concept. This concept naturally falls into the category of onsite solutions.

6.8.1 Preliminary Test. A test was conducted to investigate whether a solid bottom underneath the discharge sea chest would improve sediment control. A thin layer of walnut shell was paved on top of a piece of acrylic Plexiglas platform to simulate a section of solid sea floor. With the main circulating cooling system in operation, the discharge pushed away the thin

layer of sediment without further digging down into the sea bottom. This reduced the chance of sea-chest clogging. Figure 6-14 shows the concept of sea-floor solidifications, and Figure 6-15 shows the resulting scour patterns.

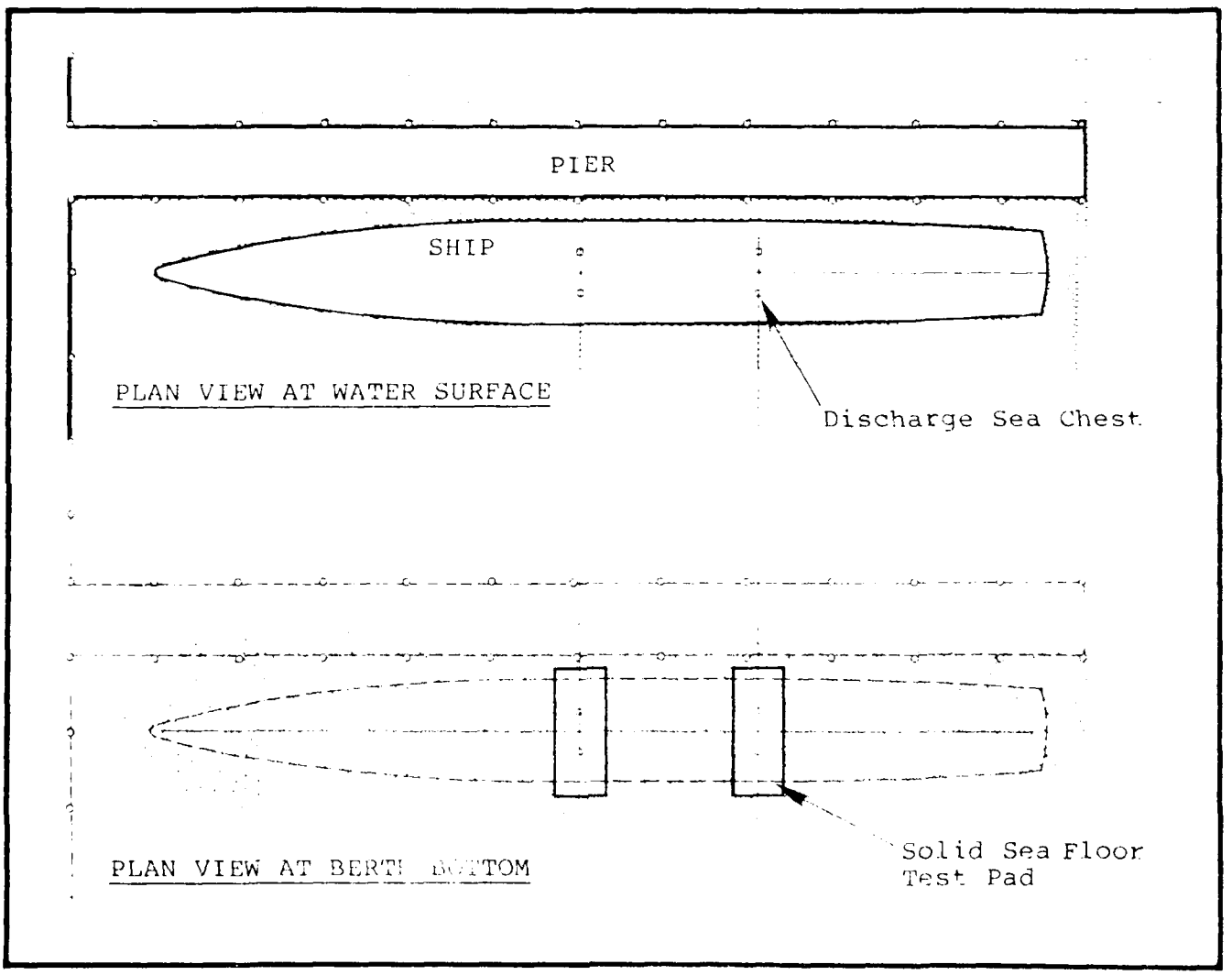

Figure 6-14
Concept of Sea Floor Solidifications

Figure 6-15
Resulting Scour Patterns

6.8.2 Recommendations. From the above-cited preliminary test, it is evident that further study of the sea floor solidifications is worth pursuing. This concept will be tested as part of the HRS study of Piers 11 and 12.

Appendix A,
Hydrodynamic Properties of Marine Organisms,
(By Dr. R.J. Diaz of VIMS)

AD-A131 645 UNDERKEEL CLEARANCE STUDY(U) HYDRO RESEARCH SCIENCE 2/2
SANTA CLARA CA A B RUDAVSKY ET AL. SEP 81 HRS-092-81
N00014-80-C-0395

UNCLASSIFIED F/G 13/10 NL

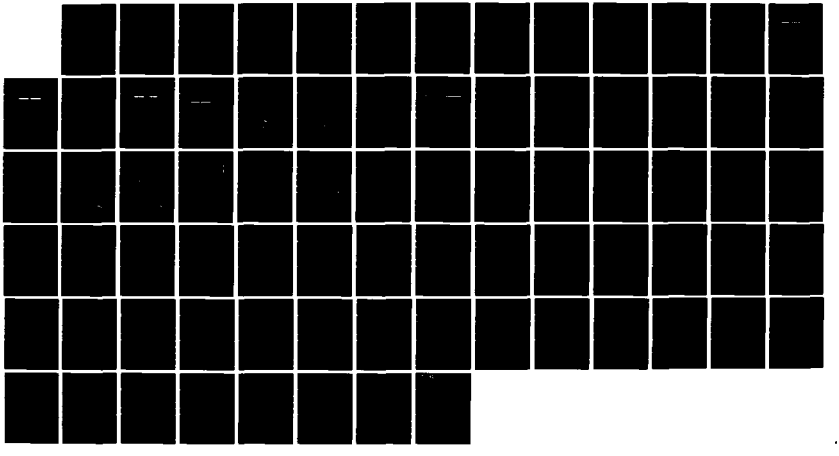

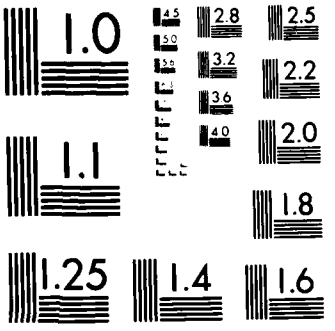

APPENDIX A
HYDRODYNAMIC PROPERTIES OF MARINE ORGANISMS
(By Dr. R. J. Diaz of VIMS)

Hydrodynamic properties of the fouling organisms were measured in the laboratory using the VIMS hydraulic flume [31] [32]. The flume has a 48-ft long by 3-ft by 3-ft test section with a smooth level floor. Current velocities in the test section were adjustable from 0 to 2.8-ft/sec. The overall uniformity of velocity versus depth is within 2 to 3%.

A.1 DENSITY OF THE ORGANISMS

Density of the organisms was measured by a volume displacement method. The volume of a given quantity of organisms was estimated from the amount of water they displaced in a 1,000 ml graduated cylinder. The mass of the same quantity was then estimated using a sartorius balance. The average density for live hydroids was 1.026-g/cc; for live bryozoans 1.087-g/cc; for dead and buried hydroids 1.128-g/cc; and for dead and buried bryozoans 1.187-g/cc. The higher densities for dead organisms resulted from the inclusion of sediment particles within the skeletal remains of the organisms.

A.2 MOTION OF ORGANISMS IN FLOW

For this series of tests, organisms were placed on the floor of the flume, and the flume velocity increased until the organisms began to roll. Several parameters were measured, including: critical flow velocity, and initiation of motion velocity. Critical flow velocity was determined for individual colonies and for a large cluster of colonies of various sizes. Flume velocity was increased from zero to the point where waving and saltation of colonies occurred. Results are summarized in Table A-1.

TABLE A-1

Critical Flow Velocity

Individual Colony Hydroids	live	0.05 fps
Individual Colony Hydroids	dead	0.22 fps
Individual Colony Bryozoans	live	0.20 fps
Individual Colony Bryozoans	dead	0.22 fps
Mixed Colonies Hydroids		0.07 to 0.08 fps
Mixed Colonies Bryozoans		0.20 to 0.23 fps

Individual live colonies of hydroids have the lowest critical flow velocity, and are very easily moved along the flat floor of the flume. Dead hydroids that have been buried have mud incorporated into their hollow skeletons, and are harder to move. With bryozoans it makes little difference as to whether they are live or dead.

When a large amount of organisms was placed in the flume test section (about 20-lb) the intertwining of the colonies increased the resistance to movement, increasing the critical flow velocity. This mix of colonies probably represents a more realistic picture of what occurs in the prototype system than the individual colony measurements.

Initiation of motion velocities, defined as the flume velocity needed to cause sustained motion of colonies, were estimated similarly to critical flow velocities. Results are summarized in Tables A-2 and A-3.

TABLE A-2

Initiation of Motion Velocity (I)

Individual live colony			
Hydroids		Bryozoans	
wet weight (grams)	velocity (fps)	wet weight (grams)	velocity (fps)
0.6	0.05	16.8	0.34
1.7	0.07	27.1	0.37
4.1	0.09	73.0	0.40
7.8	0.11	89.1	0.41

TABLE A-3

Initiation of Motion Velocity (II)

Mixed live & dead colonies	
Hydroids velocity (fps)	Bryozoans velocity (fps)
0.14 to 0.17	0.28 to 0.32

For hydroids the size of the colony strongly affects the initiation of motion velocity. With bryozoans the effect of size on velocity is not as strong. Again as with the critical flow velocity, the initiation of motion velocity is higher for a mix of colonies, and probably represents a more realistic view of the prototype.

A.3 FALL VELOCITY OF ORGANISMS

Fall velocity was determined in a standing body of water about 3-ft deep. Organisms were placed below the water surface, released, and after achieving terminal velocity timed across a measured depth of water. Results are summarized in Tables A-4 and A-5.

The size of the hydroid colony, expressed as a wet weight, influenced the fall velocity. Larger live colonies sank faster. Dead colonies of equal size to live colonies had faster fall velocities, due to the higher density of the dead colonies. With the bryozoans there was no clear relationship to size of colony and fall velocity. That dead colonies of bryozoans had smaller fall velocities than live colonies is unexplainable, and may require further testing.

TABLE A-4

Fall Velocity of Organisms (Hydroids)

Live colonies -- Winter 1980 growth --		Dead colonies -- Winter 1979 growth --	
wet weight (grams)	fall velocity (fps)	wet weight (grams)	fall velocity (fps)
158.0	0.11	23.3	0.09
50.0	0.09	12.4	0.10
29.0	0.12	6.6	0.09
7.0	0.04	3.1	0.16
2.4	0.03	0.5	0.18
0.7	0.02	0.4	0.27
0.4	0.02	0.2	0.39

TABLE A-5

Fall Velocity of Organisms (Bryozoans)

Live colonies -- Winter 1980 growth --		Dead colonies -- Winter 1979 growth --	
wet weight (grams)	fall velocity (fps)	wet weight (grams)	fall velocity (fps)
278.0	0.22	77.2	0.09
130.0	0.21	42.4	0.11
94.0	0.29	20.5	0.13
45.0	0.27	18.2	0.16
28.0	0.25	9.1	0.13
22.0	0.26	8.2	0.12
17.0	0.22	3.7	0.16
		3.3	0.21

Appendix B,
Physical Model Test Results

APPENDIX B
PHYSICAL MODEL TESTS AND RESULTS

B.1 THE PHYSICAL MODEL SETUP

B.1.1 Key Elements of Model Setup

The model of the underkeel clearance study was constructed to an undistorted linear-scale ratio, model to prototype, of 1:10. The model was built to be flexible enough to make the components readily exchangeable if the need arose for the revisions to the model structure. The model consisted of four main components:

- The facility (the HRS berthing tank)
- The model proper (the sectional sea-chest model)
- Auxiliary equipment
- Instrumentation.

B.1.2 The Berthing Tank -- The Model Housing

The sectional sea-chest model was constructed and then installed in the HRS berthing tank. This tank is a permanent HRS facility 6.3 ft wide and 6 ft deep. The side walls and floor of the tank are made of clear acrylic plastic to enable easy observation of flow patterns.

B.1.3 The Model Proper

The model proper encompassed significant sections of the bottom hull of the CVN 69 aircraft carrier, shown in Figure 4-2, where assessment of sea-chest fouling was to be performed. These critical sections included:

- Suction sea chest with strainer plate for SG Units #43 and #53
- Discharge sea chest for SG Units #45 and #57

- Main circulating system suction sea chest with inlet strainer bars for Unit #41
- Main circulating system discharge sea chest for Unit #46.

B.1.4 The Auxiliary Equipment

The actual model components were augmented by auxiliary equipment, including: sumps to store water, centrifugal pumps to circulate the flow through the model, and a system of discharge valves and butterfly valves to regulate the flow for the simulation of the sea-chest pumping conditions.

B.1.5 The Instrumentation

The primary metering devices used to measure flow velocities and pressures included: Pitot tube, current meters, dye probes, pressure transducers and piezometers, and orifice meters to monitor the flow rates. Higher velocities were measured using a conventional Pitot tube with a minimum reading of 0.3 feet per second (fps) (prototype value) and an electromagnetic water current meter with a minimum reading of 0.2 fps (prototype value).

The electromagnetic velocity meter was equipped with a calibration check mechanism to monitor the magnetic drive signal and channel amplifiers to ensure that the calibration remained the same as that preset at the factory. A calibration check was performed every time an experiment was conducted. The Pitot tube measurements were compared with the electromagnetic meter simultaneously operated in the model.

Dye meters were used to observe and record flow patterns and any other eddy formations. Subsurface patterns were determined by means of dye introduced into the model at the desired depths. The differential pressure transducers used in the pressure measurement study were equipped with replaceable diaphragms to measure pressure fluctuations from 0.1 to 25 psi.

The 2-channel oscillographic recorder recorded pressure-variation dispatches through the transducers at locations of the sea floor beneath the jet.

B.2 THE MODEL LAWS

The similitude relationships between the model and the prototype for flows in the study are based on the Froude Law. The resulting mathematical relationships between the basic hydraulic quantities of the model and the prototype are summarized in Table B-1. The scale relationships in this table can be used to transfer quantitatively the discharge, depth of flow, and the velocity of flow from the model to the prototype.

TABLE B-1
Similitude Relationships

Dimension	Ratio of model to prototype	Scale Relationships
Length	$L_r = \frac{L_m}{L_p}$	1:10
Area	$A_r = (L_r)^2$	1:100
Time	$T_r = (L_r)^{1/2}$	1:3.16
Velocity	$V_r = (L_r)^{1/2}$	1:3.16
Discharge	$Q_r = (L_r)^{5/2}$	1:316

B.3 THE STATISTICAL DESIGN DATA

B.3.1 Structural Design Data

Data pertinent to structural features of the original sea-chest design are summarized in Table B-2.

TABLE B-2
Sea-Chest Structural Features

Service Generator (SG) suction opening	37-1/8" x 30-3/8"
Service Generator discharge opening	16" circular
Main Circulation System suction opening	42-13/16" x 28-13/16"
Main Circulation System discharge opening	69-13/16" x 46-13/16"
Underkeel clearance	5', 13', and 21'

B.3.2 Hydraulic Design Data

The hydraulic design data related to the model investigations are summarized in Table B-3.

TABLE B-3
Hydraulic Design Data

SG circulation flow rate (Full Capacity)	5,890 gpm
Main Circulation System flow rate (Full Capacity)	25,000 gpm
Ship speed	0 to 15 knots

B.4 PHYSICAL MODEL LIMITATIONS

B.4.1 Similarity Limitations

Similarity between the model and the prototype was obtained in accordance with the Froude Law, which assumes

gravity as the dominant force. Since complete dynamic similitude and accurate reproduction of some properties of the prototype materials are not possible, some limitations must be imposed on the model results.

B.4.2 Scour Interpretations

Data on scour are to be considered as qualitatively reliable, since it has not yet been found practical to reproduce quantitatively the resistance to erosion of a prototype bed material in a model. The observed scour data served as a basis for determining the relative effectiveness of the types and placement of the protective elements, as well as indicating areas most vulnerable to erosive attacks.

B.4.3 Air-Entrainment Considerations

Air entrainment cannot be modeled by the Froude Law alone. Air entrainment is a function of the flow velocity, depth and distance traveled, or, in the case of a trajectory, the flight path. At present there is no acceptable method to correlate air entrainment between the model and the prototype.

B.4.4 Simulation of Turbomachinery

The sea chests were the terminal components of the model proper, therefore, neither the prototype turbomachinery nor a model scale relationship for this type of turbomachinery was established. Instead, the properly-scaled discharge quantities were used to simulate prototype turbomachinery discharges. Therefore, the model should be considered as representative only within the confines of the terminal sections of turbomachinery structures.

B.4.5 Limitations of the Sea-Chest Model

Within the scope of model interpretation and limitations, the sea-chest model proper is only a partial model taken out

of context from a total functional system. It is thus somewhat limited in its predictive applicability.

B.5 MODEL TESTS AND RESULTS

B.5.1 Jet Impinging on a Solid Boundary

B.5.1.1 Jet Regions

Three distinct regions of flow can be recognized on a circular jet impinging normally on a plate. The flow at the immediate area surrounding the jet opening tends to discharge freely, as it is not influenced by bottom boundary effects. The flow characteristics in this region are therefore designated as "free jet".

Beyond the free-jet region the jet undergoes considerable deflection. Close to the boundary, the flow becomes almost parallel to the plane wall. The flow characteristics in the vicinity of the plane-impact zone are therefore designated as the "impingement" region and the "wall jet" region. Figure B-1 illustrates a jet impinging on a solid boundary.

B.5.1.2 SG Discharge Velocity Measurements

As mentioned in Section B.1.5, the velocity distribution of the SG discharge was recorded using an electromagnetic flow meter. The observed conditions included three underkeel clearances and three pumping rates.

Figure B-2 shows the SG discharge velocity distributions.

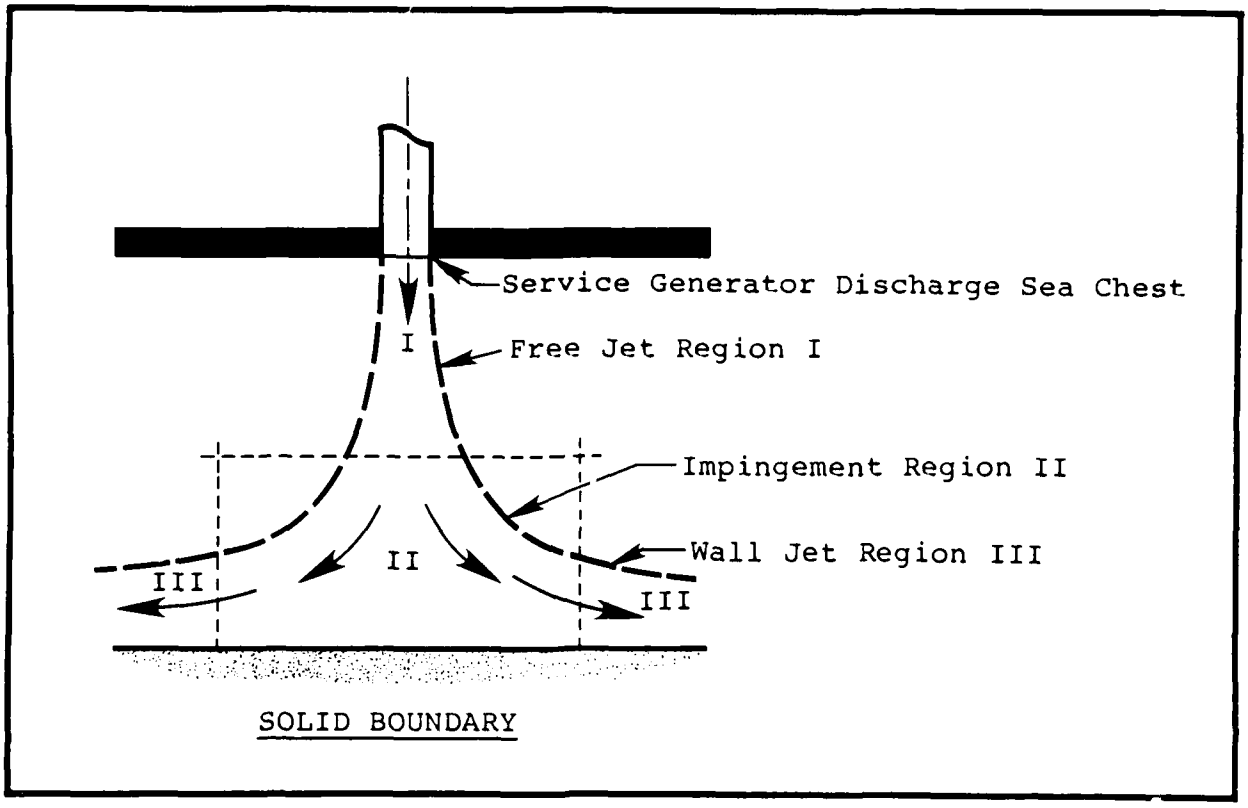

Figure B-1
Jet Impinging on a Solid Boundary

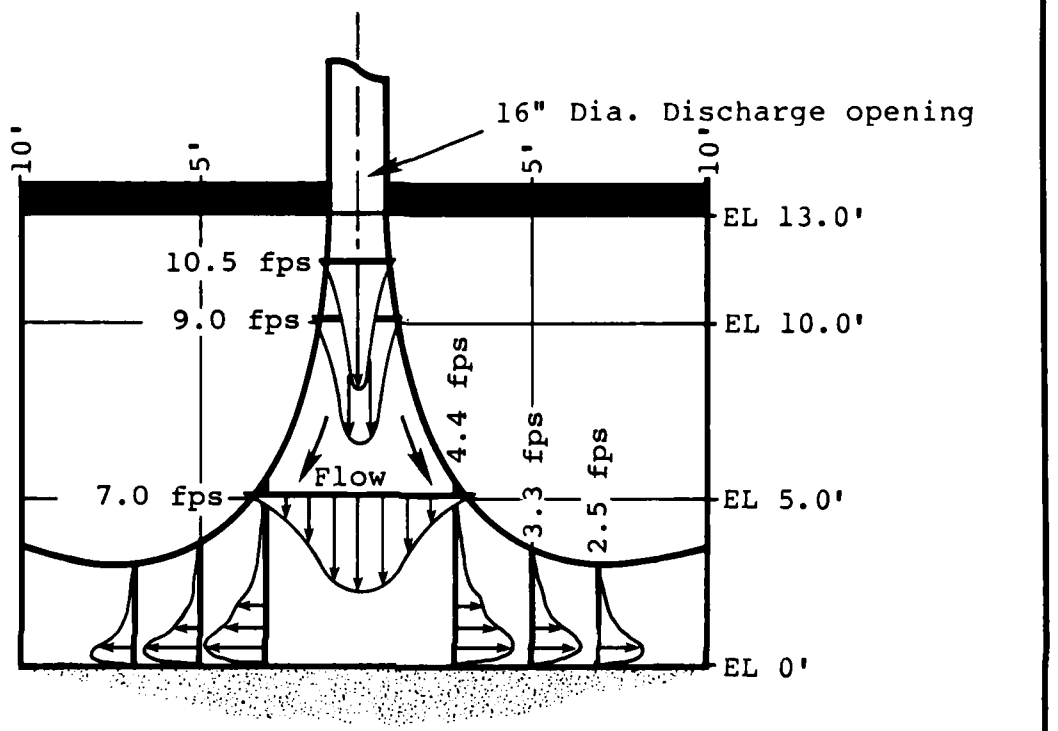

SERVICE GENERATOR DISCHARGE OPENING

Q = 5890 gpm Velocity measurements are the maximum recording for each measured plane.

Figure B-2

SG Discharge Velocity Distributions

Table B-4 is an example of the velocity data obtained from the observations.

TABLE B-4

Sample Circular Jet Velocity Data

	$(V_n)_{5\text{-ft}}/V_o$ Ratio of normal velocity measured at EL. 5 ft to the maximum exit velocity		
Underkeel Clearance	Q = 5890 gpm V_o = 10.5 fps	Q = 4800 gpm V_o = 9.5 fps	Q = 2100 gpm V_o = 4.5 fps
5 ft	0.9 - 0.95	0.9 - 0.95	0.9 - 0.95
13 ft	0.7 - 0.75	0.65	0.55
21 ft	0.55	--	--

The measurements from this study correlated with the available data of other experiments in terms of normal velocity V_n, radial velocity V_r, and bottom pressure Δp. Excellent correlations were found to exist between HRS findings and the data of other investigators.

The key variables of a jet include: the diameter of the jet nozzle D, the exit velocity V_o, the normal velocity V_n, the radial velocity V_r, the bottom pressure differential Δp, and the bottom shear stress τ.

B.5.1.3 Main Circulating System Discharge Sea-Chest Velocity Measurements

The main circulating system discharge sea chest has a circular-to-elliptical transitional cross section much like a boot. The exit velocity therefore has a skewed distribution in the direction of the stern as shown in Figure B-3.

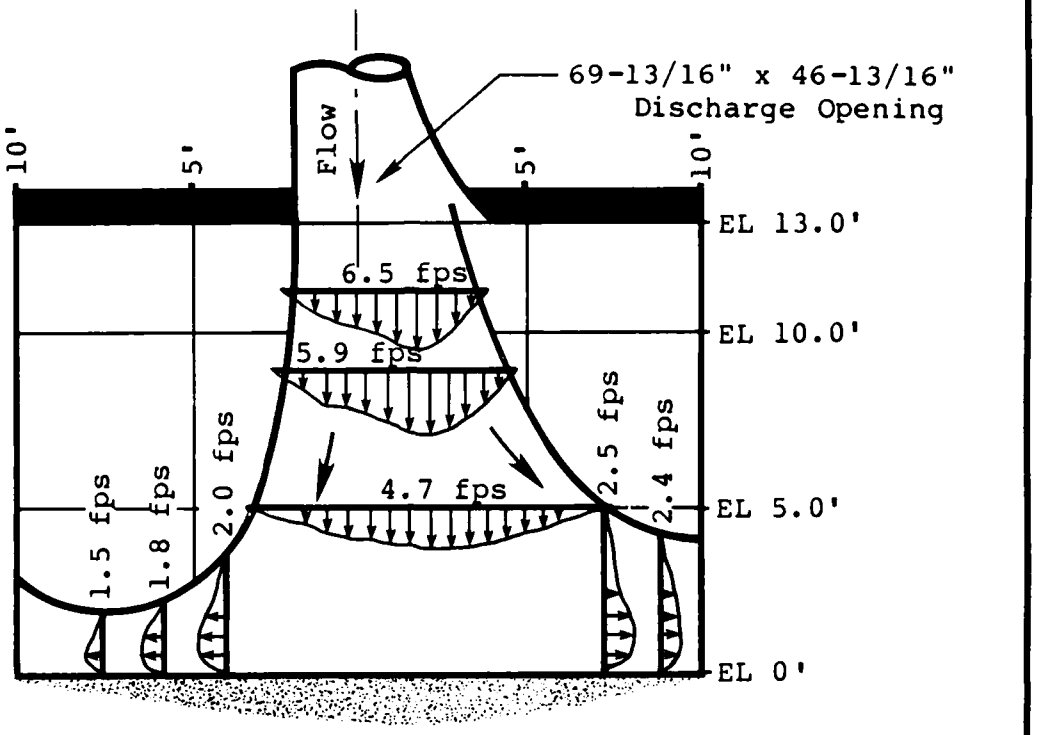

Figure B-3

Main Circulating System Discharge Sea Chest Velocity Distributions

B.5.2 Jet Impinging on a Movable Boundary

B.5.2.1 Jet Regions

The jet regions for the movable boundary can be divided into three regions: the free jet region, the impingement

region, and the boundary jet region. The jet impinging on a movable boundary is a dynamic process. It digs down to the bottom and forms a perpetuated eddy pattern, scouring the bottom materials. Figure B-4 illustrates the concept of a jet impinging on a movable boundary.

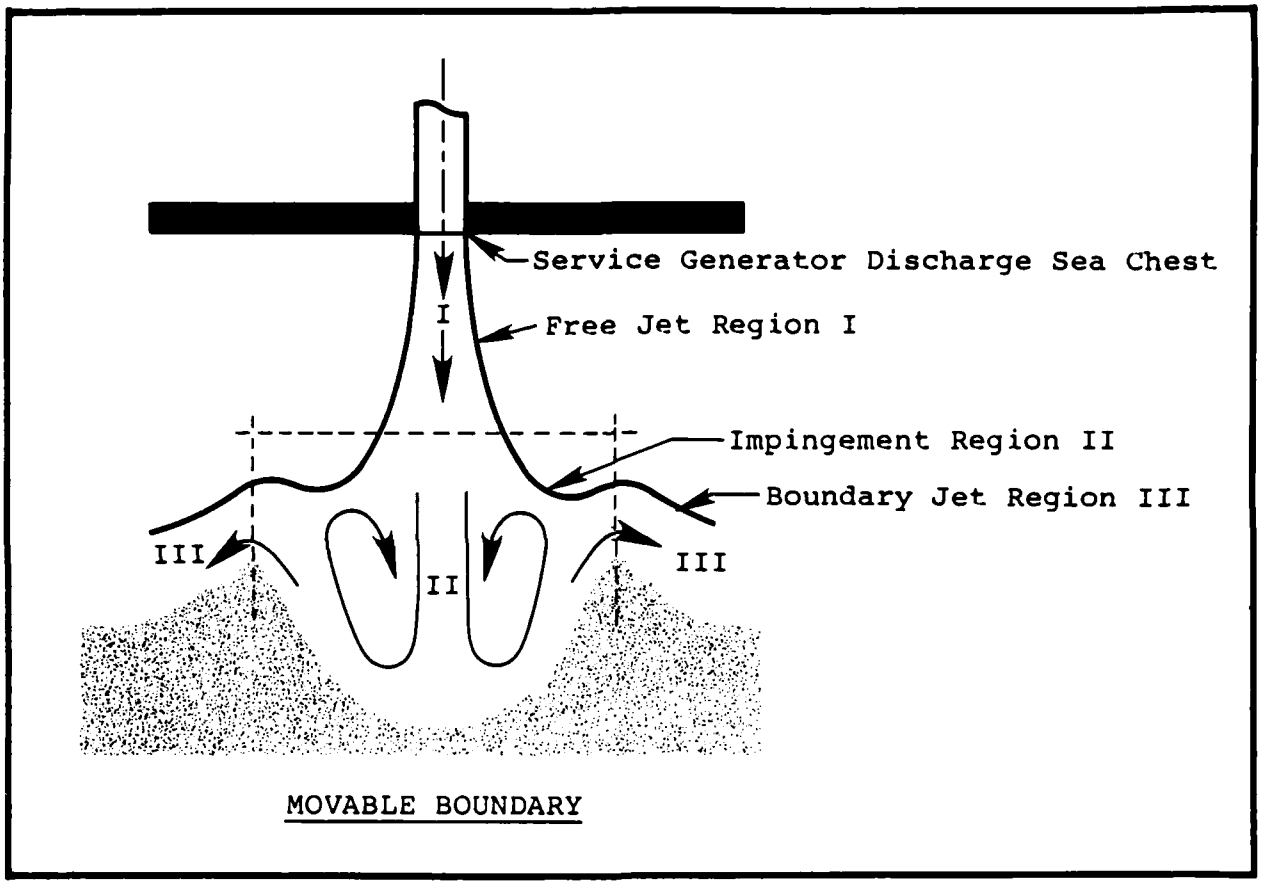

Figure B-4
Jet Impinging on a Movable Boundary

B.5.2.2 SG Discharge Velocity Measurements

The velocity distribution of the SG discharge jet impinging on a movable bottom was recorded. The model materials included sand (to simulate sand) and walnut shells (to simulate mud). The jet velocity distributions on sand and mud bottoms are presented in Figures B-5 and B-6, respectively.

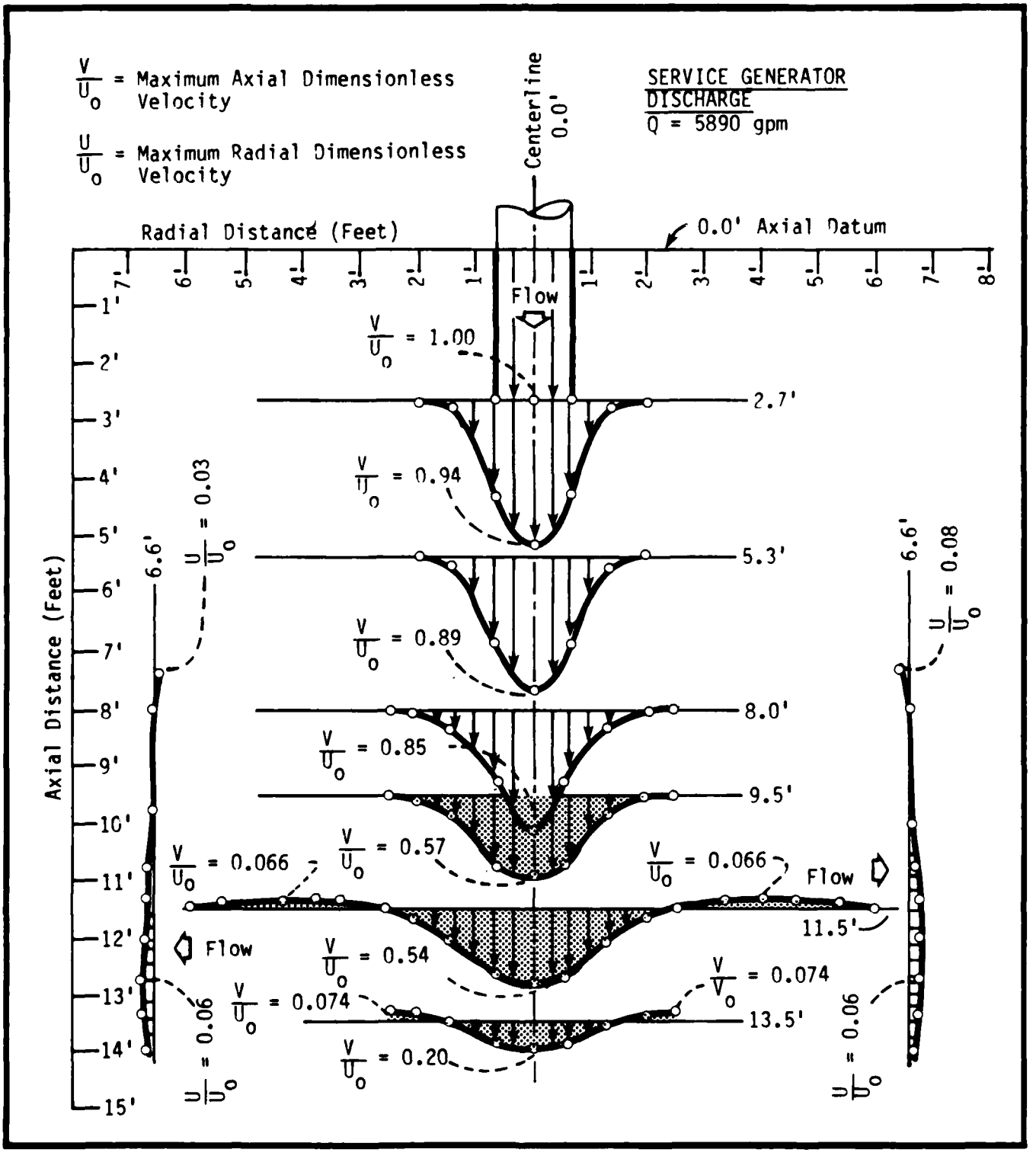

Figure B-5

Flow Field on Movable Boundary (Mud)

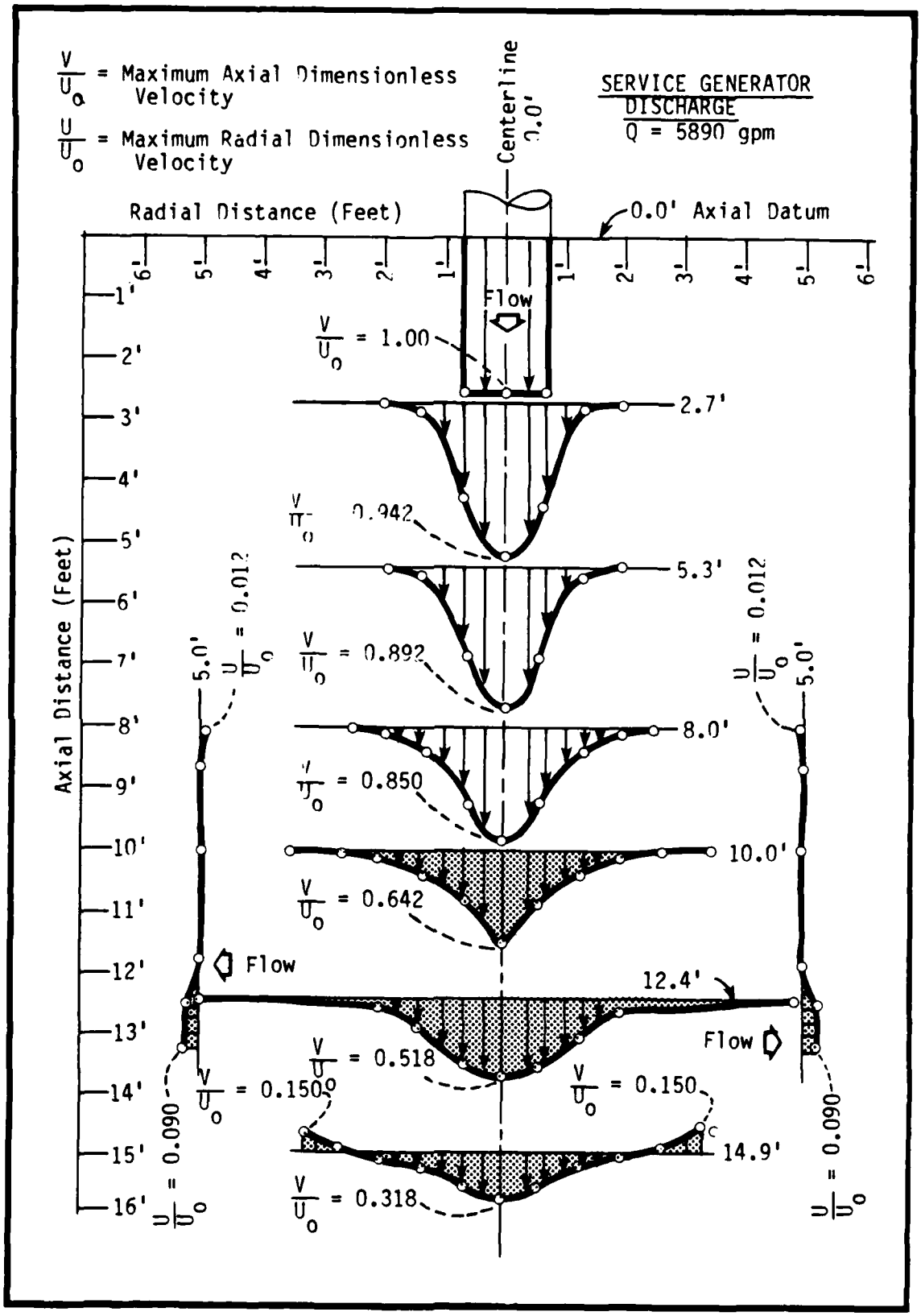

Figure B-6

Flow Field of Jet on Movable Boundary (Sand)

B.5.2.4 Scouring Mechanisms

From the jet on movable bottom tests, the following two types of scouring mechanisms were hypothesized:

Noncohesive Material (sand): the flow impinged onto the bottom layer, eroded the material, and created a scour hole in the stagnation region. The movement of the particles began when the bottom shear exceeded the critical shear. Away from the stagnation region jet flow characteristics were found, and the jet velocity decreased its strength in the radial direction. This dispersing led to deposition along the inner flanks of the scour hole -- reaching a dynamic equilibrium condition following an adequate period of time.

Cohesive Material (mud): the flow dug to the bottom and resulted in circulatory eddy patterns. Above the scour hole the boundary of the hole was bigger and deeper than the noncohesive material hole. In both cases bottom material was moved upward and carried by the current drifting under the ship, which increased the chance of sea-chest clogging.

The resulting scour holes for sand bed (to simulate sand) and walnut shell bed (to simulate mud) are shown in Figure B-7.

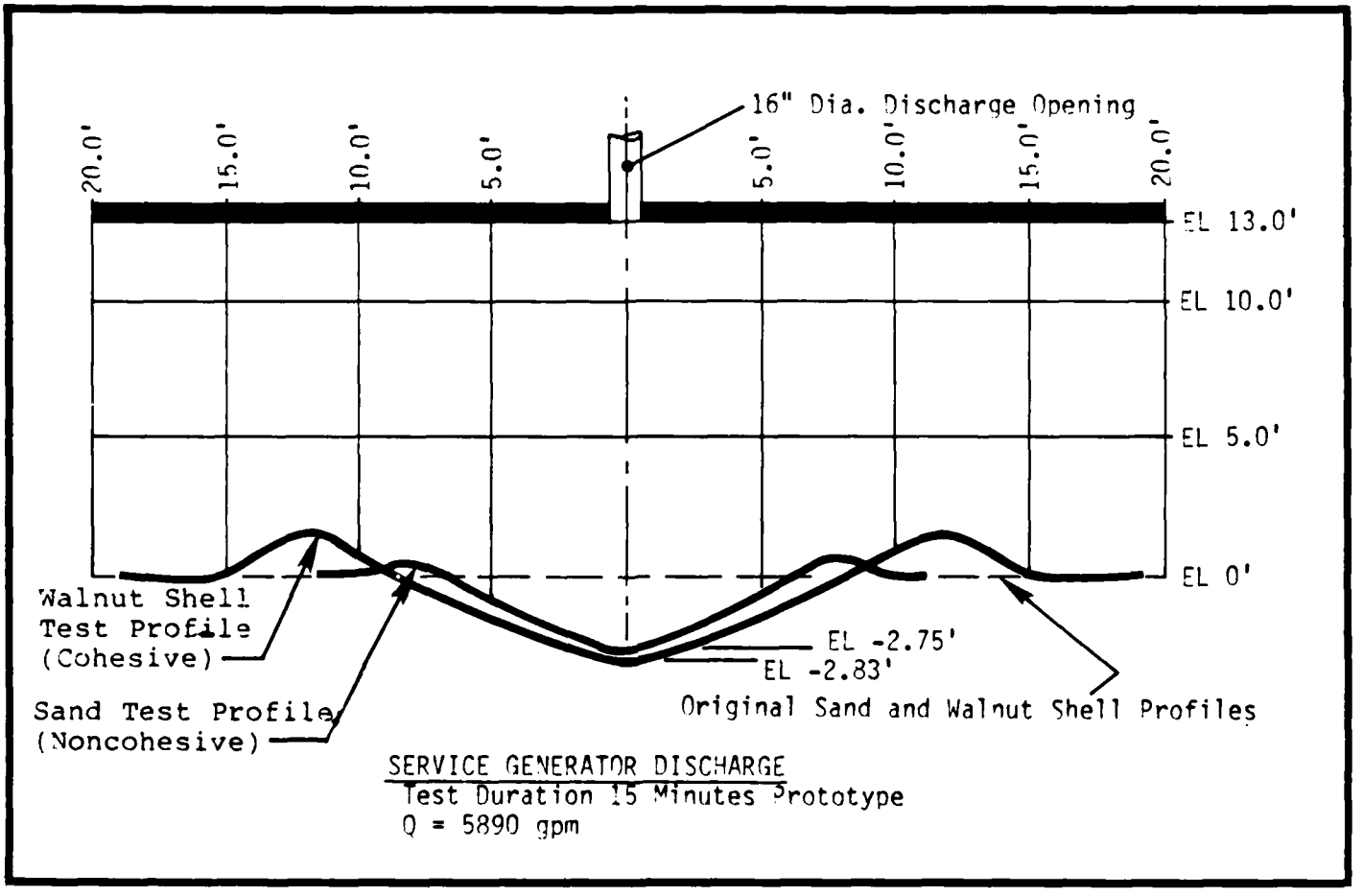

Figure B-7

Composite of Physical Model Scour Study

Appendix C,
Development of the Numerical Model

APPENDIX C
DEVELOPMENT OF THE NUMERICAL MODEL

C.1 THE ALGORITHM OF JET SIMULATION

The impingement of a jet on a flat or movable bottom has been observed by many investigators in the last two decades. [22] [24] [26] [29] The flow field of this problem has been defined in three regions: the free jet, impingement, and wall jet regions. Since laboratory data are available concerning jet impingement on a solid boundary, the present effort concerns the definition of a general equation for the problem based on the laboratory data, and the development of a numerical model to calculate the flow field under the impingement of a jet.

C.1.1 Free Jet Region

In the free jet region the flow characteristics are identical to those of the free jet. A dimensionless form of the axial velocity for a jet with diameter of the nozzle D may be obtained as follows:

$$\frac{V}{U_c} = e^{-0.0693\eta^2} \qquad \text{for } r \geq r_1 \qquad (1)$$

$$\frac{v}{U_c} = 1 \qquad \text{for } r < r_1 \qquad (2)$$

where $\eta = \dfrac{r - r_1}{b}$ and U_c is the axial velocity along the centerline, r is the radial distance from the center to the point of interest, and r_1 is the center core radius in the radial direction which can be expressed as:

$$r_1 = 0.39D - 0.065\,x \qquad \text{for } x \leq 6D \qquad (3)$$

$$r_1 = 0 \qquad \text{for } x > 6D \qquad (4)$$

where x is the axial distance from nozzle to the point of interest, and b = 0.115D + 0.087x.

C.1.2 Impingement Region

In the impingement region, the flow starts to change direction from the free jet to the wall jet. It was found that the axial velocity distributions along the radial direction for any given depth have the same form as the free jet region, that is:

$$\frac{V}{U_m} = e^{-0.0693\eta^2} \tag{5}$$

where U_m is the axial velocity at r_1 and given the following definitions:

$$\frac{U_m}{U_c} = 1, \quad \text{for } H \geq 6D \tag{6}$$

$$\frac{U_m}{U_c} = 1.15, \quad \text{for } H<6D \text{ and } H-x \leq 0.7D \tag{7}$$

$$\frac{U_m}{U_c} = 1, \quad \text{for } H<6D \text{ and } H-x>0.7D \tag{8}$$

H is the total depth from the nozzle to the flat bottom. If r_1 is greater than zero, then the axial velocity between the center to r_1 has the following form:

$$U = U_c + (U_m-U_c) \quad \lambda^2(2-\lambda^2) \tag{9}$$

where $\lambda = \frac{r}{r_1}$.

Tani and Komatsu [26] presented the jet centerline velocity with axial distance for three different water depths: four, eight, and twelve times the diameter of the nozzle. The solid line in Figure C-1 summarizes the results of their experimental data. There is difficulty in using these data to develop a general model for any total depth of interest, because there is no simple general form for the results. Based on Beltaos and Rajaratnam's study [29], a general trend for the total depth less than 5.17 nozzle diameters is presented in Figure C-2.

A new parameter was defined to analyze Tani and Komatsu's results for the total water depth equal to eight and twelve times the nozzle diameter. This parameter is U_R, the reference velocity, and is equal to the centerline velocity at the intersection of the free jet and impingement region. This point is located at a distance of about two nozzle diameters. Figure C-3 presents the result of the new approach, and shows the general form for the two different total depths.

A numerical model was developed to calculate the jet centerline velocities based on the least square fitting of Figures C-2 and C-3. If the total depth is less than six nozzle diameters, the jet centerline velocity was based on Figure C-2. Otherwise, it was based on Figure C-3. The numerical results for the jet centerline velocity is compared with the laboratory data in Figure C-1, and shows that the numerical results are in reasonable agreement with the experimental data.

C.1.3 Wall Jet Region

In the wall jet region the flow spreads out radially over the bottom. Figure C-4 illustrates the measured velocity resulting from various depths. Again, there is a general trend for the cases of the total depth of eight or twelve nozzle diameters. A least square fitting for these two curves presents the general form for the case of a total depth greater

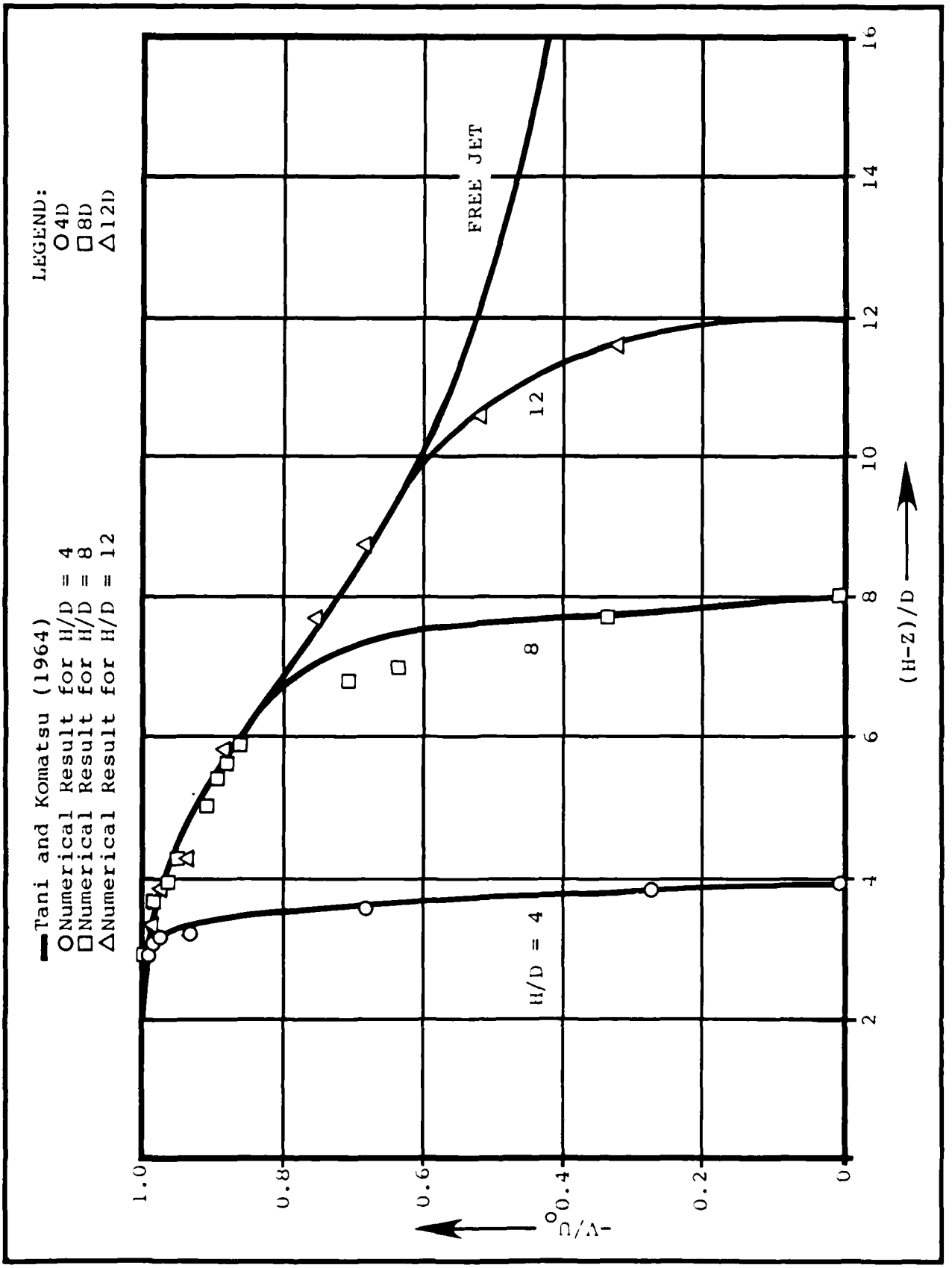

Figure C-1
Variation of Jet Centerline Velocity with Distance from Seachest Discharge

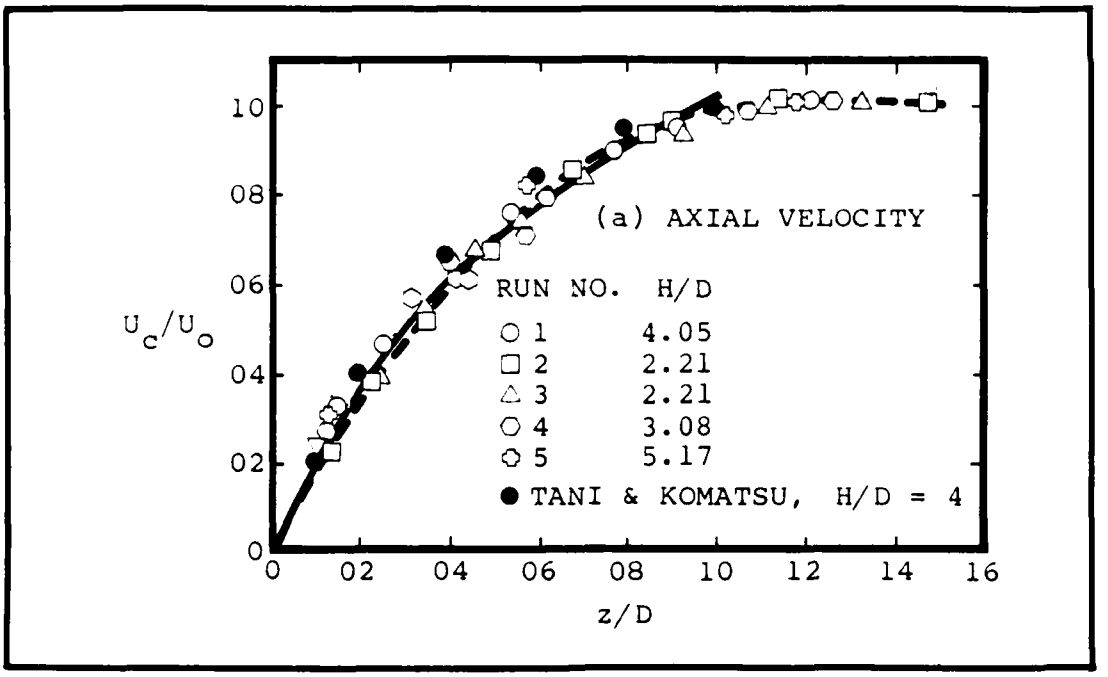

Figure C-2

Variation of Circular Jet Centerline Velocity from the Bottom (Beltaos and Rajaratnam, 1977)

than six nozzle diameters. For the case of a total depth less than six nozzle diameters, the calculation is based on the four nozzle diameter measurements.

C.1.4 The Bottom Pressure and the Shear Stress

The bottom velocity distribution derived from the surface pressure is presented in Figure C-5, and the bottom pressure distribution is shown in Figure C-6. A comparison between the numerical results and the laboratory data reveals reasonable agreement.

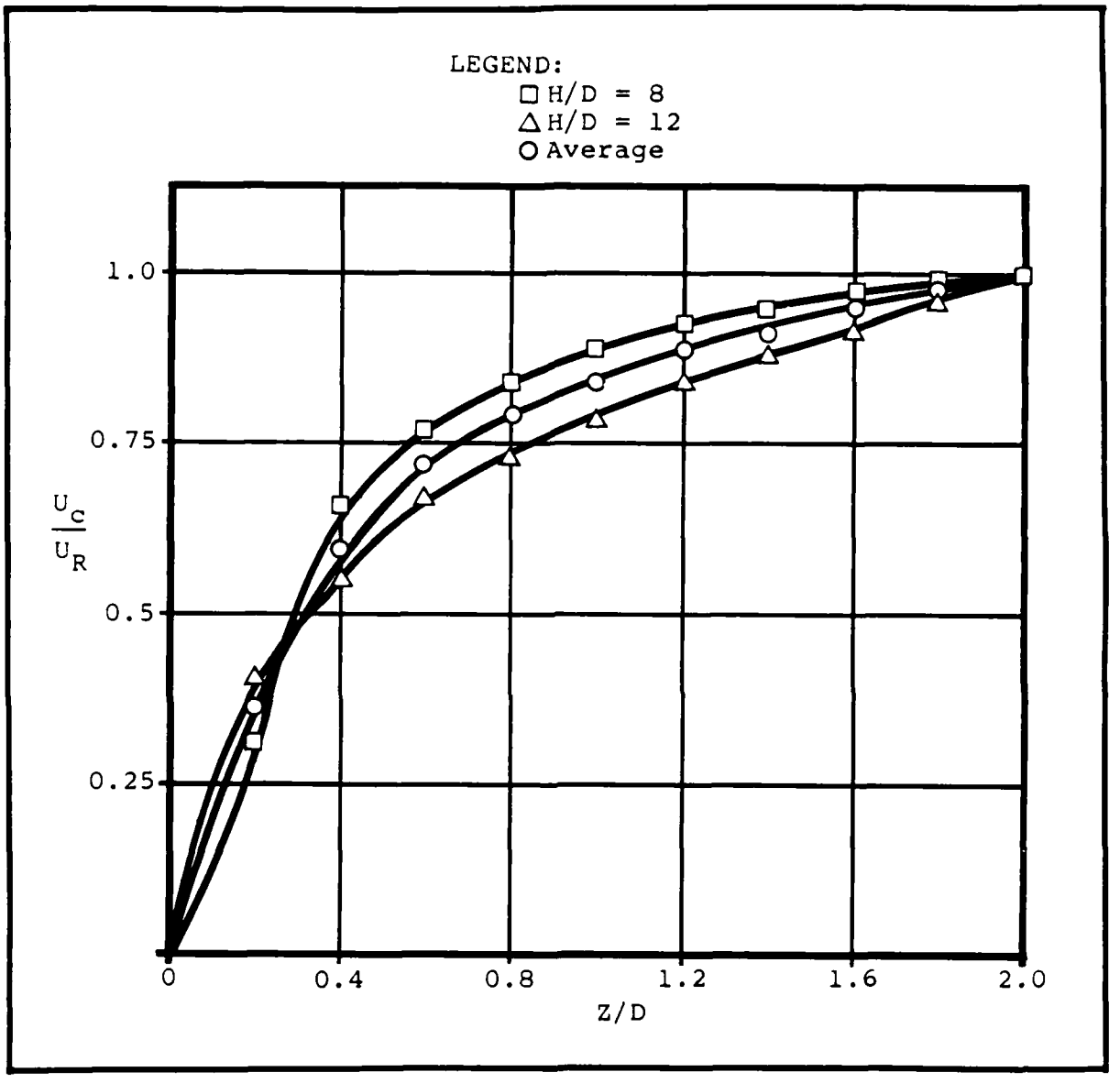

Figure C-3

Variation of Circular Jet Centerline Velocity from the Bottom

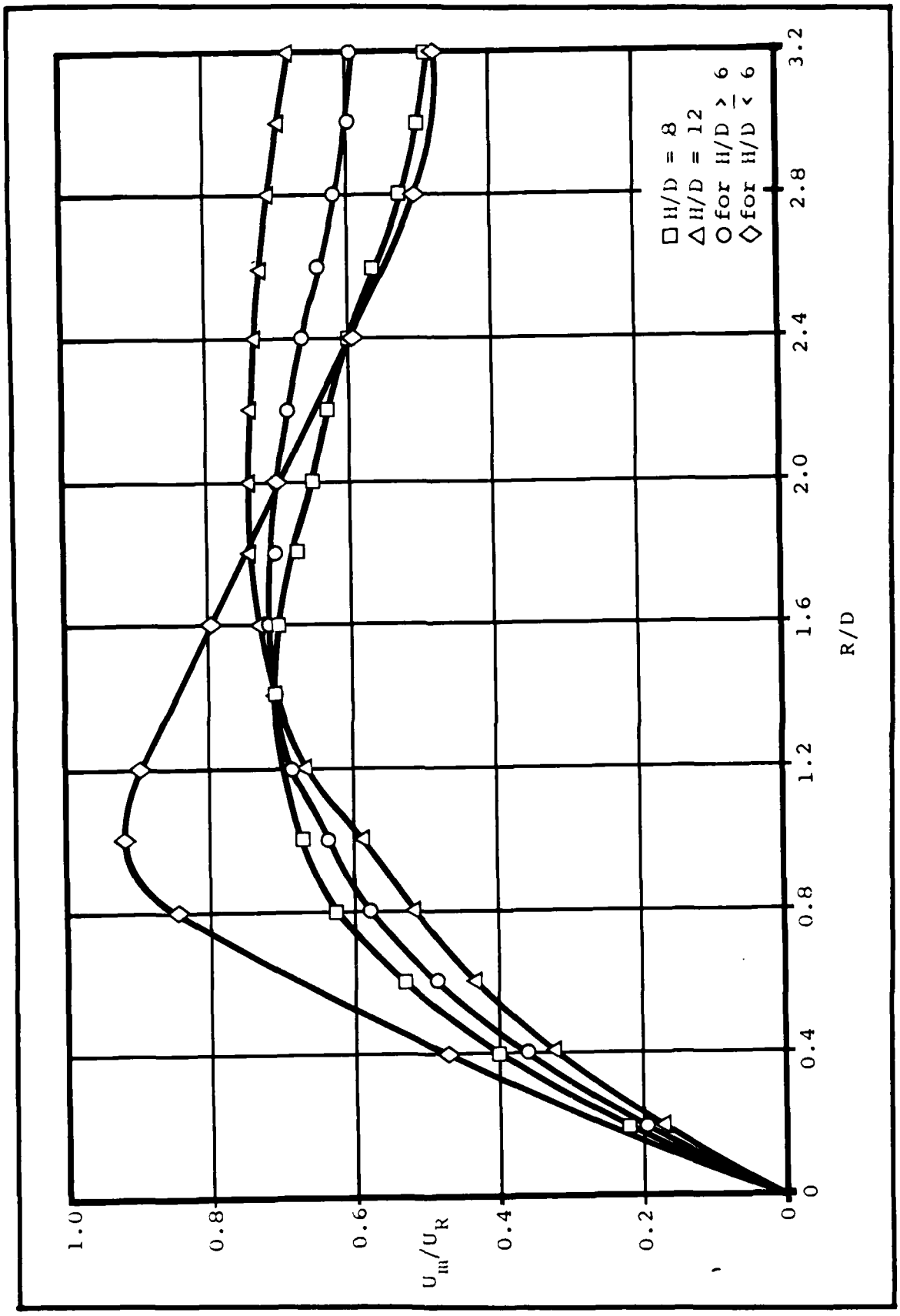

Figure C-4

Dimensionless Variation of the Radial Velocity (Peak Velocity) with Radial Distance

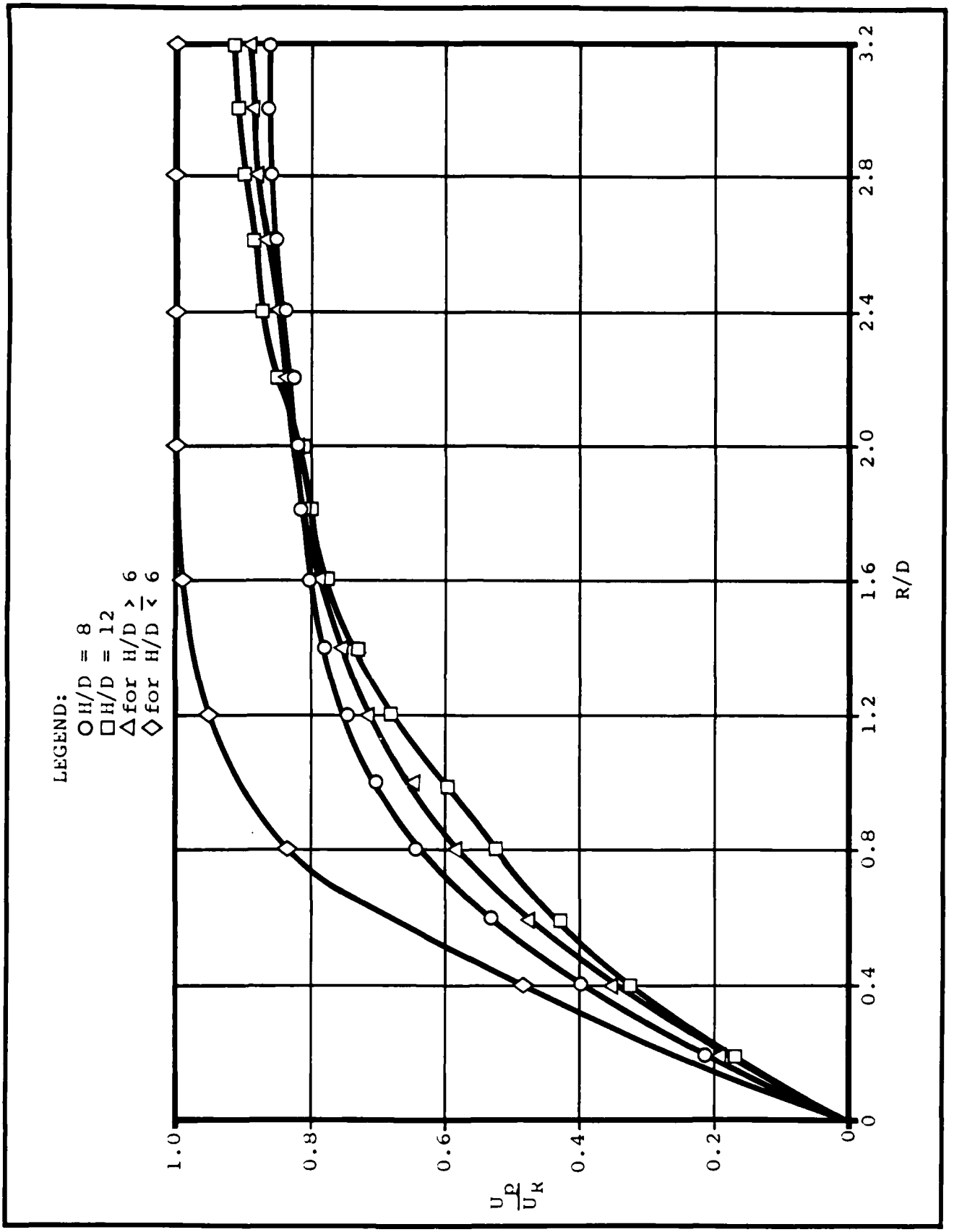

Figure C-5

Dimensionless Variation of the Radial Velocity (Derived from Surface Pressure Distribution) with Radial Distance

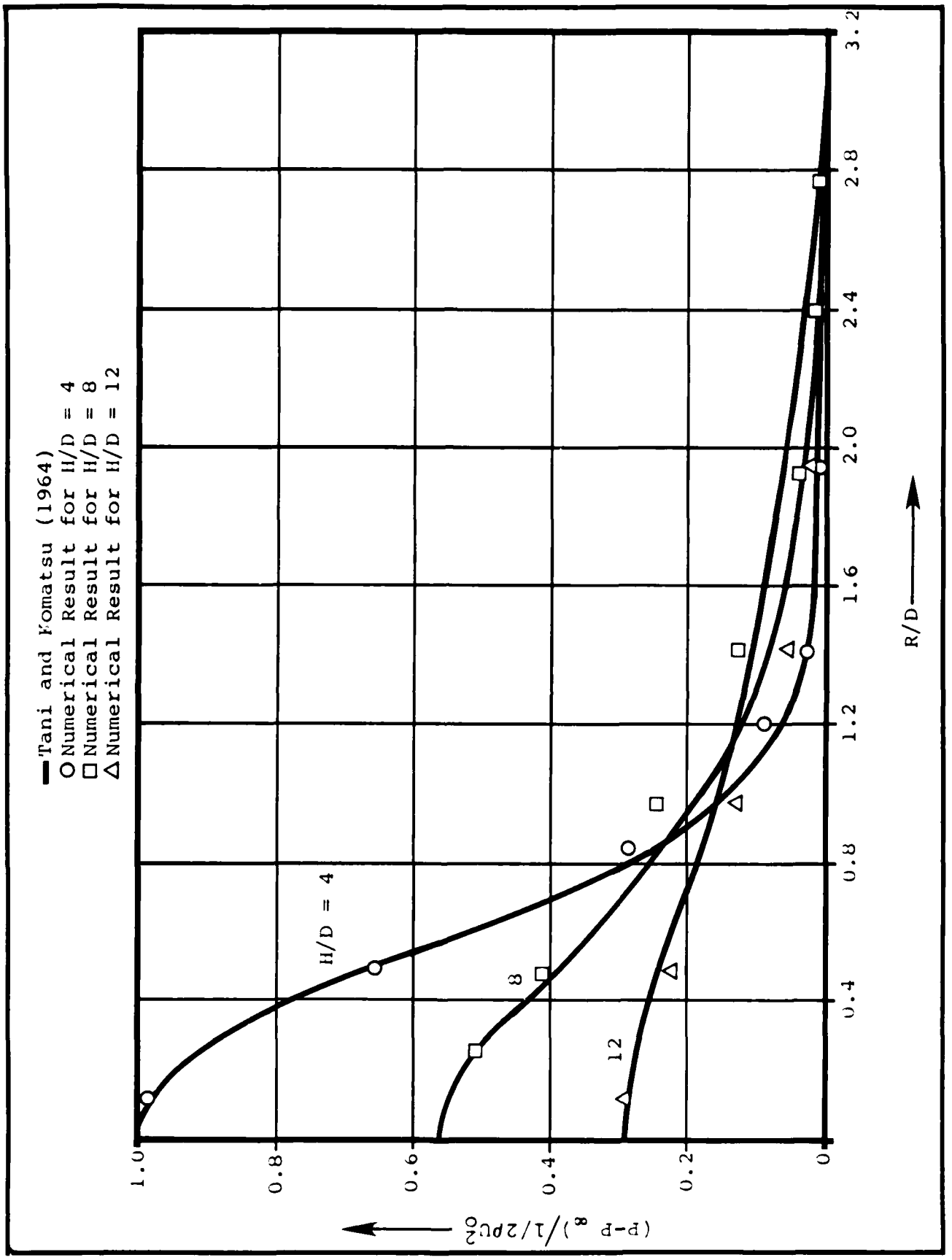

Figure C-6

Variation of Surface Pressure with Radial Distance

It was found that the shear stress can be derived from the following empirical results:

$$\tau = 1.270 \frac{\rho K}{H^2} \left(\frac{\sqrt{K}}{\nu}\right)^{-1/2} \frac{r}{H}, \quad \text{for } \frac{r}{H} < 0.03 \qquad (10)$$

and

$$\tau = 0.3 \frac{\rho K}{H^2} \left(\frac{\sqrt{K}}{\nu}\right)^{-0.3} \left(\frac{r}{H}\right)^{-2.3}, \quad \text{for } \frac{r}{H} > 0.3 \qquad (11)$$

where

ρ = the density of the fluid

$K = \frac{\pi U_o^2 d^2}{4}$

U_o = the average velocity at the jet nozzle

d = the diameter of the jet nozzle

H = the distance from the nozzle to the bottom

ν = the kinematic viscosity of the fluid

r = the radial distance from the centerline to the location of interest.

The numerical calculation for the shear stress was based on this relationship, and is shown in Figure C-7.

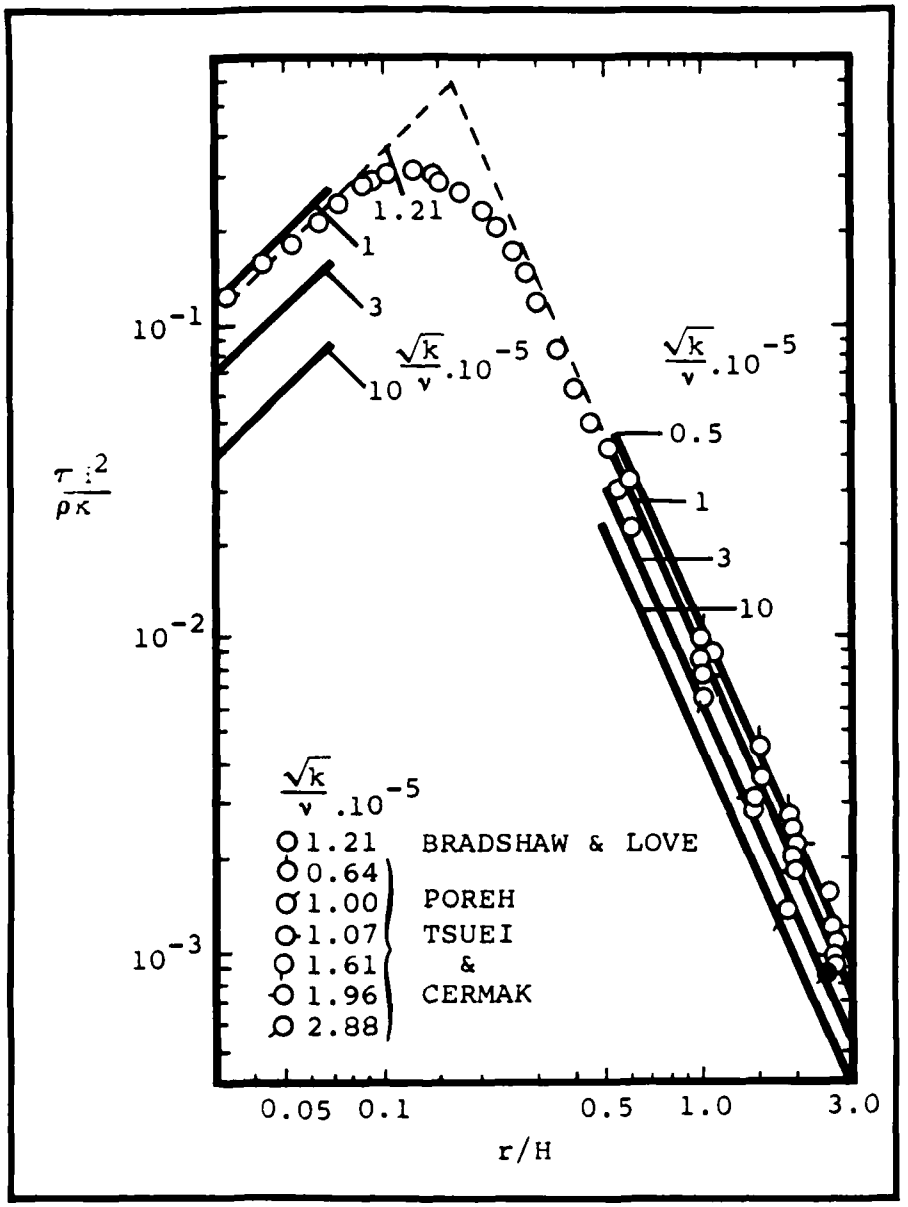

Figure C-7
Shear Stress Distribution

C.1.5 Movable Boundaries

There is little existing data on jet impingement on movable boundaries. The numerical model for the jet impingement on a movable bottom was developed in this study based on

laboratory data. The data were obtained from the tests of 5- and 13-foot underkeel clearances. The jet nozzle diameter was 16 in. Two different bottom materials were used for each depth: sand (to simulate sand), and walnut shells (to simulate mud).

C.2 THE ALGORITHM OF SINK SIMULATIONS

C.2.1 Governing Equations

In simulating the sink the flow is assumed to be inviscid, incompressible, and irrotational. The stream function, ψ, can be defined by:

$$U = \frac{1}{r} \frac{\partial \psi}{\partial z} \tag{11}$$

and

$$W = \frac{1}{r} \frac{\partial \psi}{\partial r} \tag{12}$$

where r is the radial coordinate, z is the axial coordinate, and U and W are the radial and axial components of fluid velocity, respectively. The equation of irrotationality in axisymmetric flow is:

$$\frac{\partial U}{\partial z} - \frac{\partial W}{\partial r} = 0 \tag{13}$$

Substituting Equations 11 and 12 into Equation 13 yields the following equation for the stream function:

$$\frac{\partial^2 \psi}{\partial r^2} + \frac{\partial^2 \psi}{\partial z^2} - \frac{1}{r} \frac{\partial \psi}{\partial r} = 0 \tag{14}$$

C.2.2 Boundary Conditions

The boundary conditions applied to the sink model are as follows: (1) the stream function ψ along the centerline and the surface at the bottom is a constant, and is set to zero,

(2) it is assumed that the fluid velocity U_o across the boundaries of the incoming flow is constant, therefore the stream function ψ at the sink opening is equal to $1/2\ U_o r^2$., (3) the stream function ψ on the free surface is constant and is equal to $1/2\ U_o r_o^2$, where r_o is the radius of the sink opening, and (4) the downstream stream function ψ along the axial direction at $r = R$ is set equal to the stream function value at $r = R - \Delta r$, where R is the total radial distance in the calculation, and Δr is the grid increment in the radial direction.

C.2.3 Finite Difference Form

Let ψ_{ij}, U_{ij} and W_{ij} represent $\psi(r_i, z_j)$, $U(r_i, z_j)$ and $W(r_i, z_j)$, respectively. The notation (i, j) indicates the intersecting point of the axial grid line passing through r_i and the radial grid line through z_j. The increment of the radial grid is equal to Δr, and the increment of the axial grid is equal to Δz. The finite-difference approximations of the partial derivatives then becomes:

$$\frac{\partial \psi_{ij}}{\partial r} = \frac{\psi_{i+1,j} - \psi_{i-1,j}}{2\Delta r}\ , \tag{15}$$

$$\frac{\partial^2 \psi_{i,j}}{\partial r^2} = \frac{\psi_{i+1,j} - 2\psi_{i,j} + \psi_{i-1,j}}{(\Delta r)^2} \tag{16}$$

and

$$\frac{\partial^2 \psi_{i,j}}{\partial z^2} = \frac{\psi_{i,j+1} - 2\psi_{i,j} + \psi_{i,j-1}}{(\Delta z)^2} \tag{17}$$

Substituting Equations 15, 16, and 17 into Equation 14, one obtains:

$$\psi_{i,j} = \frac{1}{\left(\frac{2}{\Delta r^2} + \frac{2}{\Delta z^2}\right)} \left(\frac{\psi_{i+1,j} + \psi_{i-1,j}}{\Delta r^2} + \frac{\psi_{i,j+1} + \psi_{i,j-1}}{\Delta z^2} - \frac{1}{r_{i,j}} \frac{\psi_{i+1,j} - \psi_{i-1,j}}{2\Delta r} \right) \tag{18}$$

When Equation 18 is applied to all the interior points, there are (m-2) (n-2) algebraic equations that automatically include the boundary conditions, where m and n are the total number of increments in the axial and radial directions of the rectangular region. Theoretically, it is possible to solve these equations for values of ψ at the interior grid points; but this direct procedure is tedious and time-consuming, especially when the number of grid points is large. The present numerical model uses the successive over-relaxation (S.O.R.) method to solve the problem. This method used the following iteration scheme for a rectangular domain instead of Equation 18:

$$\psi_{i,j}^{(k+1)} = (1-w)\psi^{k}_{i,j} + \frac{w}{(\frac{2}{\Delta r^2} + \frac{2}{\Delta z^2})}\left(\frac{\psi_{i+1,j} + \psi_{i-1,j}}{\Delta r^2}\right.$$

$$\left. + \frac{\psi_{i,j+1} + \psi_{i,j-1}}{\Delta z^2} - \frac{1}{r_{ij}} \frac{\psi_{i+1,j} - \psi_{i-1,j}}{2\Delta r}\right) \quad (19)$$

where k represents the kth iteration.

The values of ψ are computed for the next iteration by executing Equation 19 at every interior point based on the values of ψ at the current iteration. The sequence of computation starts from the upper left-most interior point, proceeds downward until reaching the bottom, and then moves to the top of the next axial line on the right.

This process is repeated until the next value of ψ at the last interior point at the lower right corner has been obtained. In this model, the values of ψ are first estimated at all interior points, in addition to those prescribed at the boundary. These values are:

$$\psi^{o}_{i,j} = \frac{1}{4} U_o r_o^2 \quad (20)$$

The value of w in Equation 19 is a constant, and

$$w = \frac{8 - 4\sqrt{4-\alpha^2}}{\alpha^2} \tag{21}$$

where

$$\alpha = \cos(\frac{\pi}{m}) + \cos(\frac{\pi}{n}).$$

The error of the stream function values is defined as:

$$\xi = \sqrt{\sum_{i=2}^{m-1}\sum_{j=2}^{n-1}(\frac{\psi_{i,j}^{k+1} - \psi_{i,j}^{k}}{\psi_{i,j}^{k}})^2 \cdot \frac{1}{(m-2)(n-2)}} \tag{22}$$

In the present model if the value of ξ is less than 0.01, the iteration will be stopped with the final value of the stream function given. The central finite-difference approximations for the axial and radial velocities are:

$$U_{ij} = \frac{1}{r_{ij}} \frac{\psi_{i,j+1} - \psi_{i,j-1}}{2\Delta z} \tag{23}$$

and

$$W_{ij} = \frac{1}{r_{ij}} \frac{\psi_{i+1,j} - \psi_{i-1,j}}{2\Delta r} \tag{24}$$

On the boundary, the forward or backward finite-difference approximations may be used for the axial and radial velocities. They are:

$$U_{ij} = \frac{1}{r_{ij}} \frac{\psi_{i,j+1} - \psi_{ij}}{\Delta z} \tag{25}$$

and

$$W_{ij} = \frac{1}{r_{ij}} \frac{\psi_{i+1,j} - \psi_{ij}}{\Delta r} \tag{26}$$

When i equals one, then r_{ij} is zero. The axial and radial velocities were then assumed to be equal the value at i equals two:

$$U_{1j} = U_{2j} \tag{27}$$

and

$$W_{1j} = W_{2j} \tag{28}$$

After the finite-difference form of the sink mode was constructed, the development of the numerical model for the sink problem proceeded.

Appendix D,
Key Words and Definition

APPENDIX D
KEY WORDS AND DEFINITIONS

Aircraft Carrier	A ship equipped with a takeoff and landing deck, and designed to serve as a base for aircraft operations.
Berthing Area	The port or harbor slips where vessels are anchored.
Critical Shear Stress	A threshold value of the shear stress, above which the particle starts to move from its resting position.
Diffuser	A structure which serves the function of spreading fluid flow through various arrangements to reduce the flow concentration or velocity intensity.
Discharge	Amount of fluid flow released from a storage or a fluid impelling system.
Draft	The vertical distance from the top of the keel plate of a vessel to the load waterline.
Fall Velocity	The average terminal settling velocity of a single particle in distilled water.
Flocculating	The collection or uniting of suspended sediment to form a mass.
fps	feet-per-second
gpm	gallons-per-minute

Keel Clearance	The clear space between a vessel's keel plate and the sea bottom.
Light off	The operation involved in preparation of a vessel's departure from a harbor.
Main Circulating Cooling System	A circulating water system that provides for cooling of a vessel's main circulating system.
Marine Organism	Biological species which exist in the marine environment.
MLW	Mean low water
Movable Boundary	A boundary that can be deformed by external pressures.
Sea Chest	A pipe between a ship's side and a flow control device for transporting water.
Sea Floor	The bottom of the ocean.
Service Generator Cooling System	A circulating water system that provides for cooling of a vessel's service generator.
SG	See Service Generator Cooling System.
Solid Boundary	A boundary that cannot be deformed by pressure force.
Solidification	A procedure which hardens a material into a solid state.

Appendix E,
Annotated Bibliography

APPENDIX E

ANNOTATED BIBLIOGRAPHY

[1] Jones, S. H., Cdr., USN., CVN 68 Class Condenser Fouling. U.S. Navy, April, 1980, 9 figs.
The condenser fouling problems of an aircraft carrier are described.

[2] Brehmer, M. L., Nichols, M. M., and Calder, D. R. Study and Control of Marine Fouling Organisms, Naval Base, Norfolk, Virginia. Virginia Institute of Marine Science, Gloucester Point, Virginia, February, 1967, 4 figs., 8 tables.
The authors investigate the biology and distribution of marine organism, including current velocity and sediment characteristics, and identify the silver hydroid and the fleshy bryozoan as being primarily responsible for condenser fouling resulting in vessel operational difficulties.

[3] Shidler, J. K. and MacIntyre, W. G., "Hydrographic Data Collection for 'Operation James River - 1964'." Data Report No. 5. Virginia Institute of Marine Science, Gloucester Point, Virginia, October, 1967, 3 figs., 5 tables.
This report presents collected hydrographic data on the James River estuary for verification of an hydraulic model and for calculation of circulation dynamics in the James River.

[4] Hoffman, J. F., "Investigation into Deep-Draft Vessel Berthing Problems at Selected U. S. Naval Facilities." Report No. 4914-801. E G & G Washington Analytical Services Center, Inc., Rockville, Maryland, October, 1980, 21 figs., 16 tables.
This report provides a detailed investigation of shoaling and addresses sediment control problems, such as retardation of deposition of sediments or flushing of resuspended sediments, in the pier slips and associated waterways of six deep-draft harbors used by the U. S. Navy. Information on marine organism fouling at Norfolk Naval Station is also presented.

[5] Nichols, M. M., "Sediments of the James River Estuary, Virginia." Memoir 133. The Geological Society of America, Inc., New York, 1972, pp. 169-212, 28 figs., 1 table.

This article reports the distribution, composition, chemistry and characteristics of the sediments in the James River Estuary, Virginia.

[6] Van Dorn, W. G., et al., "The Evaluation of Sediment Management Procedures Phase II Final Report 1975-1976." SIO Reference 77-10. Scripps Institution of Oceanography, La Jolla, California, August, 1977, 42 figs., 4 tables.

This report summarizes a study of a number of sedimentation removal techniques and recommends the resuspension of sediments by submerged hydraulic jet method. Physical model of a berthing complex using a phased array of ten radial jets was built and tested. The report also includes the current and (mud) sediment information near Pier 12 area in Norfolk Harbor.

[7] Environmental Impact Assessment: Norfolk Naval Base Complex Long-Range Maintenance Dredging Program. Arthur D. Little, Inc., Massachusetts, February, 1976, 22 figs., 19 tables.

This report provides the environmental impact assessment on the maintenance dredging for the Norfolk Naval Base Complex. Conclusions from the study indicate that the maintenance dredging will redistribute polluted sediments and adversely affect estuaraine biota.

[8] U. S. Army Corps of Engineers. Norfolk Harbor and Channels, Virginia, Deepening and Disposal, Feasibility Report and Appendices. U. S. Army Corps of Engineers, Norfolk District, July, 1980.

This report addresses and evaluates possible solutions for two problems: first, the existing disposal needs facing Norfolk Harbor and adjacent waters, and second, the need for improved and expanded channels and anchorages.

[9] Fang, C. S., et al., "Physical and Geological Studies of the Proposed Bridge-Tunnel Crossing of Hampton Roads near Craney Island." Special Report in Applied Marine Science and Ocean Engineering No. 24. Virginia Institute of Marine Science, Gloucester Point, Virginia, August, 1972, 10 figs., 20 tables.

This report is divided into four parts. Part 1 presents the hydraulic model study of the effects of a proposed river crossing structure on the tides, currents and distribution of sea salts and sediments at Hampton Roads near Craney Island. Part 2 investigates the impact from the proposed bridge-tunnel model study on the shoreline, Hampton Flats and Newport News Point area. Part 3 reports the field survey of currents in the Newport News area using the drogued buoys. Part 4 presents the hydraulic model test results of tidal currents.

[10] Chen, H. S., "A Storm Surge Model Study Volume II A Finite Element Storm Surge Analysis and its Application to a Bay-Ocean System." Special Report No. 189 in Applied Science and Ocean Engineering. Virginia Institute of Marine Science, Gloucester Point, Virginia, September, 1978, 86 figs., 9 tables.

This report describes the development of a two-dimensional storm surge model for calculation of water elevation and circulation subject to the effect of a hurricane, in the James River estuary and Chesapeake Bay area. The storm surge model was first used to simulate tides in the Chesapeake Bay until tide simulation was satisfactory, then a storm surge hindcast was conducted in the Chesapeake Bay and its Virginia Atlantic nearshore area.

[11] Jacobson, J. P. and Fang, C. S., "Flood Wave-Tide Wave Interaction on the James River During the Agnes Flood." Studies of Certain Impacts of Tropical Storm Agnes on the Chesapeake Bay and its Tributaries. Virginia Institute of Marine Science, Gloucester Point, Virginia, August, 1974, pp. 119-130.

This article summarizes the tidal height data and current measurement at the James River during the Agnes Flood. The authors concluded that the flood did significantly affect the water level in the upper portion of the tidal James. However, in the lower portion of the James River, no discernible rise was evident due to the passage of the flood wave.

[12] Namias, J. and Dunn, C. R., "The Weather and Circulation of August, 1955." Monthly Weather Review. Vol. 83, No. 8, August, 1955, pp. 163-170, 8 figs., 1 table.

This article presents the characteristic atmospheric circulation during August 1955. The weather information over the Northeast United States, where flood-producing rains associated with hurricanes Connie and Diane, are also reported.

[13] Chapman, W. T., Jr., and Sloan, Y. T., "The Paths of Hurricanes Connie and Diane." Monthly Weather Review. Vol. 83, No. 8, August, 1955, pp. 171-180, 13 figs.

This article deals with two hurricanes, Connie and Diane, which crossed the North Carolina Coast near the middle of August 1955 and inflicted great damage over a large area of the eastern seaboard. The tracks and surface maps of these hurricanes are reported.

[14] Ruzecki, E. P. and Ayres, R., "Suspended Sediments Near Pier 12, Norfolk Navy Base, on 26 June and 15 September, 1973." Data Report No. 11. Virginia Institute of Marine Science, Gloucester Point, Virginia, October, 1974, 2 figs., 30 tables.

This report summarizes the results of two suspended sediment studies near Norfolk Naval Base Pier 12 area. Salinity, temperature and current velocity information are also provided in conjunction with suspended sediment samples at five stations.

[15] Neilson, B. and Boule, M. Oceanographic, Water Quality, and Modeling Studies for the Outfall from a Proposed Nansemond Waste Water Treatment Plant. Vol. 2 An Analysis of Currents and Circulation in Hampton Roads, Virginia. Virginia Institute of Marine Science, Gloucester Point, Virginia, January, 1975, 98 pp., 39 figs., 5 tables.

The investigation of the water circulation in Hampton Roads concluded that it is dominated by tidal currents. Results of current measurements from the James River Hydraulic Model demonstrate all of the essential features of the tidal circulation in prototype.

[16] Malloy, R. J. U. S. Navy Harbor Maintenance Dredging Atlas (CONUS). (Preliminary Outline Copy) Foundation Engineering Division, Civil Engineering Laboratory, Port Hueneme, California, April, 1980, 21 figs.
This article discusses dredging and alternative methods for Navy harbors. Sediment types and sediment prevention systems are also reported.

[17] O'Connor, D. J. and Lung, W., "Suspended Solids Analysis of Estuarine Systems." ASCE Journal of the Environmental Engineering Division, Vol. 107, No. EEI, February, 1981, pp. 101-120, 12 figs.
A two-layer salinity and suspended solids model for estuarine systems is reported. The model includes the considerations of a seaward advective flow in the surface layers, landward in the bottom layer, vertical advective flow, vertical dispersion across the layer interface, and the settling of suspended solids. Velocity, salinity and suspended solids distributions of the James River estuary are also reported.

[18] Krone, R. B., "A Study of Rheologic Properties of Estuarial Sediments." Technical Bulletin No. 7. U. S. Army Corps of Engineers, Committee on Tidal Hydraulics, September, 1963, 38 figs., 10 tables.
The author provides information on rheological properties of sediments from a variety of estuaries including the stability of deposits and the characteristics of sediment during transport. Data on shear strength and relative differential viscosity of soil samples are also reported.

[19] Kranck, K., "Sediment Deposition from Flocculated Suspensions." Sedimentology, Vol. 22, No. 1, February, 1975, pp. 111-123, 10 figs.
This article reports the sediment deposition from flocculated suspensions in coastal environments which is part of the composition of mud. The nature and formation of flocculated sediments and their settling characteristics is discussed.

[20] Shelley, P. E., "Sediment Measurement in Estuarine and Coastal Areas." NASA CR 2769, National Aeronautics and Space Administration, Washington, D. C., December, 1976, 17 figs., 5 tables.

This report discusses the direct and indirect methods of measuring and preserving sediments in estuarine and coastal areas. Sediment mechanics, including sediment sources, characteristics and transport, are also discussed.

[21] Hancock, D. A., Drinnan, R. E., and Harris, W. N., "Notes on the Biology of Sertularia Argentea L." Journal, Marine Biological Association, Vol. 35, 1956, pp. 307-325, 5 figs., 4 tables.

This article presents the investigation of the biology of the hydroids including their growth and regeneration. The findings are a) the growth is seasonal, occurring mostly in the summer months and b) the regeneration of cut stems and detached side branches are possible.

[22] Poreh, M. and Hefez, E., "Initial Scour and Sediment Motion Due to an Impinging Submerged Jet." Proceedings, Twelfth Congress of the International Association for Hydraulic Research, Fort Collins, Colorado, September 11-14, 1967, Vol. 3, pp. 9-16, 10 figs.

A theoretical analysis and experimental study of the initial sediment motion and scour caused by a circular submerged jet impinging on a flat erodible boundary is presented. The region in which initial motion of sediments may occur is predicted by generalizing Shields' criterion for the critical shear stress in open channel flows.

[23] Westrich, B. and Kobus, H., "Erosion of a Uniform Sand Bed by Continuous and Pulsating Jets." Proceedings, Fifteenth Congress of the International Association for Hydraulic Research, Turkey, 1973, Vol. 1, pp. 91-98, 8 figs.

An experimental investigation of erosion of a uniform sand bed by a vertical submerged jet is presented. Analysis of results show that the momentum flux of the jet and the distance between jet nozzle and sediment bed determines the rate of scour.

[24] Kobus, H., Leister, P., and Westrich, B., "Flow Field and Scouring Effects of Steady and Pulsating Jets Impinging on a Movable Bed." Journal of Hydraulic Research, Vol. 17, No. 3, 1979, pp. 175-192, 12 figs.

The flow field and erosion pattern of a continuous and pulsating impinging jet were studied experimentally. The mean velocity field as well as the turbulent and pulsation components, wall pressure and wall shear stress distributions are reported.

[25] Yalin, M. S. and Karahan, E., "Inception of Sediment Transport." ASCE Journal of the Hydraulics Division, Vol. 105, No. HY11, November, 1979, pp. 1433-1443, 5 figs., 1 table.

This article presents the investigation on the mass transport of sediments in open channel having movable boundaries. The prediction of the critical shear stress corresponding to the inception of sediment transport in fluvial hydraulics is reported. An extended Shields' diagram is also included in this paper.

[26] Tani, I. and Komatsu, Y., "Impingement of a Round Jet on a Flat Surface." Proceedings, Eleventh International Congress of Mechanics, Munich, 1964, pp. 672-676, 7 figs.

An experimental study of circular jet impingement on a flat surface is reported. The experimental analysis was performed using similarity solution for calculating jet centerline velocity and radial velocity. The study also compares analytical results with experimental findings.

[27] Rajaratnam, N., "Plane Turbulent Compound Wall Jets." Journal of Hydraulic Research, Vol. 10, No. 2, 1972, pp. 189-203, 10 figs.

Reports a simple method of predicting the variation of the velocity and length scale and the wall shear stress for the problem of the plane wall jet. This method was based on similarity analysis, integral momentum equation, dimensional analysis and available experimental data.

[28] Beltaos, S. and Rajaratnam, N., "Impinging Circular Turbulent Jets." ASCE Journal of the Hydraulics Division, Vol. 100, No. HY10, October, 1974, pp. 1313-1328, 15 figs., 1 table.

Presents an analytical and experimental study of the impingement region of circular turbulent impinging jets. Wall pressure and velocity fields are reported. A semi-empirical method developed to predict the variation of the axial velocity is discussed as well as an analytical method developed to assess the wall shear stress profile.

[29] Beltaos, S. and Rajaratnam, N., "Impingement of Axisymmetric Developing Jets." Journal of Hydraulic Research, Vol. 15, No. 4, 1977, pp. 311-326, 8 figs., 2 tables.

An experimental and analytical study of developing jets, impinging on a smooth wall, is presented. Measurements of the velocity field and static pressure in excess of ambient and wall shear stress are reported.

[30] Kline, S. J., Abbott, D. E., and Fox, R. W., "Optimum Design of Straight-Walled Diffusers." Journal of Basic Engineering, Vol. 81, No. 9, September, 1959, pp. 321-331, 8 figs., 1 table with discussion.

This article discusses four common optimum problems in diffuser design. Included in the discussion are the effects of geometrical and non-geometrical parameters. Derivation of diffuser head losses and the minimization of this head loss are also provided.

[31] Ho, G. C., Diaz, R. J., and Neilson, B. J., "Evaluation of Ventra Vacs at Pier 12 Naval Base, Norfolk, Virginia." Special Report No. 228 in Applied Marine Science and Ocean Engineering, Virginia Institute of Marine Science, Gloucester Point, Virginia, September, 1979, 12 figs., 8 tables.

The authors summarize the field and flume study of the Ventra Vac units to resolve suction fouling problems on deep-draft vessels. Field study of currents, water quality, bathymetry and the distribution and entrainment of marine organisms at Pier 12 area is reported. Flume tests to determine the characteristics of the marine organisms are also described.

[32] Diaz, R. J. Distribution and Hydrodynamic Properties of Fouling Organisms in the Pier 12 Area of the Norfolk Naval Station. Virginia Institute of Marine Science, Gloucester Point, Virginia, 1980, 1 fig., 5 tables.

This article reports the distribution and hydrodynamic properties of the silver hydroid and fleshy bryozoans in Hampton Roads area of the Norfolk Harbor, Virginia.

Appendix F,
User's Manual-Numerical Program

APPENDIX F
USER'S MANUAL
NUMERICAL PROGRAM

F.1 ORIGIN OF THIS PROGRAM

The program documented herein was developed by Hydro Research Science (HRS, Inc.) of Santa Clara, California under ONR contract Number N00014-80-C-0395 dated 80 MAR 17.

F.2 PURPOSE OF THE PROGRAM

This simulation program has been designed to analyze underkeel flow field characteristics under the influence of combined sea chest discharge jet and suction. The purpose of the analysis is to assist in judging CVN class sea chest ingestion of suspended sediments.

The two bottom boundary conditions simulated were flat and movable bottoms. The bottom materials involved in the simulations were sand and mud.

F.3 HARDWARE AND SOFTWARE REQUIREMENTS

This numerical model has been written for standard FTN compiler executions of the CDC 7600 machine. These codes can also be compiled and executed on other machines such as IBM computer systems. The CPU time is about 5 seconds for the flat-bottom problem, and 0.7 seconds for the movable-bottom problem.

F.4 GENERAL DESCRIPTION OF THE PROGRAM

The present flat-bottom numerical model will simulate the flow field of combined jet and suction. It also simulates the bottom pressure and the bottom shear stress under the impingement of a discharger jet. The input data for the model includes: (a) the diameters of the jet and the suction, (b) the distance

from the jet center to the suction center, and (c) the flow rate and depth from the jet (or suction) to the bottom.

The jet and suction are treated separately in computation procedures. The advantage of this approach is the use of an axisymmetrical flow field assumption, which is good for both jet and suction problems.

Based on the numerical results, which showed that if the radial distance from the center of the jet (or suction) to the point of interest is greater than three jet (or suction) diammeters, then the kinematics are negligible. This was also supported by the HRS physical model test results. In the present problem, the distance from the jet center to the suction center is much greater than triple the diameter of the jet (or suction).

The flow field for a movable-bottom boundary was simulated under the impingement of a jet. The numerical model is based on HRS laboratory results. This model is for water depths of 5- and 13-ft, and for two different bottom materials (mud and sand). The diameter of the jet is 16-in., and the flow rate is 5890 gpm.

F.5 LIMITATIONS OF THE PROGRAM

Two different bottom boundary conditions are simulated: the flat bottom, and the movable bottom. The flat bottom numerical model does not have limitations. It is a general model, and can provide flow field, bottom pressure, and bottom shear stress information for any conditions.

For movable bottom boundary problems, on the other hand, this model can only provide flow field information for four different cases, including: two different depths (5- and 13-ft), and two different bottom materials (sand and mud). These conditions were based on HRS laboratory results.

F.6 INPUT REQUIREMENTS

Input requirements are summarized in the following table.

TABLE F-1

Input Requirements for Numerical Model

Card number and format	Fortran variables	Description
1 2I2	LTYPE	= 1 Flat bottom = 2 Movable bottom
1 2I2	LMAT	= 1 Bottom material is mud = 2 Bottom material is sand
1 1X, F10.7	CONCEN	The concentration of bottom material sucked into the suction
2 F6.3, 3(2X, F6.3), 2X, F8.3	DJ	The diameter of the jet (the unit is inches)
	DS	The diameter of the suction (the unit is inches)
2 F6.3, 3(2X, F6.3), 2X, F8.3	DEPTH	The axial distance from the jet (or suction) opening to the bottom (the unit is feet)
	DIS	The radial distance from the jet center to the suction center (the unit is feet)
	Q	The absolute flow rate of the jet or suction (the unit is gpm = gallons per minute)

Figure F-1 illustrates a typical input card.

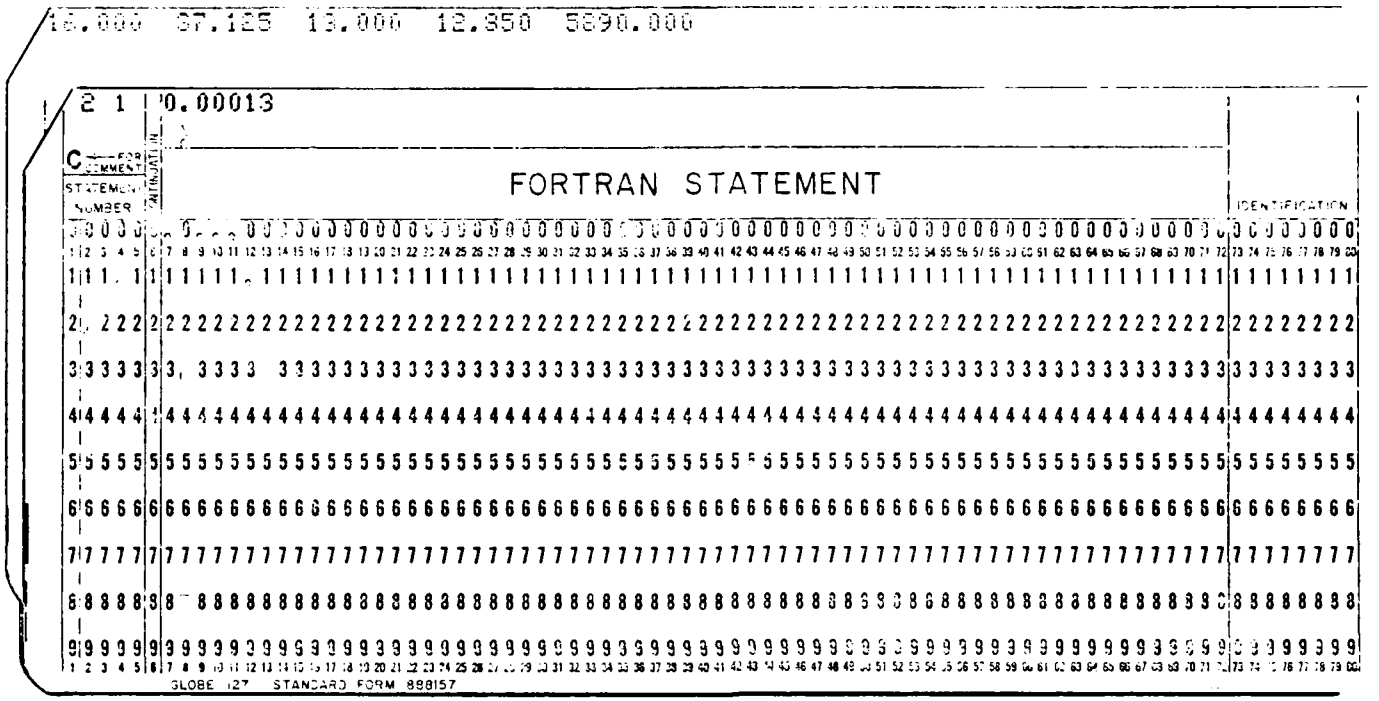

Where LTYPE = 2

LMAT = 1

CONCEN = 0.00013

DJ = 16 inches

DS = 37.125 inches

DEPTH = 13 feet

DIS = 12.85 feet

G = 5890 CPM

Figure F-1

Typical Input Card for Numerical Program

F.7 OUTPUT FORMATTING

The output first lists all the information described in the input. Then for the movable-bottom problems, it prints the axial and radial velocity field of the impingement of the jet in dimensionless form. The common denominator is the average velocity at the opening of the jet.

For the flat-bottom problems, the output shows the flow-field results under the impingement of the jet in dimensionless form, and the common denominator is the average velocity at the opening of the jet. The flow-field results under the suction are also reported in dimensionless form, which is normalized by the average velocity at the opening of the suction. The total flow-field results present the flow-field under the combination of the impingement of the jet and suction expressed in feet per second. Finally, the bottom-pressure and shear stress distribution along the radial direction is printed.

F.8 FLOW CHART

Figure F-2 illustrates the logic setup of the program.

F.9 PROGRAM LISTING

A numerical model program listing follows (refer to the following 16 pages).

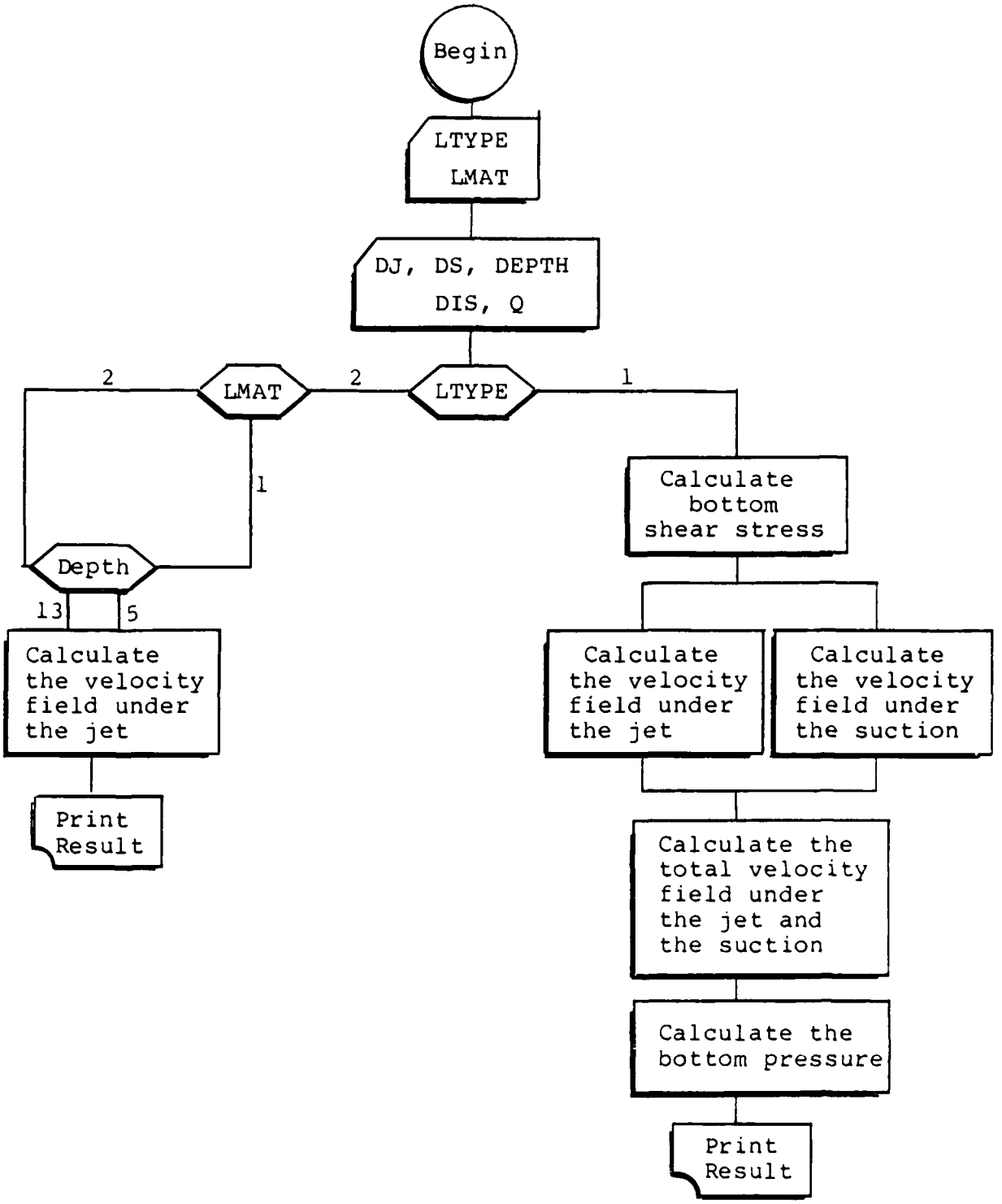

Figure F-2

Flow Chart

```
HRSSC                    **PROGRAM HRSSC(INPUT,OUTPUT,TAPE5=INPUT,TAPE6=OUTPUT)**

    1.  0000000B          PROGRAM HRSSC(INPUT,OUTPUT,TAPE5=INPUT,TAPE6=OUTPUT)
                     C*** THIS NUMERICAL MODEL IS TO DEFINE THE GENERALIZED VELOCITY FIELDS
                     C*** UNDER CAPITAL SHIPS DURING PIERSIDE STEAMING EVOLUTIONS FOR THE
                     C*** CONTRACT OF NAVAL FACILITIES ENGINEERING COMMAND.
                     C**
                     C**
    2.  0011038           DIMENSION UZJ(101,81),URJ(101,81),UZS(101,81),URS(101,81),
                         *STR(101,81),UC(101),VM(81),VP(81),RR(81),RZ(81),
                         *RAD(81),ZDE(101),PR(81),SH(81),PRDI(81),UMO(41,4),VMO(34,4)
    3.  0011038           DIMENSION NU(3),NV(3),PU(3),PV(3)
    4.  0011038           DATA (UMO(I,1),I=1,32)/3.,7.13,8.63,10.13,9.,11.,5.,0.57,
                         *0.5,0.13,0.03,0.017,0.014,0.011,0.009,0.0,0.54,0.48,0.21,
                         *0.077,0.0,-0.049,-0.066,-0.057,-0.046,-0.03,-0.02,0.2,0.15,
                         *0.0,-0.063,-0.074/
    5.  0011038           DATA (UMO(I,2),I=1,41)/3.,7.5,9.32,11.19,12.,16.,6.,0.642,
                         *0.368,0.165,0.037,0.025,0.025,0.024,0.023,0.017,0.0099,0.0049,
                         *0.0,0.518,0.443,0.226,0.049,0.033,0.03,0.026,0.025,0.017,0.,
                         *-0.015,-0.035,-0.047,-0.051,-0.047,-0.037,0.318,0.21,0.099,
                         *0.049,-0.064,-0.151/
    6.  0011038           DATA (UMO(I,3),I=1,13)/2.,2.63,3.75,4.,4.,0.73,0.37,-0.012,0.,
                         *0.71,0.046,0.0014,0./
    7.  0011038           DATA (UMC(I,4),I=1,32)/3.,1.875,3.038,4.54,8.,11.,6.,0.894,
                         *0.855,0.684,0.179,0.053,0.0105,0.0053,0.,0.795,0.752,0.566,
                         *0.137,0.021,0.,0.,-0.0013,-0.0092,-0.0237,-0.0263,0.71,0.566,
                         *0.016,-0.16,-0.113,-0.026/
    8.  0011038           DATA (VMO(I,1),I=1,34)/3.,5.,8.75,10.86,5.5,11.,7.,8.,-0.029,
                         *0.,0.,-0.009,0.011,0.029,0.043,0.054,0.06,0.051,0.031,-0.0036,
                         *0.0027,0.011,0.017,0.026,0.031,0.049,0.,0.0045,0.014,0.023,
                         *0.02,0.014,0.0029,0./
    9.  0011038           DATA (VMO(I,2),I=1,34)/3.,3.75,6.,8.25,5.,11.,9.,6.,0.,0.,-0.012,
                         *-0.0049,0.0049,0.0142,0.,0.0099,0.0173,0.0839,0.0938,0.,0.,0.,0.,
                         *0.0099,0.0173,0.0259,0.0494,0.0642,0.0074,0.0099,0.0235,0.0222,
                         *0.0074,0./
   10.  0011038           DATA (VMO(I,3),I=1,30)/3.,4.125,7.35, 8.81,0.5,11.,5.,6.,0.,
```

```
                     *-0.0015,-0.0091,-0.0121,-0.0061,0.003,0.03,0.051,0.051,0.033,
                     *0.,0.,0.,0.006,0.0212,0.033,0.0182,0.0242,0.0288,0.0242,0.0091,
                     *0./
11.    001103B        DATA (VMO(I,4),I=1,21)/2.,5.,7.25,0.,7.,8.,0.,0.,0.,0.0013,
                     *0.0158,0.0342,0.0605,0.0039,0.0053,0.0053,0.0066,0.0079,
                     *0.0132,0.0276,0.0552/
12.    011103B        READ(5,5)LTYPE,LMAT,CONCEN
13.    123237B      5 FORMAT(2I2,1X,F10.7)
                  C** LTYPE=1, IT IS FOR THE FLAT BOTTOM
                  C** LTYPE=2, IT IS FOR THE MOVABLE BOTTOM
                  C** LMAT=1, THE BOTTOM MATERIAL IS WALNUT SHELL
                  C** LMAT=2, THE BOTTOM MATERIAL IS SAND
14.    123237B        IF(LTYPE.EQ.1) WRITE(6,7)
15.    123247B      7 FORMAT(//2X,*----FLAT BOTTOM----*,//)
16.    123247B        IF(LTYPE.EQ.2) WRITE(6,8)
17.    123257B      8 FORMAT(//,2X,*----MOVABLE BOTTOM----*,//)
18.    123257B        IF(LTYPE.EQ.1) GO TO 9
19.    123260B        IF(LMAT.EQ.1) WRITE(6,12)
20.    123271B     12 FORMAT(/,2X,*----THE BOTTOM MATERIAL IS WALNUT SHELL----*,//)
21.    123271B        IF(LMAT.EQ.2) WRITE(6,14)
22.    123301B     14 FORMAT(/,2X,*----THE BOTTOM MATERIAL IS SAND----*,//)
23.    123301B      9 CONTINUE
24.    123302B        READ(5,10)DJ,DS,DEPTH,DIS,Q
25.    123315B     10 FORMAT(F6.3,2X,F6.3,2X,F6.3,2X,F6.3,2X,F8.3)
26.    123315B        WRITE(6,20)DJ,DS,DEPTH
27.    123326B     20 FORMAT(///,2X,*THE JET DIAMETER IS *,F6.3,1X,*IN*,//,2X,
                     * *THE SUCTION DIAMETER IS *,F6.3,1X,*IN*,//,2X,
                     * *THE WATER DEPTH IS *,F6.3,1X,*FEET*)
28.    123326B        WRITE(6,30)DIS,Q
29.    123336B     30 FORMAT(//,2X,*THE DISTANCE BETWEEN THE JET AND SUCTION IS *,
                     * 1X,F6.3,* FEET*,//,2X,
                     * *THE FLOW RATE OF THE JET AND SUCTION IS *, F8.3,* GPM*,//)
                  C** CHANGE INCH TO FOOT
30.    123336B        DJ=DJ/12.
31.    123337B        DS=DS/12.
                  C** CHANGE GPM TO CFS
32.    123340B        Q=Q/448.2
```

```
33.   123342B          PI=3.1415927
34.   123343B          RJ=.5*DJ
35.   123344B          RS=.5*DS
36.   123345B          VOJ=Q/(PI*RJ*RJ)
37.   123350B          VOS=-Q/(PI*RS*RS)
38.   123352B          DR=DIS/80.
39.   123354B          DZ=DEPTH/100.
40.   123356B          DRE=DEPTH/DJ
41.   123357B          IF(LTYPE.EQ.2) GO TO 6000
                  C** CALCULATE THE SKIN FRICTION (PSI) ON THE BOTTOM
                  C** ALONG THE RADIAL DIRECTION
42.   123362B          TMO=PI*VOJ*VOJ*RJ*RJ*(.3048)**4
43.   123365B          DEN=1000.
44.   123367B          CHUN=2.2/(3.2808*12.)**2
45.   123370B          TMOV=SQRT(TMO)/(10.**(-5)*.3048*.3048)
46.   123375B          DIVP=(.3/1270.*TMOV**.2)**(1./3.3)
47.   123405B          DEP2=1./(DEPTH*.3048)**2
48.   123407B          DO 90 I=1,81
49.   123413B          RD=DR*(I-1)
50.   123415B          RDD=RD/DEPTH
51.   123416B          IF(RDD.GT.DIVP) GO TO 85
52.   123421B          SH(I)=DEN*TMO*DEP2*1270.*(TMOV)**(-.5)*RDD*CHUN
53.   123435B          GO TO 90
54.   123440B       85 SH(I)=DEN*TMO*DEP2*.3*(TMOV)**(-.3)*RDD**(-2.3)*CHUN
55.   123460B       90 CONTINUE
56.   123465B          DEN=1.93
                  C** TO CALCULATE THE GENERALIZED VELOCITY FIELDS UNDER THE
                  C** JET CONDITION.
                  C*
                  C*
                  C** TO CALCULATE THE JET CENTERLINE VELOCITY ALONG THE AXIAL DIRECTION
                  C**
                  C**
57.   123466B          IF(DRE.LT.6.) GO TO 150
58.   123471B          DRSUB=DRE-2.
59.   123472B          DRE=VOJ*(.8C5-.J65*(DRSUB-7.))
```

```
60.   123476B          IF(DRSUB.LE.7) URE=VOJ*EXP(-0.054173*(DRE-5.))
61.   123512B          IF(DRSUB.GE.10.) URE=VOJ*EXP(-0.07048*(DRE-5.))
62.   123525B          II=(DEPTH-2.*DJ)/DZ
63.   123530B          I3=(3.*DJ)/DZ+1
64.   123533B          DO 110 I=1,I3
65.   123542B      110 UC(I)=VOJ
66.   123560B          DO 120 I=I3+1,II
67.   123572B          Z=DZ*(I-1)/DJ
68.   123575B          UC(I)=VOJ*(.805-.065*(Z-7.))
69.   123605B          IF(Z.LE.7.) UC(I)=VOJ*EXP(-0.054173*(Z-3.))
70.   123624B          IF(Z.GE.10.) UC(I)=VOJ*EXP(-0.07048*(Z-3.))
71.   123643B      120 CONTINUE
72.   123647B          DO 130 I=II+1,101
73.   123656B          Z=URE-DZ*(I-1)/DJ
74.   123662B      130 UC(I)=URE*(1.5574*Z-1.0776*Z*Z+.2742*Z**3)
75.   123675B          GO TO 190
76.   123676B      150 URE=VOJ*EXP(-0.054173*(DRE-4.))
77.   123710B          IF(DRE-1.1 .LE. 3.) URE=VOJ
78.   123715B          II=(DEPTH-1.1*DJ)/DZ
79.   123720B          DO 160 I=1,II
80.   123727B          Z=DZ*(I-1)
81.   123731B          IF(Z/DJ.LE.3.) GO TO 155
82.   123734B          UC(I)=VOJ*EXP(-0.054173*(Z/DJ-3.))
83.   123751B          GO TO 160
84.   123754B      155 UC(I)=VOJ
85.   123762B      160 CONTINUE
86.   123770B          DO 170 I=II+1,101
87.   123777B          Z=DZ*(I-1)
88.   124001B          Z=(DEPTH-Z)/(1.1*DJ)
89.   124005B      170 UC(I)=URE*(Z*(2.-Z))
90.   124017B      190 CONTINUE
                  C** TO CALCULATE THE VERTICAL VELOCITY ALONG THE RADIAL DISTANCE
                  C** FOR A GIVEN VERTICAL LOCATION.
                  C**
                  C**
91.   124020B          IF(DRE.LT.6) GO TO 250
```

```
     92.  124023B          RIR=6.*DJ
     93.  124024B          DO 240 I=1,101
     94.  124027B          Z=DZ*(I-1)
     95.  124031B          R1=DJ*0.39-0.065*Z
     96.  124034B          IF(Z.GE.RIR) R1=0.
     97.  124040B          B1=0.115*DJ+0.087*Z
     98.  124042B          DO 220 J=1,81
     99.  124045B          R=DR*(J-1)
    100.  124047B          IF(R.LT.R1) GO TO 210
    101.  124052B          ET=(R-R1)/B1
    102.  124054B          UZJ(I,J)=UC(I)*EXP(-0.693*ET*ET)
    103.  124075B          GO TO 220
    104.  124076B      210 UZJ(I,J)=UC(I)
    105.  124113B      220 CONTINUE
    106.  124117B      240 CONTINUE
    107.  124123B          GO TO 290
    108.  124124B      250 RIR=DEPTH-1.1*DJ
    109.  124131B          CON=0.5-0.069*(DEPTH/DJ)
    110.  124134B          DO 280 I=1,101
    111.  124137B          Z=DZ*(I-1)
    112.  124141B          R1=.39*DJ-0.065*Z
    113.  124144B          IF(Z.GE.RIR) R1=DJ*CON*(Z/DJ)**(-0.25)
    114.  124156B          B1=0.115*DJ+0.087*Z
    115.  124161B          UMM=UC(I)
    116.  124166B          IF(Z.GE.DEPTH-0.7*DJ) UMM=1.15*UC(I)
    117.  124176B          DO 270 J=1,81
    118.  124200B          R=DR*(J-1)
    119.  124202B          IF(R.LT.R1) GO TO 260
    120.  124205B          ET=(R-R1)/B1
    121.  124207B          UZJ(I,J)=UMM*EXP(-0.693*ET*ET)
    122.  124225B          GO TO 270
    123.  124226B      260 IF(UMM.EQ.UC(I)) GO TO 265
    124.  124236B          R2=(R/R1)**2
    125.  124240B          UZJ(I,J)=UC(I)+(UMM-UC(I))*R2*(2.-R2)
```

```
126.  1242578        GO TO 270
127.  1242618    265 UZJ(I,J)=UMM
128.  1242728    270 CONTINUE
129.  1242768    280 CONTINUE
                  C**
                  C**
                  C** CALCULATE THE RADIAL VELOCITIES FOR THE JET PROBLEM
                  C**
                  C**
130.  1243028    290 IF(DRE.LT.6.) GO TO 350
131.  1243068        DO 310 J=1,81
132.  1243118        R=(DR*(J-1))/DJ
133.  1243148        IF(R.LE.1.2) VM(J)=URE*(1.070848*R-0.5313*R*R+.1042*R**3)
134.  1243318        IF(R.GT.1.2 .AND. R.LE.3.2) VM(J)=URE*(.2120061+
                     * .8004053*R-.3953057*R*R+.0559883*R**3)
135.  1243478        IF(R.GT.3.2) VM(J)=URE*(.56-.075*(R-3.2))
136.  1243608    310 CONTINUE
137.  1243638        GO TO 390
138.  1243648    350 DO 360 J=1,81
139.  1243718        R=(DR*(J-1))/DJ
140.  1243748        IF(R.LE.1.2) VM(J)=URE*(1.05*R+.40625*R*R-.546875*R**3)
141.  1244118        IF(R.GT.1.2 .AND. R.LE.2.4) VM(J)=URE*(.9-.25*(R-1.2))
142.  1244258        IF(R.GT.2.4) VM(J)=URE*(.6-.1875*(R-2.4))
143.  1244368    360 CONTINUE
144.  1244418    390 DO 400 I=1,101
145.  1244468        DO 400 J=1,81
146.  1244518    400 URJ(I,J)=0.
147.  1244758        B2=.444*DJ
148.  1244768        IY=(DEPTH-2.6*B2)/DZ+1
149.  1245038        DO 410 J=1,81
150.  1245068        VMA=VM(J)
151.  1245128        DO 410 I=IY,101
152.  1245248        Y=(DEPTH-DZ*(I-1))/B2
153.  1245368        IF(Y.GE.1.5 .AND. Y.LE.2.6) URJ(I,J)=VMA*(.579-.494*Y+.0697*Y*Y)
```

```
154.   124547B          IF(Y.GE..25 .AND. Y.LT.1.5) URJ(I,J)=VMA*(.9900968+.8873709*Y-
                       *  1.974826*Y*Y+.6967529*Y**3)
155.   124567B          IF(Y.GE.0. .AND. Y.LT..25) URJ(I,J)=VMA*(.47+6.9456422*Y-
                       *  31.225658*Y*Y+47.692356*Y**3)
156.   124636B        410 CONTINUE
                     C**
                     C**
                     C** TO CALCULATE THE GENERALIZED VELOCITY FIELDS UNDER THE
                     C**  SUCTION CONDITION (BASED ON POTENTIAL THEORY).
                     C**
                     C**
                     C** SET INITIAL CONDITION
                     C**
157.   124614B            SM=-VOS*RS*RS*.5
158.   124616B            DO 415 I=1,101
159.   124622B            DO 415 J=1,81
160.   124625B            UZS(I,J)=0.
161.   124633B        415 STR(I,J)=.5*SM
162.   124642B            DO 420 I=1,101
163.   124644B        420 STR(I,1)=0.
164.   124662B            DO 430 J=1,81
165.   124664B        430 STR(101,J)=0.
166.   124704B            DO 440 J=1,81
167.   124706B            R=DR*(J-1)
168.   124710B            STR(1,J)=-VOS*R*R*.5
169.   124723B        440 IF(R.GE.RS) STR(1,J)=SM
170.   124730B            DZ2=1./(DZ*DZ)
171.   124731B            DR2=1./(DR*DR)
172.   124734B            DZR=.5/(DZ2+DR2)
173.   124736B            DO 460 J=2,81
174.   124740B            R=DR*(J-1)
175.   124742B            RZ(J)=.5/(R*DZ)
176.   124750B        460 RR(J)=.5/(R*DR)
177.   124757B            RR(1)=0.
178.   124757B            API=(COS(PI/101.)+COS(PI/81.))**2
179.   124775B            OMI=(8.-4.*SQRT(4.-API))/API
180.   125005B            ITR=0
181.   125006B            DO 600 L=1,200
```

```
      DO 550 J=2,80
      IF(J.EQ.80) GO TO 520
      DO 510 I=2,100
  510 STR(I,J)=(1.-OMI)*STR(I,J)+OMI*DZR*(DZ2*(STR(I+1,J)+STR(I-1,J))
     * +DR2*(STR(I,J+1)+STR(I,J-1))-RR(J)*(STR(I,J+1)-STR(I,J-1)))
      GO TO 550
  520 DO 530 I=2,100
  530 STR(I,J)=(1.-OMI)*STR(I,J)+OMI/(2.*DZ2+DR2+RR(J))*(DZ2*
     * (STR(I+1,J)+STR(I-1,J))+DR2*STR(I,J-1)+RR(J)*STR(I,J-1))
  550 CONTINUE
      ITR=ITR+1
      IF(ITR.LE.50) GO TO 580
      ERR=0.
      DO 560 I=2,100
      DO 560 J=2,80
  560 ERR=ERR+(STR(I,J)-UZS(I,J))**2
C** UZS(I,J) REPLACED THE PREVIOUS STREAM FUNCTION VALUE TO SAVE THE
C** MEMORY, LATER UZS(I,J) WILL BECOME THE VERTICAL VELOCITY
      ERR=SQRT(ERR/(99.*79.))
      IF(ERR.LT.0.01) GO TO 650
  580 DO 590 I=2,100
      DO 590 J=2,80
  590 UZS(I,J)=STR(I,J)
  600 CONTINUE
  650 WRITE(6,670)ITR,ERR
  670 FORMAT(/,1X,*TOTAL INTERATION = *,I4,*  ERROR = *,E13.6)
      DO 690 I=1,101
  690 STR(I,81)=STR(I,80)
      DO 700 I=2,100
      II=I
      DO 700 J=2,80
      JJ=82-J
      UZS(II,JJ)=-RR(J)*(STR(I,J+1)-STR(I,J-1))
  700 URS(II,JJ)=RZ(J)*(STR(I+1,J)-STR(I-1,J))
      UZS(1,81)=VOS
      URS(1,81)=0.
```

```
HRSSC                    **PROGRAM HRSSC(INPUT,OUTPUT,TAPE5=INPUT,TAPE6=OUTPUT)**

  214.   1254028          UZS(1,1)=0.
  215.   1254048          URS(1,1)=(STR(2,81)-STR(1,81))*RZ(81)*2.
  216.   1254058          UZS(101,1)=0.
  217.   1254068          URS(101,1)=(STR(101,81)-STR(100,81))*RZ(81)*2.
  218.   1254118          UZS(101,81)=0.
  219.   1254128          URS(101,81)=0.
  220.   1254128          DO 710 I=2,100
  221.   1254158          UZS(I,81)=-STR(I,2)/(DR*DR)*2.
  222.   1254268          URS(I,81)=0.
  223.   1254328          UZS(I,1)=UZS(I,2)
  224.   1254428      710 URS(I,1)=URS(I,2)
  225.   1254558          DO 720 J=2,80
  226.   1254608          JJ=82-J
  227.   1254618          UZS(101,JJ)=0.
  228.   1254668          UZS(1,JJ)=-RR(J)*(STR(1,J+1)-STR(1,J-1))
  229.   1255108          URS(1,JJ)=RZ(J)*2.*(STR(2,J)-STR(1,J))
  230.   1255238      720 URS(101,JJ)=RZ(J)*2.*(STR(101,J)-STR(100,J))
                     C** CALCULATE THE BOTTOM PRESSURE (PSI) DISTRIBUTION ALONG
                     C** THE RADIAL DISTANCE DUE TO THE  EXISTANCE OF THE JET
  231.   1255428          IF(URE.LT.6.) GO TO 850
  232.   1255448          DO 840 I=1,81
  233.   1255478          RD=DR*(I-1)
  234.   1255518          RDD=RD/DJ
  235.   1255528          IF(RDD.LE.1.6) VP(I)=URE*(1.070848*RDD-.5313*RDD*RDD+.1042*RDD**3)
  236.   1255678          IF(RDD.GT.1.6 .AND. RDD.LE.2.8) VP(I)=URE*(.72112-.09726*RDD+
                         * .1256*RDD*RDD-.026125*RDD**3)
  237.   1256058          IF(RDD.GT.2.3) VP(I)=URE*.86
  238.   1256148      840 CONTINUE
  239.   1256178          GO TO 870
  240.   1256208      850 DO 860 I=1,81
  241.   1256258          RD=DR*(I-1)
  242.   1256278          RDD=RD/DJ
  243.   1256308          IF(RDD.LE.2.) VP(I)=URE*(1.0729167*RDD+.9765625*RDD*RDD-
                         * 2.0638021*RDD**3+1.1230469*RDD**4-.2034505*RDD**5)
```

```
244.  1256518        IF(RDD.GT.2.) VP(I)=URE
245.  1256618   860 CONTINUE
246.  1256648   870 VIN=VOJ*VCJ
247.  1256678       DO 880 I=1,81
248.  1256728   880 PR(I)=.5*DEN*(VIN-VP(I)**2)/144.
249.  1257138       DIPR=.5*DEN*VIN/144.
250.  1257158       DO 1000 I=1,81
251.  1257268       PRDI(I)=(PR(I)-PR(81))/DIPR
252.  1257268       PR(I)=PRDI(I)*DIPR
253.  1257328  1000 RAD(I)=DR*(I-1)
254.  1257448       DO 1100 I=1,101
255.  1257468  1100 ZDE(I)=DZ*(I-1)
256.  1257658       WRITE(6,1810)VCJ
257.  1257748  1810 FORMAT(//,2X,*THE JET ENTRANCE CENTRAL VELOCITY = *,E12.5,
                  **  FEET/SEC*,//)
258.  1257748       WRITE(6,1850)
259.  1260028  1850 FORMAT(///,2X,*--THE VERTICAL VELOCITY DISTRIBUTION FOR THE *,
                  **JET (DIMENSIONLESS FORM)--*,///)
260.  1260028       DO 1860 I=1,101
261.  1260048       DO 1860 J=1,81
262.  1260078       UZJ(I,J)=UZJ(I,J)/VCJ
263.  1260168  1860 URJ(I,J)=URJ(I,J)/VCJ
264.  1260248       DO 2000 K=1,5
265.  1260278       I1=18*(K-1)+1
266.  1260308       I2=18*K-1
267.  1260328       IF(I2.GT.81) I2=81
268.  1260368       WRITE(6,3000)(RAD(J),J=I1,I2,2)
269.  1260668       DO 1900 I=1,101,2
270.  1260708  1900 WRITE(6,3100)ZDE(I),(UZJ(I,J),J=I1,I2,2)
271.  1261348  2000 CONTINUE
272.  1261408       WRITE(6,2040)
273.  1261478  2040 FORMAT(///,2X,*--THE RADIAL VELOCITY DISTRIBUTION FOR THE *,
                  **JET (DIMENSIONLESS FORM)--*,///)
274.  1261478       DO 2100 K=1,5
275.  1261518       I1=18*(K-1)+1
276.  1261538       I2=18*K-1
277.  1261558       IF(I2.GT.81) I2=81
278.  1261618       WRITE(6,3000)(RAD(J),J=I1,I2,2)
```

```
279.    1262118         DO 2050 I=1,101,2
280.    1262138   2050 WRITE(6,3100)ZDE(I),(URJ(I,J),J=11,12,2)
281.    1262578   2100 CONTINUE
282.    1262638         WRITE(6,2110)VCS
283.    1262738   2110 FORMAT(//,2X,*THE SUCTION ENTRANCE CENTRAL VELOCITY = *,E12.5,
                     ** FEET/SEC*,//)
284.    1262738         DO 2120 I=1,101
285.    1262758         DO 2120 J=1,81
286.    1263008         UZJ(I,J)=UZJ(I,J)*VCJ
287.    1263078         URJ(I,J)=URJ(I,J)*VCJ
288.    1263108         UZS(I,J)=UZS(I,J)/VOS
289.    1263128   2120 URS(I,J)=-URS(I,J)/VOS
290.    1263208         WRITE(6,2140)
291.    1263278   2140 FORMAT(///,2X,*--THE VERTICAL VELOCITY DISTRIBUTION FOR THE*,
                     ** SUCTION (DIMENSIONLESS FORM)--*,///)
292.    1263278         DO 2200 K=1,5
293.    1263318         I1=18*(K-1)+1
294.    1263338         I2=18*K-1
295.    1263358         IF(I2.GT.81) I2=81
296.    1263418         WRITE(6,3000)(RAD(J),J=11,12,2)
297.    1263718         DO 2150 I=1,101,2
298.    1263738   2150 WRITE(6,3100)ZDE(I),(UZS(I,J),J=11,12,2)
299.    1264378   2200 CONTINUE
300.    1264438         WRITE(6,2240)
301.    1264528   2240 FORMAT(///,2X,*--THE RADIAL VELOCITY DISTRIBUTION FOR THE *,
                     **SUCTION (DIMENSIONLESS FORM)--*,///)
302.    1264528         DO 2300 K=1,5
303.    1264548         I1=18*(K-1)+1
304.    1264568         I2=18*K-1
305.    1264608         IF(I2.GT.81) I2=81
306.    1264648         WRITE(6,3000)(RAD(J),J=11,12,2)
307.    1265148         DO 2250 I=1,101,2
308.    1265168   2250 WRITE(6,3100)ZDE(I),(URS(I,J),J=11,12,2)
309.    1265628   2300 CONTINUE
310.    1265668         DO 2320 I=1,101
311.    1265718         DO 2320 J=1,81
312.    1265748         UZS(I,J)=UZS(I,J)*VOS
313.    1266038         URS(I,J)=URS(I,J)*VCS
```

```
314.    1266048         UZJ(I,J)=UZJ(I,J)+UZS(I,J)
315.    1266058    2320 URJ(I,J)=URJ(I,J)+URS(I,J)
316.    1266148         WRITE(6,2340)
317.    1266238    2340 FORMAT(///,2X,*--THE VERTICAL VELOCITY DISTRIBUTION FOR THE*,
                       */,2X,*--SUM OF THE JET AND THE SUCTION (FT/SEC)--*,///)
318.    1266338         DO 2400 K=1,5
319.    1266428         I1=18*(K-1)+1
320.    1266518         I2=18*K-1
321.    1266618         IF(I2.GT.81) I2=81
322.    1266708         WRITE(6,3000)(RAD(J),J=I1,I2,2)
323.    1266808         DO 2350 I=1,101,2
324.    1266878    2350 WRITE(6,3100)ZDE(I),(UZJ(I,J),J=I1,I2,2)
325.    1267338    2400 CONTINUE
326.    1267378         WRITE(6,2440)
327.    1267468    2440 FORMAT(///,2X,*--THE RADIAL VELOCITY DISTRIBUTION FOR THE *,
                       */,2X,*--SUM OF THE JET AND THE SUCTION (FT/SEC)--*,///)
328.    1267468         DO 2500 K=1,5
329.    1267508         I1=18*(K-1)+1
330.    1267528         I2=18*K-1
331.    1267548         IF(I2.GT.81) I2=81
332.    1267608         WRITE(6,3000)(RAD(J),J=I1,I2,2)
333.    1270108         DO 2450 I=1,101,2
334.    1270128    2450 WRITE(6,3100)ZDE(I),(URJ(I,J),J=I1,I2,2)
335.    1270568    2500 CONTINUE
336.    1270628         WRITE(6,2600)
337.    1270718    2600 FORMAT(///,2X,*LIST THE BOTTOM PRESSURE AND THE SKIN FRICTION *,
                       * *ALONG THE RADIAL DISTANCE*,//,2X,*RADIAL DISTANCE*,4X,
                       * *    PRESSURE (PSI)  *,4X,*  SKIN FRICTION (PSI)*,//)
338.    1270718         DO 2700 I=1,81
339.    1270738         RD=DR*(I-1)
340.    1270758         RDD=RD/DJ
341.    1270768    2700 WRITE(6,3200)RD,PR(I),SH(I),RDD,PRDI(I)
342.    1271338    3000 FORMAT(//,15X,*RADIAL DISTANCE (FOOT)*,//,1X,
                       * *  VER. DIS.  *,9(1X,E12.5),//)
343.    1271338    3100 FORMAT(10(1X,E12.5))
344.    1271338    3200 FORMAT(3X,E12.5,9X,E12.5,12X,E12.5,5X,E12.5,5X,E12.5)
345.    1271338         GO TO 9000
346.    1271338    6000 CONTINUE
```

```
                      C**
                      C**
                      C** CALCULATE THE VELOCITY FIELD FOR A MOVABLE BOTTOM UNDER A JET
                      C**
                      C**
     347.   127136B          IF(DEPTH.EQ.13.) I=LMAT
     348.   127142B          IF(DEPTH.EQ.5.) I=LMAT+2
     349.   127146B          KUT=UMO(1,I)+0.2
     350.   127156B          KVT=VMO(1,I)+0.2
     351.   127165B          DO 6100 J=1,KUT
     352.   127175B          J1=J+1
     353.   127175B          J2=J1+KUT
     354.   127176B          PU(J)=UMO(J1,I)*DJ
     355.   127211B          J3=UMO(J2,I)+0.2
     356.   127222B  6100    NU(J)=J3
     357.   127231B          DO 6200 J=1,KVT
     358.   127240B          J1=J+1
     359.   127240B          J2=J+2+KVT
     360.   127242B          PV(J)=VMO(J1,I)*DJ
     361.   127255B          J3=VMO(J2,I)+0.2
     362.   127266B  6200    NV(J)=J3
     363.   127275B          STV=VMO(2+KVT,I)
     364.   127304B          KMAX=0
     365.   127305B          DO 6210 J=1,KUT
     366.   127315B  6210    IF(KMAX.LT.NU(J)) KMAX=NU(J)
     367.   127332B          IF(DEPTH.EQ.5.) GO TO 6500
     368.   127333B          ITOL=3
     369.   127334B          DZ=2.*DJ
     370.   127335B          R1R=6.*DJ
     371.   127337B          DO 6240 J=1,ITOL
     372.   127347B          Z=DZ*J
     373.   127350B          R1=0.39*DJ-0.065*Z
     374.   127358B          IF(Z.GE.R1R) R1=0.
     375.   127357B          B1=0.115*DJ+0.087*Z
     376.   127361B          ZD=Z/DJ
     377.   127426B          IF(ZD.LE.3.) UCV=VOJ
```

```
378.  127366B          IF(ZD.GT.3. .AND.ZD.LE.7.) UCV=VOJ*EXP(-0.054173*(ZD-3.))
379.  127402B          DO 6220 J1=1,KMAX
380.  127411B          R=0.5*DJ*(J1-1)
381.  127414B          IF(R.LT.R1) GO TO 6215
382.  127417B          ET=(R-R1)/B1
383.  127421B          UZJ(J1,J)=UCV*EXP(-0.693*ET*ET)/VOJ
384.  127441B          GO TO 6220
385.  127442B    6215  UZJ(J1,J)=UCV/VOJ
386.  127454B    6220  CONTINUE
387.  127461B    6240  CONTINUE
388.  127465B          GO TO 6550
389.  127466B    6500  ITOL=1
390.  127467B          DZ=DJ
391.  127471B          Z=DZ
392.  127471B          R1=0.39*DJ-0.065*Z
393.  127474B          B1=0.115*DJ+0.087*Z
394.  127477B          DO 6510 J=1,KMAX
395.  127507B          R=0.5*DJ*(J-1)
396.  127512B          IF(R.LT.R1) GO TO 6520
397.  127515B          ET=(R-R1)/B1
398.  127517B          UZJ(J,1)=VOJ*EXP(-0.693*ET*ET)/VOJ
399.  127534B          GO TO 6510
400.  127535B    6520  UZJ(J,1)=1.
401.  127544B    6510  CONTINUE
402.  127552B    6550  CONTINUE
403.  127553B          WRITE(6,1810)VOJ
404.  127562B          WRITE(6,1850)
405.  127570B          DO 6600 J=1,KMAX
406.  127577B    6600  RAD(J)=0.5*DJ*(J-1)
407.  127617B          KPMA=9
408.  127617B          IF(KMAX.LT.9) KPMA=KMAX
409.  127623B          WRITE(6,3000)(RAD(J),J=1,KPMA)
410.  127650B          DO 6620 J=1,ITOL
411.  127657B          Z=DZ*J
412.  127660B    6620  WRITE(6,3100)Z,(UZJ(J1,J),J1=1,KPMA)
413.  127715B          I1=8
414.  127716B          I2=I1+NU(1)
415.  127717B          I3=I2+NU(2)
```

```
      DO 6630 J=1,KUT
      IF(J.EQ.1) IST=I1
      IF(J.EQ.2) IST=I2
      IF(J.EQ.3) IST=I3
      IEND=9+IST-1
      IF(NU(J).LT.9) IEND=NU(J)+IST-1
 6630 WRITE(6,3100)PU(J),(UMU(J1,I),J1=IST,IEND)
      IF(KMAX.LE.9) GO TO 7000
      KST=10
      WRITE(6,3000)(RAD(J1),J1=KST,KMAX)
      DO 6650 J=1,ITCL
      Z=DZ*J
 6650 WRITE(6,3100)Z,(UZJ(J1,J),J1=KST,KMAX)
      I1=17
      I2=I1+NU(1)
      I3=I2+NU(2)
      DO 6680 J=1,KUT
      IF(NU(J).LE.9) GO TO 6670
      IF(J.EQ.1) IST=I1
      IF(J.EQ.2) IST=I2
      IF(J.EQ.3) IST=I3
      IEND=IST+NU(J)-10
      WRITE(6,3100)PU(J),(UMU(J1,I),J1=IST,IEND)
      GO TO 6680
 6670 WRITE(6,3100)PU(J)
 6680 CONTINUE
 7000 CONTINUE
      WRITE(6,7100)
 7100 FORMAT(///,2X,*--THE RADIAL VELOCITY DISTRIBUTION UNDER THE *,
     * *JET (DIMENSIONLESS FORM)--*,//,15X,
     * *RADIAL DISTANCE (FOOT)*,/)
      WRITE(6,7110)(PV(J),J=1,KVT)
 7110 FORMAT(/,1X,*  VER. DIS. (FT)  *,8(1X,E12.5))
      IF(KVT.EQ.2) GO TO 7260
      I1=9
      I2=I1+NV(1)
      I3=I2+NV(2)
      DO 7250 J=1,I1
```

```
      POS=(STV+0.5*(J-1))*DJ
      I4=I1+J-1
      I5=I2+J-1
      I6=I3+J-1
      A=VMO(I4,I)
      B=VMO(I5,I)
      IF(NV(3).GE.J) C=VMO(I6,I)
      IF(NV(1).GE.J .AND. NV(2).GE.J .AND. NV(3).GE.J)
     * WRITE(6,7400)POS,A,B,C
      IF(NV(1).GE.J .AND.NV(2).LT.J .AND. NV(3).GE.J)
     * WRITE(6,7410)POS,A,C
      IF(NV(1).GE.J .AND. NV(2).GE.J .AND. NV(3).LT.J)
     * WRITE(6,7400)POS,A,B
      IF(NV(1).GE.J .AND. NV(2).LT.J .AND. NV(3).LT.J)
     * WRITE(6,7400)POS,A
7250  CONTINUE
7400  FORMAT(3X,E12.5,6X,E12.5,1X,E12.5,1X,E12.5)
7410  FORMAT(3X,E12.5,6X,E12.5,1X,E12.5)
7420  FORMAT(3X,E12.5,19X,E12.5)
      GO TO 8000
7260  I1=7
      I2=I1+NV(1)
      DO 7270 J=1,7
      POS=(STV+0.5*(J-1))*DJ
      I4=I1+J-1
      I5=I2+J-1
      A=VMO(I4,I)
      B=VMO(I5,I)
7270  WRITE(6,7400)POS,A,B
      I5=I2+7
      POS=(STV+0.5*7.)*DJ
      B=VMO(I5,I)
      WRITE(6,7420)POS,B
8000  SUVOL=Q*CONCEN*60.
      WRITE(6,8010)SUVOL
8010  FORMAT(///,3X,*THE SUCTION RATE OF THE BOTTOM MATERIAL IS  *,
     *E13.6,* CU. FT. / MIN. *)
9000  CONTINUE
      END
```

Appendix G,
Conversion Factors, Customary to SI Units of Measurements

APPENDIX G

CONVERSION FACTORS, CUSTOMARY TO SI UNITS OF MEASUREMENTS

Units of measurement used in this report can be converted as follows:

Multiply	By	To Obtain
inch	2.540* - 02	meter
foot	3.048* - 01	meter
micron	1.000* - 06	meter
foot/second	3.048* - 01	meter/second
centimeter/second	1.000* - 02	meter/second
pound	4.537* - 01	kilogram
gram/cubic centimeter	1.000* + 03	kilogram/cubic meter
cubic foot/second	2.832* - 02	cubic meter/second
gallons/minute	6.310* - 05	cubic meter/second